Structural Engineering Report No. 136

SHEAR BEHAVIOR OF LARGE DIAMETER FABRICATED STEEL CYLINDERS

by

J. MOK

A. E. ELWI

June, 1986

RECENT STRUCTURAL ENGINEERING REPORTS

Department of Civil Engineering

University of Alberta

105. *Fatigue Strength of Two Steel Details* by K.A. Baker and G.L. Kulak, October 1982.

106. *Designing Floor Systems for Dynamic Response* by C.M. Matthews, C.J. Montgomery and D.W. Murray, October 1982.

107. *Analysis of Steel Plate Shear Walls* by L. Jane Thorburn, G.L. Kulak, and C.J. Montgomery, May 1983.

108. *Analysis of Shells of Revolution* by N. Hernandez and S.H. Simmonds, August 1983.

109. *Tests of Reinforced Concrete Deep Beams* by D.M. Rogowsky, J.G. MacGregor and S.Y. Ong, September 1983.

110. *Shear Strength of Deep Reinforced Concrete Continuous Beams* by D.M. Rogowsky and J.G. MacGregor, September 1983.

111. *Drilled-In Inserts in Masonry Construction* by M.A. Hatzinikolas, R. Lee, J. Longworth and J. Warwaruk, October 1983.

112. *Ultimate Strength of Timber Beam Columns* by T.M. Olatunji and J. Longworth, November 1983.

113. *Lateral Coal Pressures in a Mass Flow Silo* by A.B.B. Smith and S.H. Simmonds, November 1983.

114. *Experimental Study of Steel Plate Shear Walls* by P.A. Timler and G.L. Kulak, November 1983.

115. *End Connection Effects on the Strength of Concrete Filled HSS Columns* by S.J. Kennedy and J.G. MacGregor, April 1984.

116. *Reinforced Concrete Column Design Program* by C-K. Leung and S.H. Simmonds, April 1984.

117. *Deflections of Two-way Slabs under Construction Loading* by C. Graham and A. Scanlon, August 1984.

118. *Effective Lengths of Laterally Unsupported Steel Beams* by C.D. Schmitke and D.J.L. Kennedy, October 1984.

119. *Flexural and Shear Behaviour of Large Diameter Steel Tubes* by R.W. Bailey and G.L. Kulak, November 1984.

120. *Concrete Masonry Prism Response due to Loads Parallel and Perpendicular to Bed Joints* by R. Lee, J. Longworth and J. Warwaruk.

121. *Standardized Flexible End Plate Connections for Steel Beams* by G.J. Kriviak and D.J.L. Kennedy, December 1984.

122. *The Effects of Restrained Shrinkage on Concrete Slabs* by K.S.S. Tam and A. Scanlon, December 1984.

123. *Prestressed Concrete Beams with Large Rectangular Web Openings* by T. do M.J. Alves and A. Scanlon, December 1984.

124. *Tests on Eccentrically Loaded Fillet Welds* by G.L. Kulak and P.A. Timler, December 1984.

125. *Analysis of Field Measured Deflections Scotia Place Office Tower* by A. Scanlon and E. Ho, December 1984.

126. *Ultimate Behaviour of Continuous Deep Reinforced Concrete Beams* by D.R. Ricketts and J.G. MacGregor, January 1985.

127. *The Interaction of Masonry Veneer and Steel Studs in Curtain Wall Construction* by W.M. McGinley, J. Warwaruk, J. Longworth and M. Hatzinikolas, May 1985.

128. *Evaluation of Existing Bridge Structure by Nondestructive Test Methods* by L. Mikhailovsky and A. Scanlon, May 1985.

129. *Finite Element Modelling of Buried Structures* by D.K. Playdon and S.H. Simmonds, October 1985.

130. *Behaviour and Ultimate Strength of Transversely Loaded Continuous Steel Plates* by K.P. Ratzlaff and D.J.L. Kennedy, November 1985.

131. *Inelastic Lateral Buckling of Steel Beam-Columns* by P.E. Cuk, M.A. Bradford and N.S. Trahair, December 1985.

132. *Design Strengths of Steel Beam-Columns* by N.S. Trahair, December 1985.

133. *Behaviour of Fillet Welds as a Function of the Angle of Loading* by G.S. Miazga and D.J.L. Kennedy, March 1986.

134. *Inelastic Seismic Response of Precast Concrete Large Panel Coupled Shear Wall Systems* by M.R. Kianoush and A. Scanlon, March 1986.

135. *Finite Element Prediction of Bin Loads* by A.H. Askari and A.E. Elwi, June 1986.

136. *Shear Behavior of Large Diameter Fabricated Steel Cylinders* by J. Mok and A.E. Elwi, June 1986.

SHEAR BEHAVIOR OF LARGE DIAMETER FABRICATED STEEL CYLINDERS

by

J. Mok

A.E. Elwi

Structural Engineering Report #136

Department of Civil Engineering

University of Alberta

Edmonton, Alberta, Canada

June 1986

ABSTRACT

The shear behaviour of large diameter fabricated steel cylinders is investigated analytically. The analysis is based on a nonlinear geometric finite element formulation coupled with a von Mises elastic-perfectly-plastic material response. The effects of initial imperfections as well as the boundary conditions on the shear behaviour of the cylindrical shells are examined. The development of a tension field in certain cases is also investigated.

The study relies on program NISA "Nonlinear Incremental Structural Analysis", a description of which is included. The analytical stage consists of two parts. The first part involves a numerical analysis of several cylinders with different edge conditions. The second part includes a numerical analysis of the actual problem with radius to thickness ratio (R/t) equal to 250. A series of numerical analyses has been carried out under different edge conditions and magnitudes of initial imperfections.

The objective was to identify the behaviour parameters in shear and the tension field contribution after buckling of the shell had occurred.

An analytical theory which recognizes the tension field contribution to the overall shear strength has been developed. The conclusions drawn from the analytical study are then compared with the existing experimental results of transversely loaded cylindrical shells (R/t = 250).

ACKNOWLEDGEMENTS

This study was made possible by the National Science and Engineering Research Council of Canada Grant No. A5877. Thanks are extended to Dr. G.L. Kulak of the Department of Civil Engineering, University of Alberta for his permission to use Fig. 2.6 and to Nola Shaw for her careful typing of the manuscript.

TABLE OF CONTENTS

Chapter Page

Chapter Page

LIST OF TABLES

LIST OF FIGURES

LIST OF SYMBOLS

a_1 = contribution of the first mode to the intial displacement pattern

A = cross-sectional area of a cylinder

b = axial or circumferential dimension of panel, whichever is smaller (except where noted)

C = compression buckling coefficient for a thin-walled cylinder

D = flexural stiffness of panel per unit length

$= [\frac{Et^3}{12(1-v^2)}]$

E = elastic modulus

E_s = secant modulus

E_t = tangent modulus

f_b = compressive stress on the extreme fiber

f_v = shear stress at the neutral axis

F = critical shear stress coefficient, established by the geometry of panel and type of edge support

$K_{t_1}, K_{t_2}, K_{y_1}, K_{y_2}$ = dimensionless parameters dependent on R/t, E, v, σ_y

K_t, K_{y_s}, K_{y_t} = dimensionless parameters dependent on E, σ_y, R, L, t, v, F

L = length of a cylinder

M = bending moment

P = transverse shear

P_b = actual buckling load

P_{cr} = predicted buckling load according to Batdorf's theory

Q = scaling factor

R = radius of a cylinder

t = cylinder wall thickness or plate thickness

$[T]$ = transformation matrix

U = unevenness factor

$\{v\}, v$ = deviation from the best fit line

Δv = deviation between two imperfection values

V = shear force

V_b = shear strength component from beam action

V_t = shear strength contribution from tension field action

V_u = ultimate shear strength of a cylinder

V_y, V_{ys} = shear yield strength of a cylinder

V_{yt} = tensile yield strength of a cylinder

Z = curvature parameter of a curved panel

α_m = capacity reduction factor for uniform axial compression and pure flexure

γ_s = nondimensional buckling parameter

ζ = angle of inclination of tension field stress

ζ' = angle of inclination of maximum principal stress of combined stress conditions

η = plasticity reduction factor

ν = Poisson's ratio

σ_{cr} = classical elastic buckling stress of a thin-walled cylinder

σ_t = tension field stress

σ_u = nominal stress in the u-direction

σ_v = nominal stress in the v-direction

σ_y = yield stress

σ_{ys} = static yield stress

$\sigma_{u\ell}$ = ultimate buckling stress of a thin-walled cylinder

$[\sigma]$ = stresses in global coordinates system

$[\sigma']$ = stresses in local coordinates system

$[\sigma_{MAX}]$ = stresses at maximum load level

$[\Delta\sigma]$ = difference in stresses at two load levels

τ_{cr} = critical shear stress

τ_{uv} = shear stress in the plane u-v

τ_{xy} = shear stress in the plane x-y

τ_y = shear yield stress

$\{\phi\}$ = eigenvector of the models

ϕ_x, ϕ_y, ϕ_z = the three translational components of the eigenvector

Δ = nondimensional buckling parameter

1. INTRODUCTION

1.1 Large Diameter Fabricated Steel Cylinders

Large diameter fabricated steel cylinders are widely used in many civil engineering structures such as columns, stacks, storage tanks and conveyor galleries. Although most of these structures are susceptible to buckling, structural specifications do not give complete design information on the buckling of these members.

A research program into the behaviour of large diameter fabricated steel cylinders was initiated at the University of Alberta in 1982. Tests on the behaviour of tubular members subjected to axial compression and bending were carried out by Pinkney et al. (1982, 1983), Stephens et al. (1982), and Bailey and Kulak (1984). The shear behaviour of large diameter steel cylinders under transverse loading was also examined (Bailey and Kulak, 1984). This report is a continuation of that work.

In this study, the behaviour of large diameter steel cylinders loaded primarily in shear is investigated. The analytical phase of the study focuses on the effects of initial imperfections, edge conditions, and shell geometry on the critical loads and the load response of the shells.

1.2 Statement of Problem

The shear behaviour of thin cylindrical shells has not been studied until recent years. There are limited sources

of literature on this topic, and the data base is very small at the present time.

For thin cylindrical shells loaded in shear, the problem can be very complicated. Although theories exist for obtaining the shear strength of curved panels and cylinders in pure shear, the additional stresses due to bending are ignored, and the post-buckling strength remains unknown.

Recent tests on the shear loading of large diameter fabricated steel cylinders have been performed by Bailey and Kulak (1984), and the test data for the experiment are available. The purpose of this study is to investigate the shear behaviour of thin cylindrical shells, using in particular the geometry of the shell employed in the experimental work conducted by Bailey and Kulak (1984).

1.3 Objectives

The objectives of this study are:

1. To analyse, in transverse shear, large diameter fabricated steel cylinders with radius-to-thickness ratio of 250.
2. To compare the results of a finite element analysis with previously obtained experimental test results on similar specimens and, where applicable, with classically based theoretical predictions.
3. To investigate the buckling behaviour of transversely loaded cylindrical shells and to

confirm the existence of a tension field after buckling occurs.

4. To develop an ultimate shear strength equation for cylindrical shells loaded in shear.
5. To make recommendations for further testing.

2. LITERATURE REVIEW

2.1 Introduction

This chapter presents a review of previous work done on the buckling of cylindrical shells. First the general instability phenomena of cylindrical shells are discussed, followed by a review of shell buckling under axial compression and bending. Next, previous work done on transversely loaded cylinders is discussed, including a review of the classical solution based on the small-deflection theory, and a review of related experimental studies. The effects of geometric and material imperfections, and boundary conditions on the buckling capacity of the shells are also discussed. This review draws among other sources on the reviews prepared by Stephens et al. (1982).

2.2 Instability Phenomena of Cylindrical Shells

Cylinders are common shell configurations in structural applications. The stability of cylindrical shells can be a very complex problem. However, stability equations for cylindrical shells have been available in the literature since the late 1800s. Earliest solutions for cylinders subjected to axial compression were presented by Lorenz (1911). Solutions for buckling under uniform lateral pressures were given by Southwell (1913, 1914) and by von Mises (1914). In 1932, Flügge presented a comprehensive

treatment of cylindrical shell stability, including combined loading and cylinders subjected to bending. Results for cylinders subjected to torsional loading were given by Schwerin (1925) and Donnell (1933).

Regardless of the mode of failure, elastic shell structures may suffer two classes of instability phenomena (Krätzig et al. 1982, 1983). The first class is the classical or bifurcation buckling (Fig. 2.1a). This type of buckling is characterized by the fact that, as the load passes through its critical stage, a perfect structure passes from its unbuckled equilibrium configuration to an infinitesimally close buckled equilibrium configuration. The point at which this happens is known as the bifurcation point, beyond which there exists more than one physically admissible equilibrium state. The primary path continues beyond the bifurcation point, but equilibrium is unstable in this region. The secondary path, which branches from the primary path, represents the stable buckled equilibrium configuration. Curve A in Fig. 2.1a is the classical eigenvalue problem of shell stability, in which all prebuckling deformations are neglected. If the prebuckling deformations are influential, extended eigenvalue problems have to be solved. This influence may be linear (curve B) or non-linear (curve C). Once the bifurcation points have been found the behaviour of the shell in the postbuckling region has to be investigated (Krätzig et al. 1982, 1983).

The second type of instability phenomena is known as

snap-through buckling (Fig. 2.1b). This phenomenon is characterized by a visible and sudden jump at a constant load from one equilibrium configuration to another equilibrium configuration for which displacements are larger than in the first. This phenomenon is typical for perfect shells under certain load conditions and for shells with imperfection patterns. However, a correct tracing of the non-linear load-displacement path may be insufficient if the shell suffers bifurcation buckling before having reached its limit point (curve D1 in Fig. 2.1b). In this case, a simultaneous eigenvalue analysis has to be carried out (Krätzig et al. 1982, 1983).

Buckling may be further classified as either elastic or inelastic. In the case of elastic buckling, local or overall instability occurs before the material has reached its yield point. In inelastic buckling, some parts of the cross-section may yield before buckling occurs, and the load response of the structure must, therefore, include the yield point of the material.

The early theories developed for stability problems of thin cylindrical shells were restricted to geometrically perfect members, elastic material behaviour, and linear relationships between displacements, strains, and curvatures. Since these classical stability approaches are based on the assumption of infinitesimal displacements, consideration of initial geometric imperfection is thus precluded. This approach has been pursued mainly by

Southwell (1914), Flügge (1932), Donnell (1934), and Timoshenko (1961) on axially loaded cylindrical shells, and by Brasier (1927), Flügge (1932), and Seide and Weingarten (1961) on flexurally loaded cylindrical shells.

2.3 Effect of Geometric Imperfections

Structural systems can never be built precisely as planned and inevitably contain small imperfections associated with geometrical errors and material defects. These imperfections can drastically change the response of the system (Fig. 2.2).

Buckling loads for fabricated steel cylindrical shells are far more difficult to predict than for members manufactured in mills because of the relatively large magnitudes of imperfection and residual stress levels which result from the production process. Moreover, tests have shown that the buckling strength of thin cylindrical steel shells is very sensitive to geometric boundary conditions of the test specimens. The lack of agreement between the predicted values and the tested values have been generally attributed to specimen imperfections (geometric and material) and poorly modelled boundary conditions.

Koiter (1945, 1963) incorporated finite initial imperfections into his general nonlinear stability theory. It is shown that, in general, the larger the initial imperfection, the smaller the buckling load. In his derivation, Koiter initially assumed that the imperfections

were axisymmetric in shape. Tests showed good correlation between theory and experiment. Further investigation by Koiter shows that interaction between axisymmetric and asymmetric imperfections may result in a more pronounced reduction in strength (Fig. 2.3).

Recent studies of the effects of imperfections on the buckling strength, as performed by Arbocz (1974) and Babcock (1974), have shown that it is possible to predict reasonably well the buckling load using numerical techniques applied to single and multiple mode imperfection shapes and to statistically random imperfection amplitudes. Further investigation by Arbocz and Babcock (1976) has progressed to the point where the buckling load can be predicted with considerable accuracy provided that the actual imperfection profiles are mapped and used in the calculation.

Recently, Pinkney et al. (1982, 1983) were able to predict the buckling load of axially loaded cylindrical shells with a good degree of accuracy using the finite element program NISA80 developed by Ramm (1980). In the analysis, a bilinear elastic-perfectly-plastic material response was used, initial imperfections, measured by Stephens et al. (1982), were incorporated and the equilibrium path was traced up to and beyond the limit point. The predictions obtained using this analysis compared closely with the experimental results. It was concluded that the first mode of buckling of the corresponding perfect cylinder, appropriately scaled,

provides a suitable initial configuration for the determination of the limit point. The appropriate scale factor for first mode amplitude corresponds to the largest measured imperfections on any generator of the surface.

2.4 Effect of Boundary Conditions

In recent years, the emphasis in both theoretical and experimental studies on the buckling of thin cylindrical shells has been directed at the effect of geometric imperfections, and has overshadowed the equally important problem of the influence of boundary conditions. Singer and Rosen (1976) report that for stiffened shells, and in particular for closely stiffened shells, the effect of geometric imperfections is less pronounced. Hence the reduction in predicted buckling loads and scatter of test results is less severe, provided the boundary conditions are adequately accounted for. The effect of experimental boundary conditions has also been extensively discussed by Almroth (1965), Hoff and Soong (1964), and Weller et al. (1974). The effects can be separated into two major items. These are the effect of nonlinear prebuckling deformation caused by the end constraint of the test shell, and the effect of end fixity on the buckling load and its associated buckling mode.

The realization of this fact has motivated recent theoretical and experimental studies aimed at better understanding of the influence of boundary conditions and

their more precise assessment.

2.5 Cylinders Under Axial Compression and Bending

As mentioned in section 2.2, earliest attempts on the problems of axially compressed cylindrical shells were mainly done by Southwell (1914), Flügge (1932), Donnell (1934), and Timoshenko (1961). As a result of this work, it was shown that the elastic buckling of axially loaded thin unstiffened cylindrical shells depends on a number of parameters. These include dimensional parameters such as length (L), radius (R), and thickness (t), and material properties such as the modulus of elasticity (E) and Poisson's ratio (ν). Depending on the geometry of the shells, they can be classified as

1. Short cylinders ($L/R < 1.72\ (t/R)^{1/2}$). These buckle in a manner similar to that of axially compressed flat plates and stub columns.
2. Long cylinders ($L/R > 2.85\ (R/t)^{1/2}$). These fail as long columns due to overall instability prior to local buckling.
3. Intermediate cylinders ($1.72(t/R)^{1/2} \leq L/R \leq 2.85\ (R/t)^{1/2}$). These buckle locally in either an axisymmetric mode or an asymmetric mode.

For intermediate cylinders, buckling is independent of length and mode of buckling (Flügge 1932, Timoshenko 1961). For a cylinder with simply supported edges, the classical elastic buckling stress is given as (Timoshenko

and Gere 1961)

$$\sigma_{cr} = CE \frac{t}{R} \tag{2.1}$$

$$\text{where} \quad C = \frac{1}{[3(2 - \nu^2)]^{1/2}} \tag{2.2}$$

In the intermediate to long cylinder transition region, buckling mode interaction may lead to a reduction of the critical buckling stress. Prior to the transition from local to overall buckling which occurs at $L/R \cong 2.85\ (R/t)^{1/2}$, it is possible that the asymmetric local buckling mode will couple with the overall buckling mode resulting in a critical stress as low as 60% of the classical value.

The assumption of elastic material behaviour is valid as long as the buckling stress is below the proportional limit of the material. The modulus of the material, however, becomes a function of the stress level if the stresses are above the proportional limit. In the inelastic range, the decrease in the material modulus causes a decrease in the stiffness of the member and, hence, a corresponding reduction in the buckling strength.

The NASA shell stability design guide (1968) recommends that for inelastic local buckling, the elastic modulus, E, be mulitplied by a plasticity reduction factor, η, to reflect the variation in material stiffness with the stress level. The recommended plasticity reduction factor is given

as

$$\eta = \frac{(E_s E_t)^{1/2}}{E} \tag{2.3}$$

where E_s and E_t are the secant and tangent modulii, respectively.

Experiments performed to verify the predicted values of the classical shell stability theory have shown that the actual buckling strength of thin-walled cylinders is quite different from the buckling strength predicted by the linear theory. For axially loaded cylinders, test results often average 1/2 to 1/3 of the classical value. In addition to lack of agreement with predictions, the test results show large scatter.

Initially the discrepancy between theory and experiment was attributed to test specimen end effects. However refinement of the linear shell buckling theories to account for these effects has shown that boundary conditions have little effect on the buckling strength of intermediate cylinders.

In 1941 von Kármán and Tsien showed, using approximate numerical analysis based on the elastic nonlinear finite-displacement theory by Donnell (1934), that equilibrium states involving large displacements can be maintained at loads far less than the critical bifurcation load obtained from the classical approach.

Initial imperfection of shell geometry was first

introduced into non-linear stability analysis by Koiter (1945). In his work, he was able to predict the maximum load that can be maintained before buckling occurs and relate this load to the size of the imperfection which causes the buckling. The inclusion of initial imperfections not only provides an explanation for buckling at loads less than the classical value, but also helps to account for the large amount of scatter of test results.

In an attempt to reduce the data scatter, Miller (1977) considered a modified form of the nondimensional buckling parameter proposed by Plantema (1946). Miller's parameter is

$$\Delta = \alpha_m \cdot C \frac{Et}{\sigma_y R} \tag{2.4}$$

$$\text{where} \quad \alpha_m = -0.041 - 0.473 \log \left(\frac{UR}{t}\right) \tag{2.5}$$

The classical elastic buckling stress as indicated by Eq. 2.1 is modified by a capacity reduction factor, α_m, based on the approximate imperfection theory of Donnell and Wan (1950). In Eq. 2.5, U is the unevenness factor which reflects the initial level of cylinder wall imperfection (geometric and material), and is considered to depend on the method of construction. Based on the available test data, Miller suggested that the unevenness factor U be 0.0005 for fabricated cylinders. With imperfection accounted for in this manner, a lower bound curve through the data points

represents an empirical equation for the plasticity reduction factor, η, applicable to nonhomogenous, sharp-yielding mild steels. Miller's buckling strength formula is

$$\frac{\sigma_{u\ell}}{\sigma_y} = \eta\ \alpha_m\ C\ \frac{E\ t}{\sigma_y R} \qquad (2.6)$$
$$= \eta\Delta$$

where
$$\eta = 1.0 \qquad \text{for } \Delta \leq 0.55 \qquad (2.7a)$$
$$\eta = \frac{0.45}{\Delta} + 0.18 \qquad \text{for } 0.55 < \Delta < 1.6 \qquad (2.7b)$$
$$\eta = \frac{1.31}{(1 + 1.15\Delta)} \leq \frac{1}{\Delta} \qquad \text{for } \Delta \geq 1.6 \qquad (2.7c)$$

Recently, the American Society of Mechanical Engineers (ASME) adopted a modified form of Miller's formula for their specification on "Metal Containment Shell Buckling Design Method" (1980) which forms an appendix to the ASME Boiler and Pressure Vessel Code. Eq. 2.5 was modified such that

$$\alpha_m = 0.207 \qquad \text{for } 600 \leq \frac{R}{t} \leq 1000 \qquad (2.8a)$$
$$\left.\begin{aligned} \alpha_m &= 1.52 - 0.473 \log\left(\frac{R}{t}\right) \\ \alpha_m &= 300\ \frac{\sigma_y}{E} - 0.033 \end{aligned}\right\} \text{ lesser value} \quad \text{for } \frac{R}{t} < 600 \qquad (2.8b),\ (2.8c)$$

The changes were made strictly to improve the correlation between predicted and test results. In addition, the ASME code restricts the application of their formula, defined by Eqs. 2.6 and 2.8, to cylinders with wall thicknesses not less than 6.35 mm.

Stephens et al. (1982) developed a semi-empirical

design formula, based on their tests and a review of tests by others, for axially compressed structural quality fabricated steel cylindrical shells. It is shown that the observed effect of geometric imperfections on the buckling strength can be approximated by the imperfection theory of Koiter. The local buckling of fabricated steel tubes subjected to uniform compression occurs at a stress considerably less than the classical elastic buckling stress. The semi-empirical formula developed is based on a buckling parameter γ_s, where

$$\gamma_s = (E/\sigma_{ys})^{1/2}(t/R)^{3/2} \tag{2.9}$$

Using this parameter, a series of best fit curves to available test data yields the following equations:

$$\frac{\sigma_{u\ell}}{\sigma_{ys}} = 119.3\ \gamma_s \qquad \gamma_s \leq 0.0036 \tag{2.10}$$

$$\frac{\sigma_{u\ell}}{\sigma_{ys}} = 1.625 + 0.489 \log \gamma_s \qquad 0.0036 < \gamma_s < 0.0527 \tag{2.11}$$

$$\frac{\sigma_{u\ell}}{\sigma_{ys}} = 1.0 \qquad \gamma_s \geq 0.0527 \tag{2.12}$$

More recent studies by Pinkney et al. (1982, 1983) have shown that, using the finite element technique, the equilibrium path of axially loaded cylinders can be traced up to and beyond the limit point. The predicted ultimate stresses are in excellent agreement with those found

experimentally provided initial imperfections are incorporated in the shell geometry.

Extensive work has been done on the bending of cylindrical shells. The classical solution for local buckling of flexurally loaded shells is usually attributed to Flügge (1932). In his analysis, it is shown that the critical stress induced by bending is 30% larger than the classical axial stress given by Eq. 2.1.

Seide and Weingarten (1961) performed a numerical small-displacement analysis of the flexural case which indicated that the flexural buckling stress is approximately equal to the compressive buckling stress. This approximation is also cited by other researchers. Stephens et al. (1982) suggest that a lower bound on the flexural buckling capacity of fabricated steel cylinders can be approximated on the basis of the test results for uniformly compressed cylinders. This can be explained by the fact that the strain gradient present in a flexurally loaded member permits a higher maximum compressive stress than would be the case for a uniformly compressed member. Bailey and Kulak (1984) also performed tests on both unstiffened and longitudinally stiffened cylindrical shells loaded in bending. These tests were designed to add to the data base started by Stephens et al. (1982).

2.6 Cylinders Under Shear Loading

Shear stresses in cylindrical shells can be induced by

torsional or transverse loading. In this study, only shear stresses due to transverse loading are investigated.

The ultimate shear strength of fabricated steel cylinders loaded in transverse shear is governed by many factors. These can be divided into three groups, the specimen geometry, the material properties, and the support and loading conditions. Failure can occur as local instability or subsequent to yielding of material.

Two types of local instability are possible; namely compression buckling and shear buckling, as shown in Fig. 2.4. Compression buckling may occur at regions where the compressive normal stress due to bending exceeds the critical buckling stress. This mode of failure is sensitive to the boundary conditions. Shear buckling may occur in regions where the critical shear stress is exceeded. The critical shear stress depends on the geometric and material properties of the shell and can be dependent on the boundary conditions as well.

When the shell geometry does not lead to local instability, transversely loaded cylinders may fail by yielding of material, which can be shear yielding or tensile yielding. Shear yielding may initiate when the shear stress in the cross-section due to the applied load exceeds the shear yield stress. This type of yielding is common in relatively "thick" cylinders in which local intability is not likely to occur. Tensile yielding can occur in a transversely loaded shell when the tensile stresses

developed in the tension field, if it exists, exceeds the tensile yield stress. This type of material failure is most likely to occur in thin shells with considerable fixity at the supporting edges in order that tension field action may develop (Fig. 2.5).

Little experimental or theoretical work that deals with the shear loading of cylindrical shells can be found in the literature. Theoretical solutions for the critical shear stress of curved rectangular panels have been developed by Batdorf et al. (May, 1947). The solution is based on small-deflection theory for curved panels with simply supported and clamped edges. The critical shear stress is given as

$$\tau_{cr} = K_s \frac{\pi^2 D}{b^2 t} \tag{2.13}$$

where K_s is the critical shear stress coefficient established by the geometry of the panel and the type of the edge supports, D is the flexural stiffness of panel per unit length, b is the smaller of the axial or the circumferential dimension, t is the thickness. K_s is obtained by solving the equation of equilibrium using the Galerkin Method for the case of simply supported conditions. Estimated results are also given for curved rectangular panels having clamped edges. Values of K_s are plotted against a curvature parameter Z given as

$$Z = \frac{b^2}{Rt} \sqrt{1 - \nu^2} \tag{2.14}$$

The curved rectangular panels tested in Batdorf's study have a range of $1 \leq Z \leq 1000$. In the present study, the shells under investigation have a value of $Z \cong 949$.

Lundquist (1932, 1933, 1935) examined the behaviour of thin cylindrical shells under pure torsion, pure bending, and combined transverse shear and bending. In his study on combined transverse shear and bending, it is assumed that ordinary beam theory applies. Hence the compressive stress on the extreme fibre and the shear stress at the neutral axis are, respectively, given by

$$f_b = \frac{M}{\pi R^2 t} \tag{2.15}$$

$$f_v = \frac{V}{\pi R t} \tag{2.16}$$

Eq. 2.15 is divided by Eq. 2.16 to obtain

$$\frac{f_b}{f_v} = \frac{M}{RV} \tag{2.17}$$

The nondimensional term in Eq. 2.17 is descriptive of the loading condition since it is clear, from purely physical considerations, that the shear V and the moment M relative to the size of the cylinder should be considered in the analysis of the test results.

Lundquist has shown that for large values of $\frac{M}{RV}$ $\left(3 \leq \frac{M}{RV} < 12\right)$, failure occurs in bending by a sudden

collapse of the outermost compression fibers in the same manner as in the pure-bending tests. The stress on the extreme fiber, calculated by the ordinary beam theory, and the size of the buckles are both equal to their respective values for a cylinder of the same dimensions in pure bending. It is, therefore, reasonable to suppose that at these M/RV values the bending strength of a thin-walled cylinder should approach the strength of a cylinder of the same dimensions in pure bending.

For small values of $\frac{M}{RV}$, $\left(0 \leqslant \frac{M}{RV} < 2\right)$, failure occurs in shear by the formation of diagonal buckles on the sides of the cylinder. The size and form of the buckles at failure are the same as those that occur at failure for a cylinder of the same dimensions in torsion. As M/RV approaches zero, the shearing stress on the neutral axis at failure, calculated by the ordinary beam theory, is approximately 1.25 times the allowable shearing stress in torsion. This is logical since there is a stress gradient effect in transverse shear which is absent in torsional shear.

At intermediate values of M/RV, there is a transition from failure by bending to failure by shear that is accompanied by a reduction in strength. A chart is developed (Lundquist, 1935), to allow for the reduction in strength for use in calculating the strength of thin-walled cylinders in combined transverse shear and bending.

Wilson and Olsen (1941) performed an extensive study on

cylindrical shells subjected to a variety of loading conditions, including axial compression, transverse shear, bending, and combined loading. Schilling (1965) has also conducted a considerable number of local buckling tests on tubes under combined loading conditions. He suggested that for elastic buckling, the critical shear stress in transverse shear be taken as 1.25 times the critical shear stress in torsion. In the inelastic case, it is conservative to assume that the critical shear stresses are the same for transverse shear and torsion.

Recently, Bailey and Kulak (1984) performed some tests on cylindrical shells loaded in transverse shear. In the experiment, two cylindrical shells were tested. The shear specimens consisted of a cylinder with fixed ends, loaded in the centre, with two thinner portions in the regions of minimum moment. The thinner sections were intended to fail in shear, and measurements of imperfections were concentrated in these areas. It was observed that the first shear specimen, with an R/t ratio of 251, failed as a consequence of a series of inclined buckles forming in the shear spans followed by compression buckles in the extreme fibres. The shear buckles were all at about the same angle, 25°, relative to the longitudinal axis, and approximately symmetric about both the longitudinal axis and the centre of the specimen. Buckles due to compressive longitudinal stresses were also observed in the compression region of the thinner section. Fig. 2.6 shows the buckled specimen.

It is suggested by Bailey and Kulak that tension field action develops after the shell buckles, and that the total shear capacity consists of two portions, namely the 'beam action' shear and the 'tension field action' shear. They suggest that a form of the relationship might be

$$V_u = K_{t_1} V_t \qquad \text{(high R/t ratio)} \qquad (2.18)$$

$$V_u = K_{y_1} V_y + K_{t_2} V_t \qquad \text{(intermediate R/t ratio)} \qquad (2.19)$$

$$V_u = K_{y_2} V_y \qquad \text{(low R/t ratio)} \qquad (2.20)$$

where K_{t_1}, K_{t_2}, K_{y_1} and K_{y_2} are dimensionless parameters which depend on R/t, E, ν and σ_y.

In conclusion, Bailey and Kulak noted that the R/t ratio is an important factor in determining the failure mode of a shell loaded in transverse shear. For a given yield strength, shells with a low R/t ratio are expected to fail as a consequence of yielding, while those with a high R/t value may buckle long before yielding occurs. Also, the contribution of the tension field to the shear strength of a cylinder increases as the R/t of the shell increases.

2.7 Post-Buckling Behaviour

As discussed in the previous section, tension field action may exist after buckling occurs in a transversely loaded cylindrical shell. One type of structural member that is often loaded primarily in shear is the plate girder. In North American Practice the shear strength of

plate girders is usually obtained using a tension field theory in the form developed by Basler (1961). This theory recognizes the fact that after a plate loaded in shear buckles, the load-carrying mechanism changes, showing significant post-buckling strength. The theory suggests that the shear strength consists of both buckling and post-buckling contributions. Prior to buckling, shear capacity is due to beam action, while after buckling shear resistance results from the formation of a tension field in the web. In stiffened plate girders, this field forms diagonally between vertical stiffeners. The analogous part of the cylindrical shell would be a ring stiffener or support which acts as reaction points for the field. Adaptation of this theory to other structural systems loaded mainly in shear has been attempted with considerable success. Thornburn et al. (1983) and Timler and Kulak (1983) investigated the behaviour of steel plate shear walls under lateral loads which might result from the action of wind or seismic forces. Good correlation between predicted values based on a tension field assumption and actual values was obtained.

Although no such theory for transversely loaded cylinders has been found in the literature, it may be possible to adapt the tension field theory to the analysis in this study.

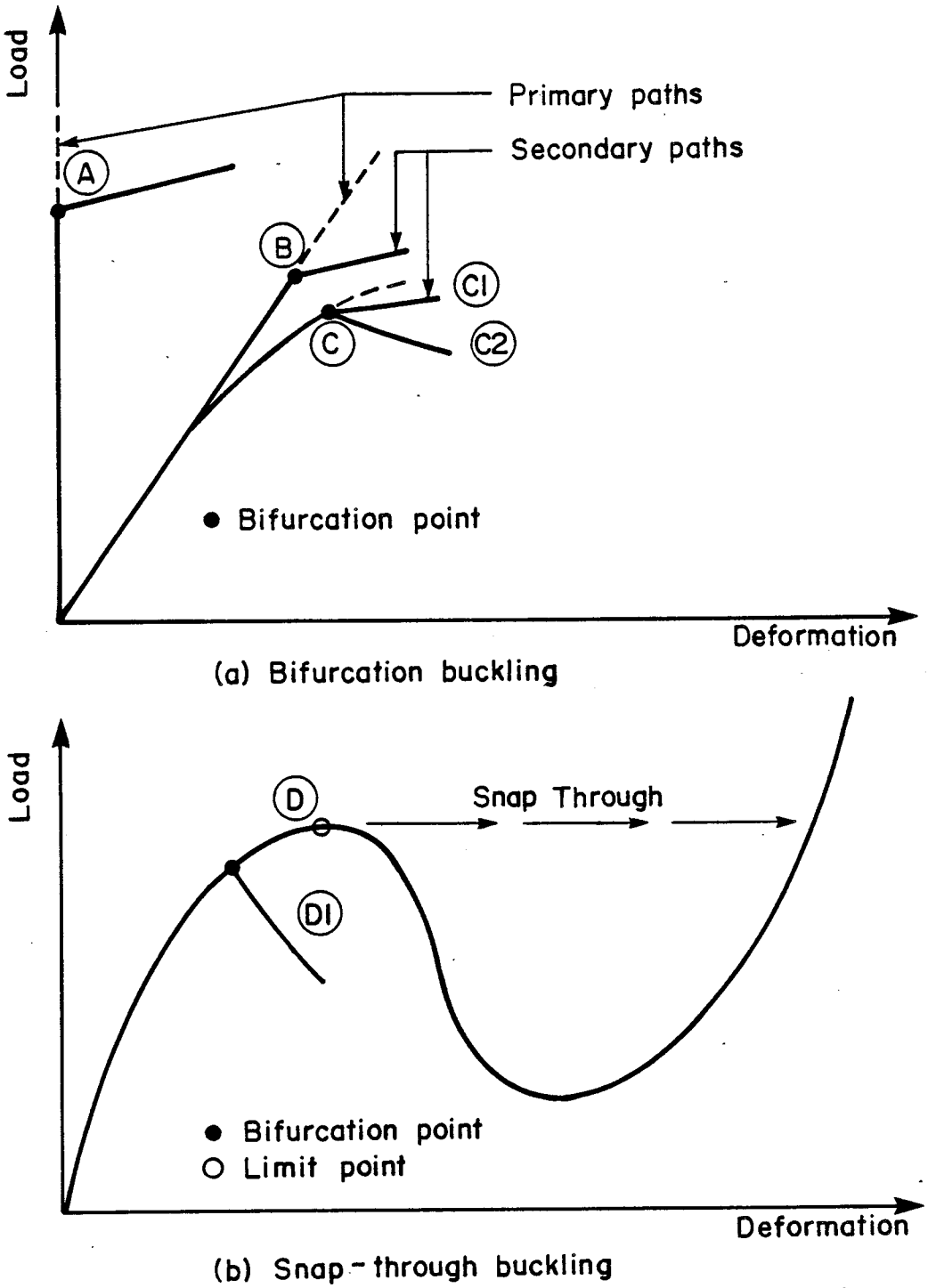

Figure 2.1 Buckling Phenomena of Shell Structures

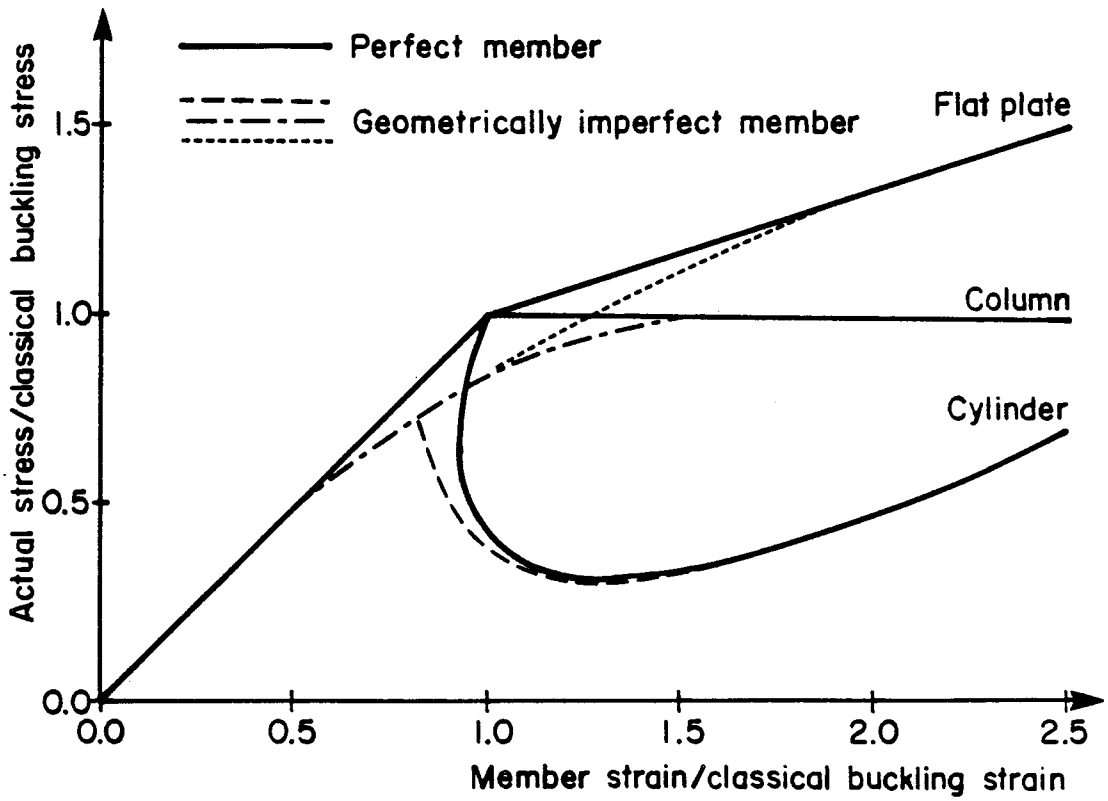

Figure 2.2 Effect of Geometric Imperfections on Load Response in Axially Loaded Structures

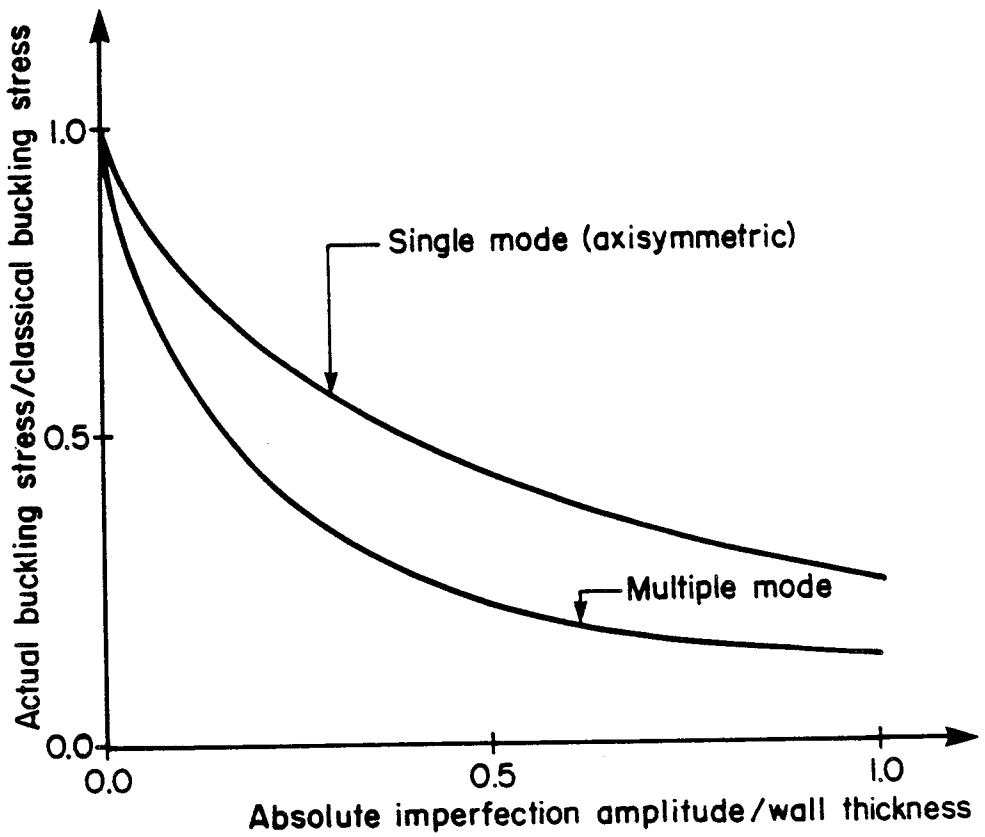

Figure 2.3 Effect of Single and Multiple Mode Imperfections on the Buckling Strength of Thin-Walled Cylinders Under Axial Load

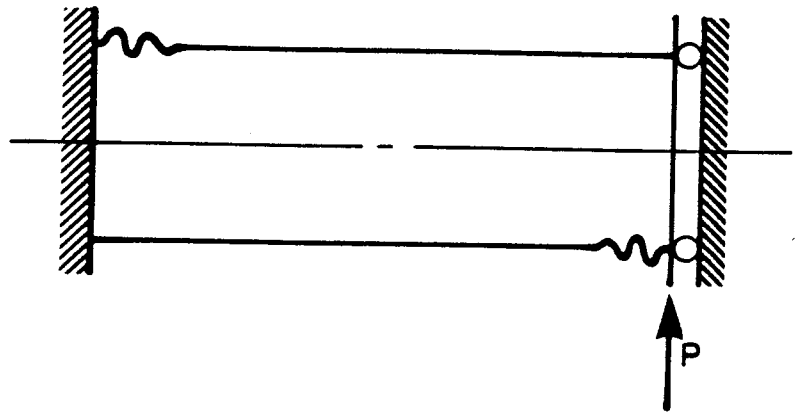

(a) Flexural buckling

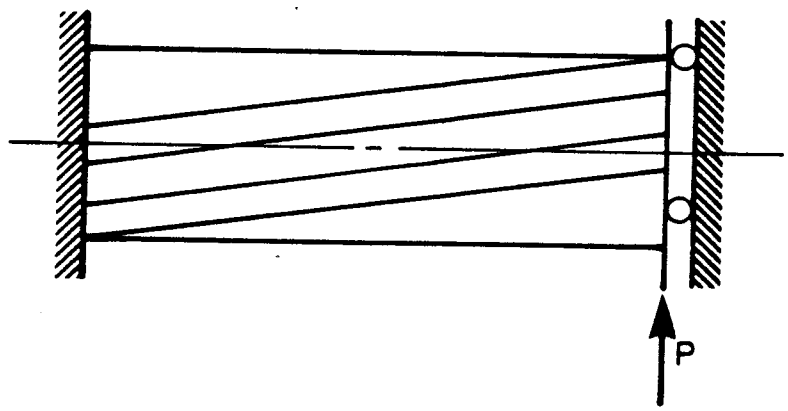

(b) Shear buckling

Figure 2.4 Types of Local Instability of Transversely Loaded Shells

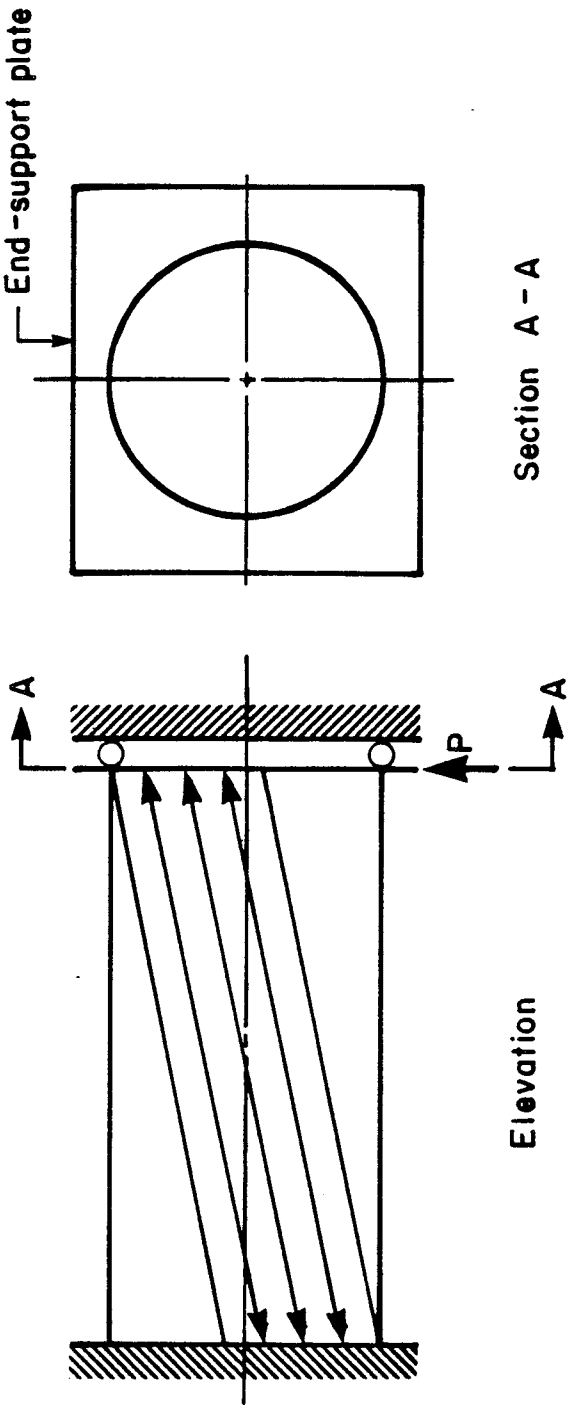

Figure 2.5 Tension Field Action of a Shell Buckled in Shear Mode

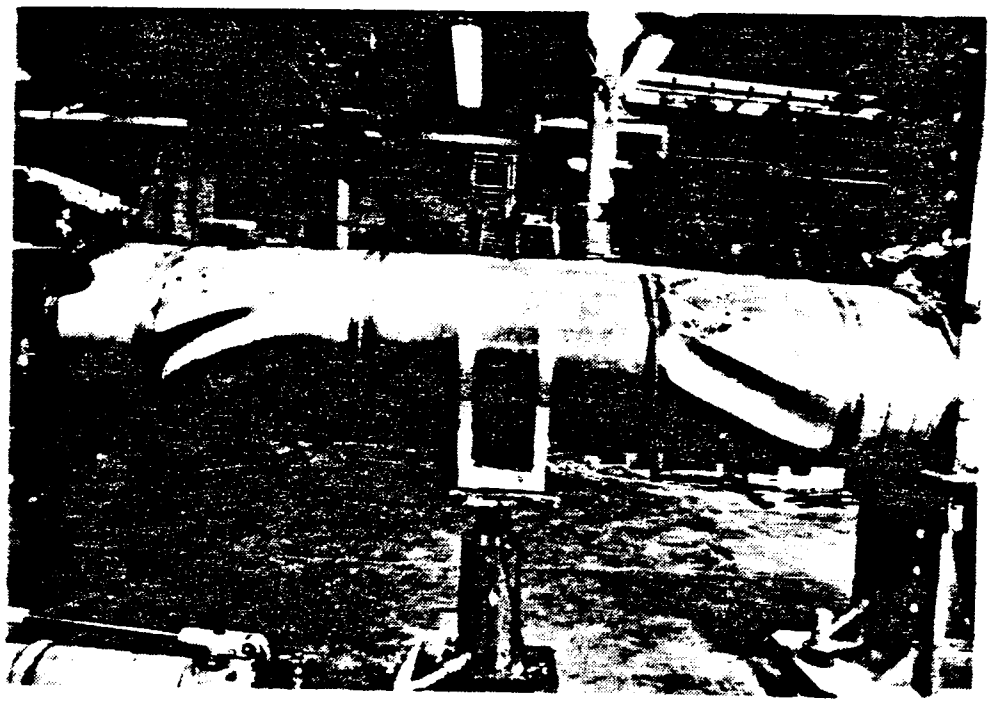

(a) East Face

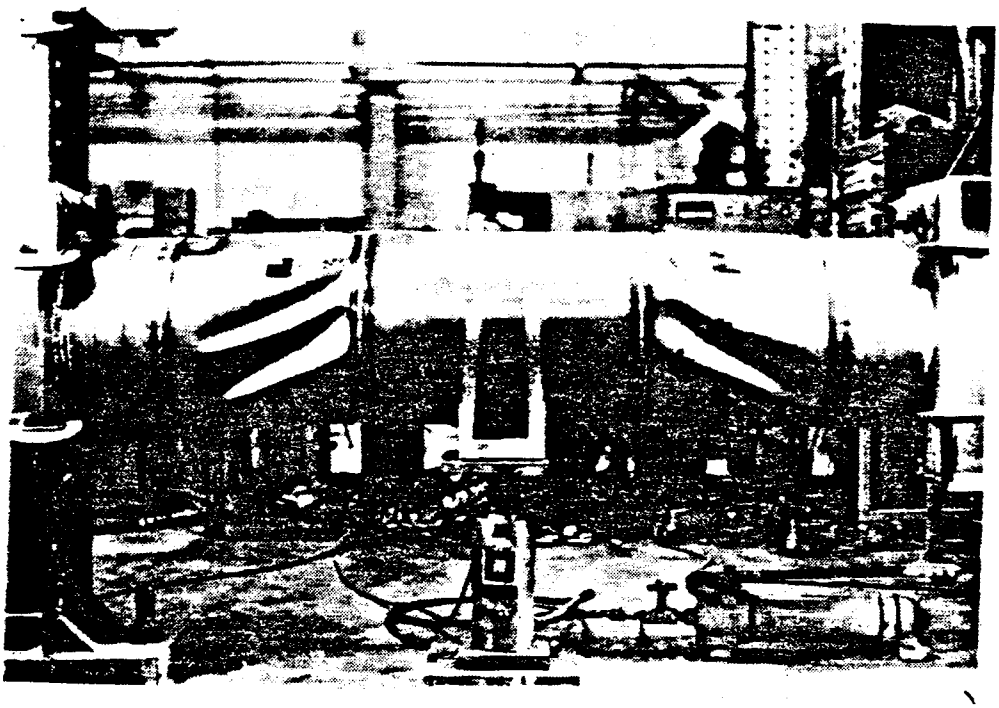

(b) West Face

Figure 2.6 Buckled Shape of Bailey's First Shear Specimen (After Bailey and Kulak)

3. PRELIMINARY INVESTIGATION

3.1 Introduction

As mentioned in section 2.6, Bailey and Kulak (1984) performed two tests on the transverse loading of thin cylindrical shells. Both shells showed an inclined buckling pattern. However, only the first specimen (R/t = 251) is dealt with in this study. The second specimen (R/t = 78) falls outside the scope of this work. It was found that the first shear specimen (R/t = 251) buckled in an inclined pattern at an angle of 24° to the horizontal (see Figure 2.6). It was suggested that the buckling pattern obtained may depend on the experimental set-up and the boundary conditions.

The objective of this preliminary study is twofold. First, it is necessary to find out the effect of the experimental set-up and support conditions on the buckling pattern of the shell. Second, it is desirable to carry out the linear buckling analysis for a series of shells in order that the modal shapes obtained from these analyses can be used as the basis for the initial geometric imperfections for the shells in the next stage of the analysis.

3.2 Basis of Analysis

The main thrust of this study is to theoretically investigate the shear buckling behaviour of thin-walled fabricated steel cylinders. Two approaches may be

adopted. An attempt may be made to obtain a closed form solution, or the problem may be investigated numerically. However, the complexity of the problem may render the first approach untenable. On the other hand, the finite element method (Zienkiewicz 1977; Cook 1981; Bathe 1982) has been developed to a great degree of sophistication as a numerical analysis tool. Such variables as geometric nonlinearities, material models and geometric imperfections are readily accommodated in a finite element analysis. Therefore, the finite element technique is adopted as the basis of this study. In particular, Program NISA80 (Ramm, 1980), which emphasizes stability problems, has been chosen as a numerical analysis tool.

3.3 General Description of Program NISA80

The nonlinear incremental structural analysis program NISA80 (Ramm, 1980) is a finite element code encompassing small displacement formulation as well as large displacement, large strain, total Lagrangian formulation and large displacement, small strain, updated Lagrangian formulation. The program accommodates elastic and elastic-plastic strain hardening material models. The range of elements represented includes truss, beam, two-dimensional plane stress, plane strain axisymmetric, three-dimensional solid and doubly curved shell elements. In addition, the program performs eigenvalue analysis on nonlinear element groups. The program employs a skyline type equation-solver

(Everstine, 1979). A variety of incremental solution strategies are made available. These include the standard and modified Newton-Raphson strategies (Zienkiewicz and Irons 1970; Webster 1980; Cook 1981) as well as the so-called Riks-Wempner or constant-arc-length technique (Wempner 1971; Riks 1979; Crisfield 1980; Ramm 1980). The Newton-Raphson iteration methods often fail in the neighborhood of critical points. The stiffness matrix approaches singularity, requiring an increasing number of iterations and even smaller load steps, and the solution finally diverges. The Riks-Wempner method is a relatively recent solution strategy designed to overcome these problems and to trace the load response beyond the critical points.

Several investigators (Brendel et al. 1981; Ramm 1980) have used the NISA80 code in association with stability oriented problems. In particular Pinkney et al. (1982, 1983) used the program to theoretically investigate the behaviour of axially compressed cylinders. In addition the Pinkney group at the University of Manitoba, has recently concluded a theoretical investigation of buckling under pure bending using the same program.

3.4 Preliminary Analysis

3.4.1 Series A

The objective of series A is to investigate the effects of the experimental set-up and support conditions on the buckling pattern of the shell.

Series A consists of three identical geometrically perfect cylindrical shells (R/t = 250) of 808.5 mm length. The shells have a mid-surface radius of 190 mm and a constant thickness of 0.76 mm throughout. These dimensions are similar in outline to the Bailey and Kulak (1984) first shear specimen. The configuration of the models is shown in Fig. 3.1.

Model A1 is designed to simulate a "fixed-end" problem loaded in shear with unrestrained vertical and horizontal translations at the loading edge (Fig. 3.2a). In order to prevent premature local failure, the loading edge is stiffened by coupling the vertical translations (Z-displacements) of all the nodes on this face. Model A2 is a "free-cantilever" problem loaded in bending (Fig. 3.2b). The y-rotations of all nodes on the loading edge are coupled so that the loading edge remains perpendicular to the longitudinal axis of the deflected shell. Model A3 is also designed as a 'free-cantilever" problem but loaded in shear (Fig. 3.2C). The loading edge is stiffened by nine vertical truss elements. The y-rotations of all the nodes on the loading edge are coupled as well. Details of the boundary conditions for the three models are listed in Table 3.1. The material and geometric properties are given in Table 3.2.

In the present analysis, a 6 x 6 uniform mesh with 36 bicubic 16-node Lagrangian 3-D degenerated plate-shell elements is employed for each of the three models. A 3 x 3

Gaussian integration scheme is adopted in the plane of each element. Integration in the thickness direction is based on a 3-point gauss rule. An elastic isotropic material model is used. Eigenvalue analysis is carried out using the subspace iteration technique (Bathe 1982) on each model.

In models A1 and A3, transverse load is applied in the vertical direction (Z-direction) at all the nodal points on the loading edge in order to produce similar loading effects as in the case of uniform transverse shear. In model A2, horizontal coupled forces are applied at all nodes above and below the neutral axis of the loading edge to simulate an external moment. The loading conditions and the finite element meshes used for the three models are shown in Fig. 3.3.

The analysis of series A shows that the linear buckling load for model A1 is 16.76 kN. Based on Batdorf's small displacement theory for curved rectangular panels, the critical loads for the simply-support and clamped-edge cases are 17.77 kN and 18.21 kN respectively. Good agreement exists between the results from the finite element analysis and Batdorf's theory. For model A2, the linear buckling load is equivalent to a single external moment of 131 N.m. The linear buckling load for model A3 is 19.87 kN. No comparison is made to the predicted values based on Batdorf's equation since it does not apply to a "free-cantilever" problem.

The first buckling modes of the three models are shown

in Fig. 3.4. Diagonal buckles are found in model A1, similar to those obtained in Bailey and Kulak's first shear specimen. Model A1, however, has a constant thickness throughout the longitudinal direction, compared to the varying thicknesses in the three spans of Bailey and Kulak's test specimen. Hence, it is concluded that the diagonal shear buckles obtained in Bailey and Kulak's experiment are not a result of the experimental set-up. In model A2 no diagonal buckles are found. Instead, a compression buckling mode appears to take place.

In model A3, a combination of the diagonal shear buckling mode and the compression buckling mode is predicted instead of a pure shear buckling pattern. It is concluded, from the above observations, that the diagonal shear buckling mode depends on the loading conditions as well as the boundary conditions.

3.4.2 Series B

The objective of series B is to generate, from the linear buckling analyses, the first buckling modes for a series of shells in order that the modal shapes obtained can be used in the preparation of initial geometric imperfections for the shells in the next stage of the analysis. In this series the models closely approximate the geometry and the thicknesses of the Bailey and Kulak (1984) first specimen.

Series B consists of four geometrically perfect

cylindrical shells with varying thicknesses in the longitudinal direction. The shells are 808.5 mm long and have a mid-surface radius of 190 mm. Each model is made up of two end spans and a test span. The term "span" refers to a length of the cylinder with a constant thickness. The test spans are the cylinder sections with smaller thicknesses. The test span, which is the "thinner" section with a thickness of 0.76 mm, has a radius to thickness ratio of 250 and is intended to fail first. The two end spans are twice as thick as the test span. Models B1 and B2 have the same configuration while models B3 and B4 are identical in geometry. The configurations of the models are shown in Fig. 3.5.

Model B1 is designed to simulate a "fixed-end" problem with unrestrained vertical translations but restrained horizontal movement at the loading edge (Fig. 3.6a). The loading edge is stiffened by coupling the vertical translations of all the nodes on this face in order to prevent premature local failure.

Model B2 provides a "free-cantilever" condition (Fig. 3.6b). The loading edge is stiffened by coupling the y-rotation of all the nodes on the loading edge. Model B3 and model B4 simulate "fixed-end" conditions with restrained and unrestrained horizontal translations respectively (Fig. 3.6c and 3.6d). For these two models, the loading edge is 72.5 mm from the far end and is stiffened by coupling the vertical translations of the nodes on the loading edge.

Table 3.3 shows the details of the boundary conditions for the four models. The material and geometric properties are listed in Table 3.4.

In the present analysis, a 6 x 6 uniform mesh is employed for models B1 and B2 while a nonuniform 6 x 6 mesh is adopted for models B3 and B4. In both cases, thirty-six bicubic 16-node Lagrangian 3-D degenerated plate-shell elements are used for each model. A 3 x 3 Gaussian integration scheme is employed in the plane of each element. Integration in the thickness direction is based on a 3-point Gauss rule. An elastic isotropic material model is used. Eigenvalue analysis is carried out using the subspace iteration technique (Bathe 1982) on each model.

For all models except B2, transverse load is applied in the vertical direction at all nodes on the loading edge. Model B2 is intended to generate the bending buckling mode. For this model, horizontal coupled forces are applied above and below the neutral axis on the loading edge in order to produce the similar loading effect as in the case for pure bending. The loading conditions and the finite element meshes used are shown in Fig. 3.7 for models B1 and B2 and in Fig. 3.8 for models B3 and B4.

The analysis shows that the linear buckling loads are 33.4 kN, 34.4 kN and 34.3 kN for models B1, B3 and B4 respectively. Model B2 is not included since it is loaded in a different manner. Using Batdorf's classical equation for curved rectangular panels, the critical loads for the

simply-supported and clamped-edge cases for models B1, B3 and B4 are calculated. They are 30.4 kN and 32.4 kN for model B1, 32.1 kN and 33.1 kN for models B3 and B4 respectively. Table 3.5 shows these values and indicates that there is good agreement between the results from the finite element analysis and Batdorf's equation.

The first buckling modes obtained from the linear buckling analyses for models B1, B3 and B4 are shown in Fig. 3.9. All three modes exhibit the chracteristic diagonal buckling pattern similar to that obtained in Bailey and Kulak's first specimen. The angle of inclination of the buckles with respect to the horizontal falls in the range of 15° to 20°.

Fig. 3.10 shows the first buckling mode for model B2 which was loaded differently and was intended to generate the bending buckling mode. This buckling mode, along with the shear buckling modes obtained in models B1, B3 and B4, are subsequently used in preparing the initial geometric imperfections for the shells.

3.5 Initial Geometric Imperfections

As mentioned in Chapter 2, it is possible to predict, reasonably well, the buckling load using single and multiple mode imperfection shapes scaled to statistically random imperfection amplitudes. Even better results can be obtained if the actual imperfection profiles are mapped and used in the calculation.

In the experimental work carried out by Bailey and Kulak (1984), extensive geometric imperfection measurements were taken for the first shear specimen. The actual imperfection profiles at different sections of the shell are shown in Fig. 3.11. The initial imperfections were measured, relative to an arbitrary datum, along each of the 32 circumferential generators, at 41 longitudinal locations for a total of 1312 measurements.

In order to correlate the prediction of ultimate strength with that obtained experimentally it is necessary to incorporate the actual (measured) imperfections into the analysis. Arbocz (1982) presents a good discussion on how initial imperfection measurements on full scale structures can be used effectively to develop improved design criteria. In the present study, a rational technique for using measured imperfections to obtain effective initial imperfections for use in the analysis is adapted from the work by Pinkney et al. (1982, 1983).

In the present analysis, only the initial geometric imperfections in the test spans are considered since the effects on the buckling load are more pronounced in these "thinner" regions. Based on the measurements by Bailey and Kulak, a straight line was fitted to each of the 32 circumferential sets of observations in each of the two test spans by the method of least squares. The straight line obtained was assumed to be a generator of the corresponding perfect shell for the test span. The deviation of each

measured value from the line was assumed to be the initial deflection at the observation point. The magnitudes of the initial imperfections are as given in Tables 3.6 and 3.7. Fig. 3.12 defines v and Δv. Tables 3.6 and 3.7 show the mean absolute and root-mean-square initial imperfections defined as follows.

$$|v|_{mean} = \frac{1}{n} \sum_{i=1}^{n} |v| \tag{3.1}$$

and

$$v_{RMS} = \left[\frac{1}{n} \sum_{i=1}^{n} v_i^2\right]^{1/2} \tag{3.2}$$

It is necessary to estimate the magnitude of the first mode of buckling that would result in the same ultimate load as the true initial shell imperfections. For this, the initial imperfections may be described in terms of the modal shapes as

$$\{v\} = \sum_{i=1}^{n} a_1 \{\phi_i\} \tag{3.3}$$

Using the orthogonality rule (Clough and Penzien 1975), the contribution of the first mode is given as

$$a_1 = \frac{\{\phi\}_1^T \{v\}}{\{\phi_1\}^T \{\phi_1\}} \tag{3.4}$$

Noting that only radial translations are measured, the

vector $\{\phi_i\}$ of Eq. 3.3 is adapted as

$$\{\phi_i\} = \{(\phi_x^2 + \phi_y^2 + \phi_z^2)^{1/2}\}_i \qquad (3.5)$$

Although this vector is not strictly radial, it is approximately so.

The second problem (the initial geometric imperfections are measured at locations different from the nodal points of the finite element model) makes it necessary to interpolate between observations in the longitudinal direction in order to obtain an initial displacement vector {v} of the same order as the eigenvectors $\{\phi\}_i$. No interpolation is made in the circumferential direction since the observation points are very close, although not exactly, to the nodal points in this direction. It is assumed that the effect due to this approximation is negligible.

The third problem is solved by searching all available sets of measurements against Eq. 3.4 for a maximum value to be used as a scaling factor for the eigenvectors.

For test span 1 of Bailey and Kulak's specimens, twelve longitudinal measurements are available at each of the thirty-two circumferential generators. Each generator is fitted to a polynomial of degree twelve. For test span 2, a polynomial of degree fourteen is used since fourteen longitudinal measurements are available at each generator. After the polynomials are established, coordinates of the nodal points are fed in, and the initial displacement

vectors {v} at the nodal points are thus obtained. The vectors {v} are now of the same order as the restricted eigenvectors $\{\phi\}_i$.

Using Eq. 3.4, the first-mode component a_1 is extracted from the interpolated initial displacement at all generators in each test span for each model. Setting n equal to 1 in Eq. 3.3 and using the values of a_1, the sets of eigenvectors {v}, appropriately scaled by a_1, are generated. These eigenvectors {v} are then quantified as before. Tables 3.8 and 3.9 compare the experimental imperfection measurements with those resulting from the above analysis for test span 1 and test span 2 respectively.

It can be seen that there is little agreement between the scaled mode-1 imperfection measures and the experimental measures. It is interesting to note that the location of the maximum scaled mode-1 imperfection does not necessarily correspond to the location for the maximum experimental measurement. Also, the scaled mode-1 imperfection values obtained from test span 1 are relatively higher than those obtained from test span 2. Hence, it is suggested that the values from test span 1 be used to determine the effective initial imperfections.

From Table 3.8, the maximum scaled mode-1 imperfection values are 1.400 mm, 1.890 mm, 1.390 mm and 1.910 mm, and the average values are found to be 1.080 mm, 1.393 mm, 1.136 mm and 1.450 mm for models B1, B2, B3 and B4 respectively. These values lie between one and a half to three times the

thickness in the test spans. Hence, it is recommended that the maximum scaled mode-1 imperfection value be twice the thickness in the test spans.

In order to study the effect of initial imperfection on the buckling strength of the shells, different scaled mode-1 imperfection values are used for the models in later analysis. These imperfections are superimposed onto the perfect shell geometry.

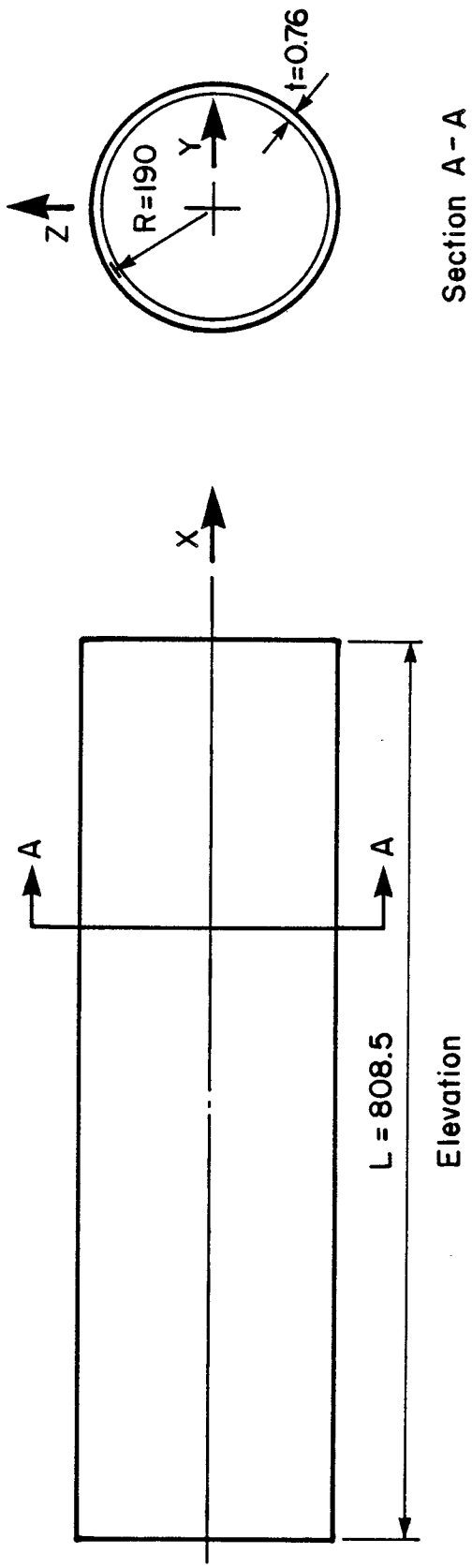

Figure 3.1 Configuration of Models in Series A

(a) MODEL A1: Fixed-end problem

(b) MODEL A2: Free-cantilever problem

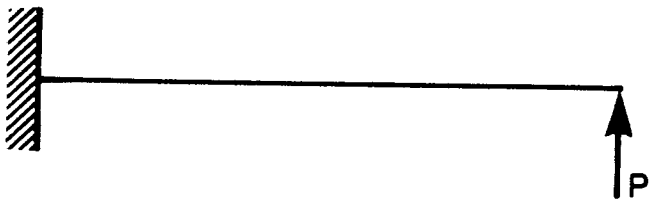

(c) MODEL A3: Free-cantilever problem

Figure 3.2 End Conditions of Models in Series A

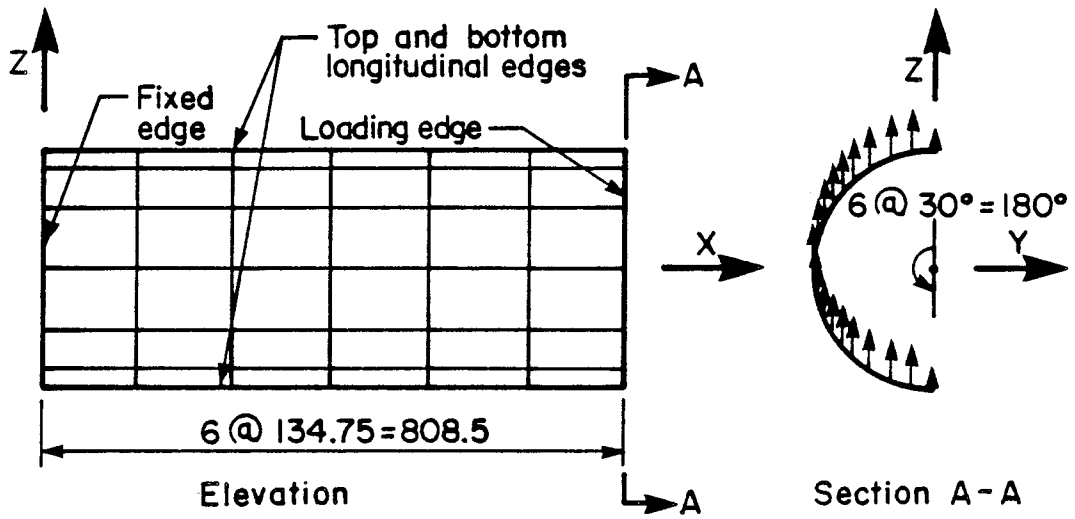

(a) MODELS A1 and A3

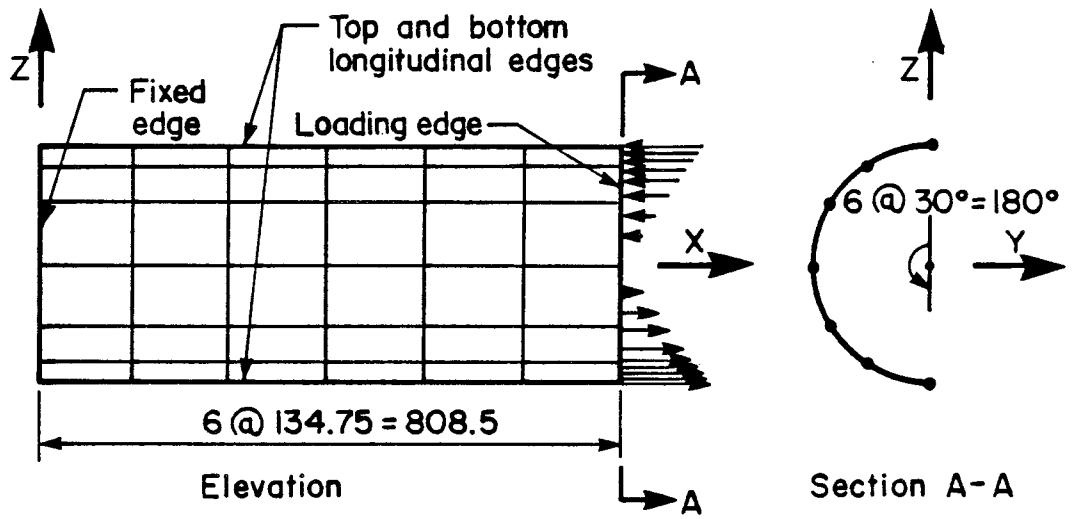

(b) MODEL A2

Figure 3.3 Uniform 6x6 Finite Element Meshes and Loading Conditions of Models in Series A

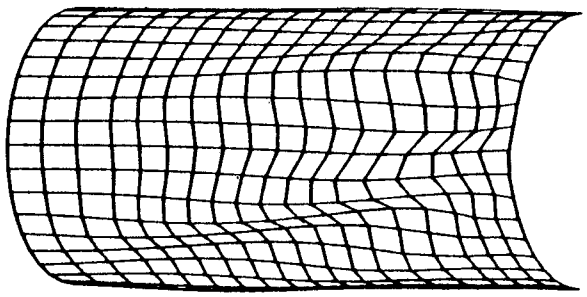

(a) Model A1

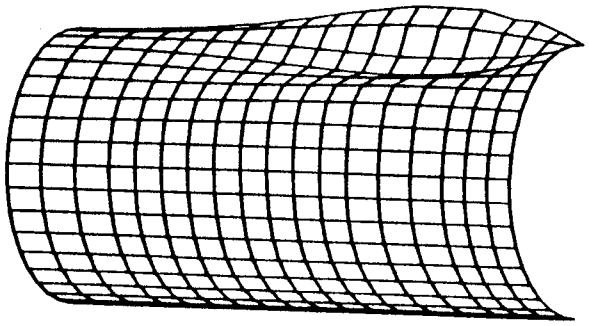

(b) Model A2

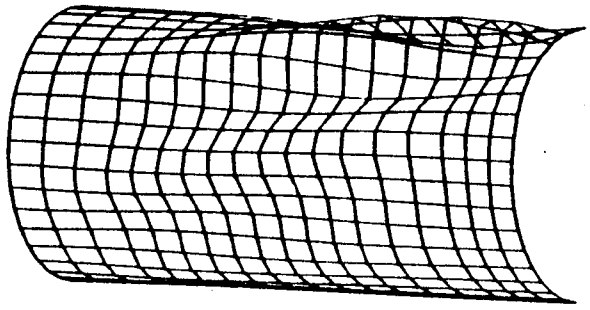

(c) Model A3

Figure 3.4 First Buckling Modes of Models in Series A

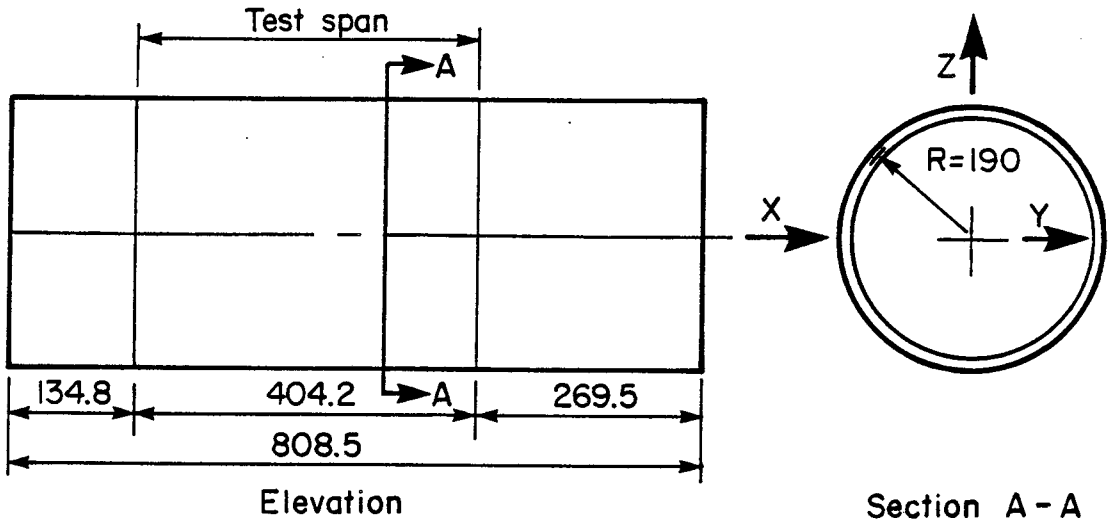

(a) MODELS B1 and B2

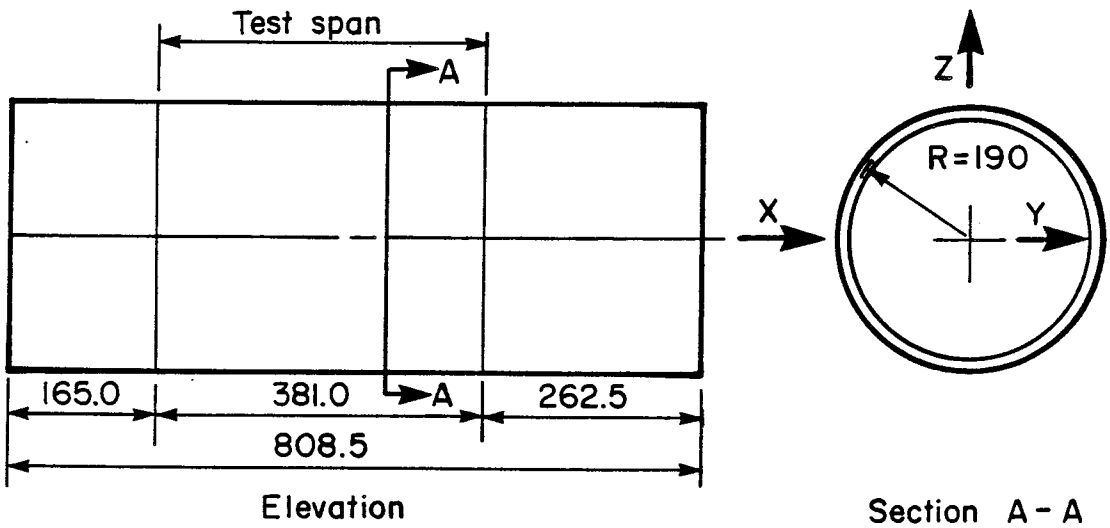

(b) MODELS B3 and B4

Test span : t = 0.76 mm
Other span : t = 1.52 mm
R = Radius of mid-surface (all spans)

Figure 3.5 Configurations of Models in Series B

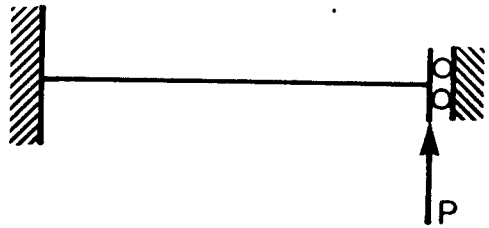

(a) MODEL B1 : Fixed-end problem

(b) MODEL B2 : Free-cantilever problem

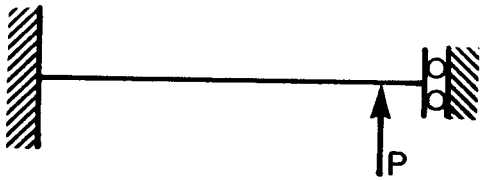

(c) MODEL B3 : Fixed-end problem

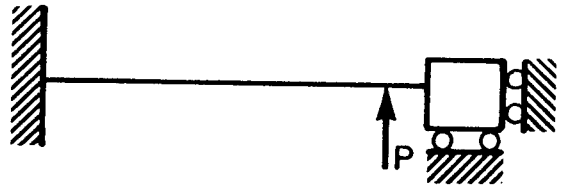

(d) MODEL B4 : Fixed-end problem

Figure 3.6 End Conditions of Models in Series B

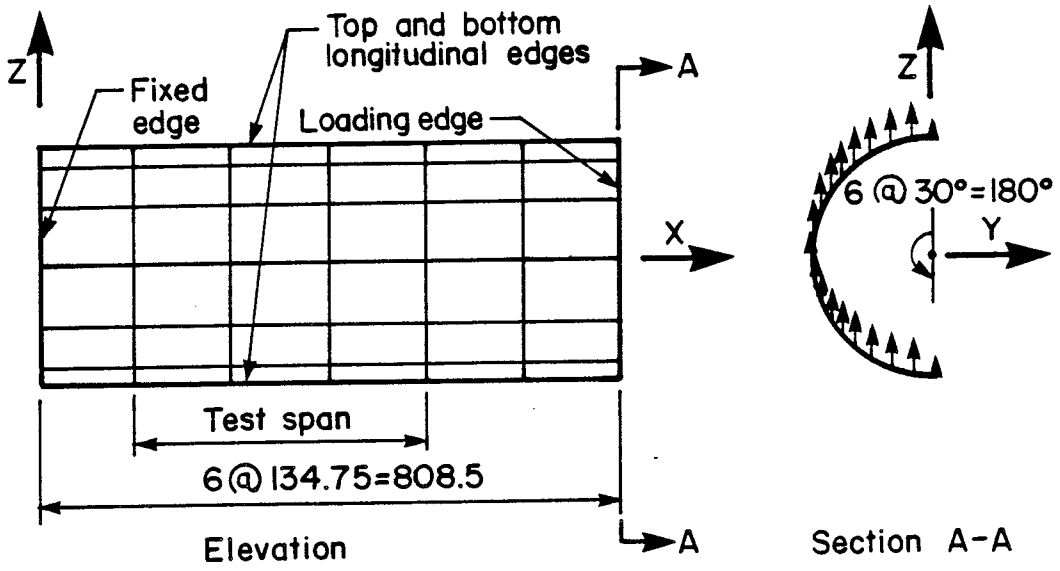

(a) MODEL B1

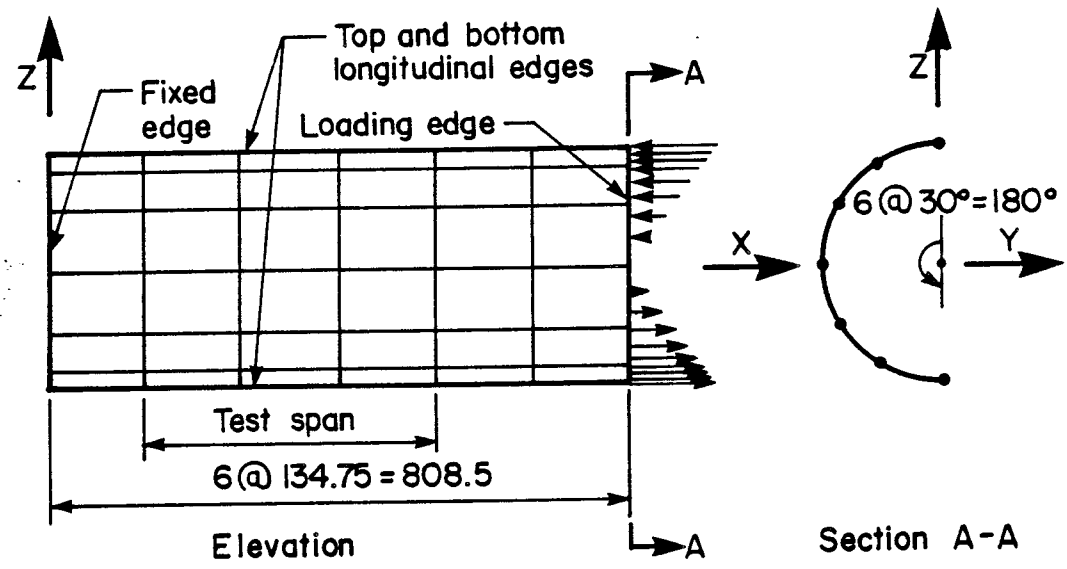

(b) MODEL B2

Figure 3.7 Uniform 6x6 Finite Element Meshes and Loading Conditions of Models B1 and B2 in Series B

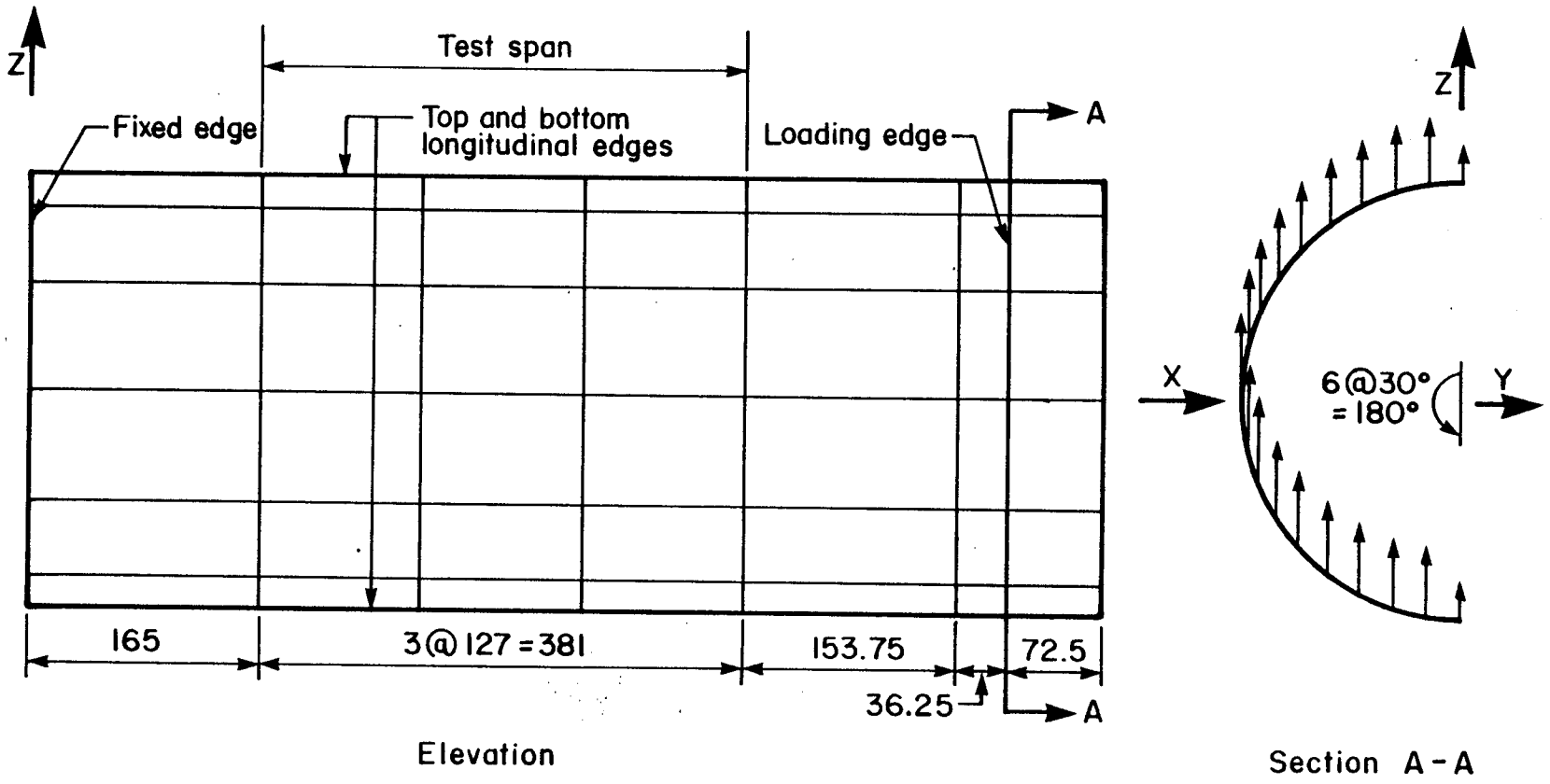

Figure 3.8 Nonuniform 6x6 Finite Element Meshes and Loading Conditions of Models B3 and B4 in Series B

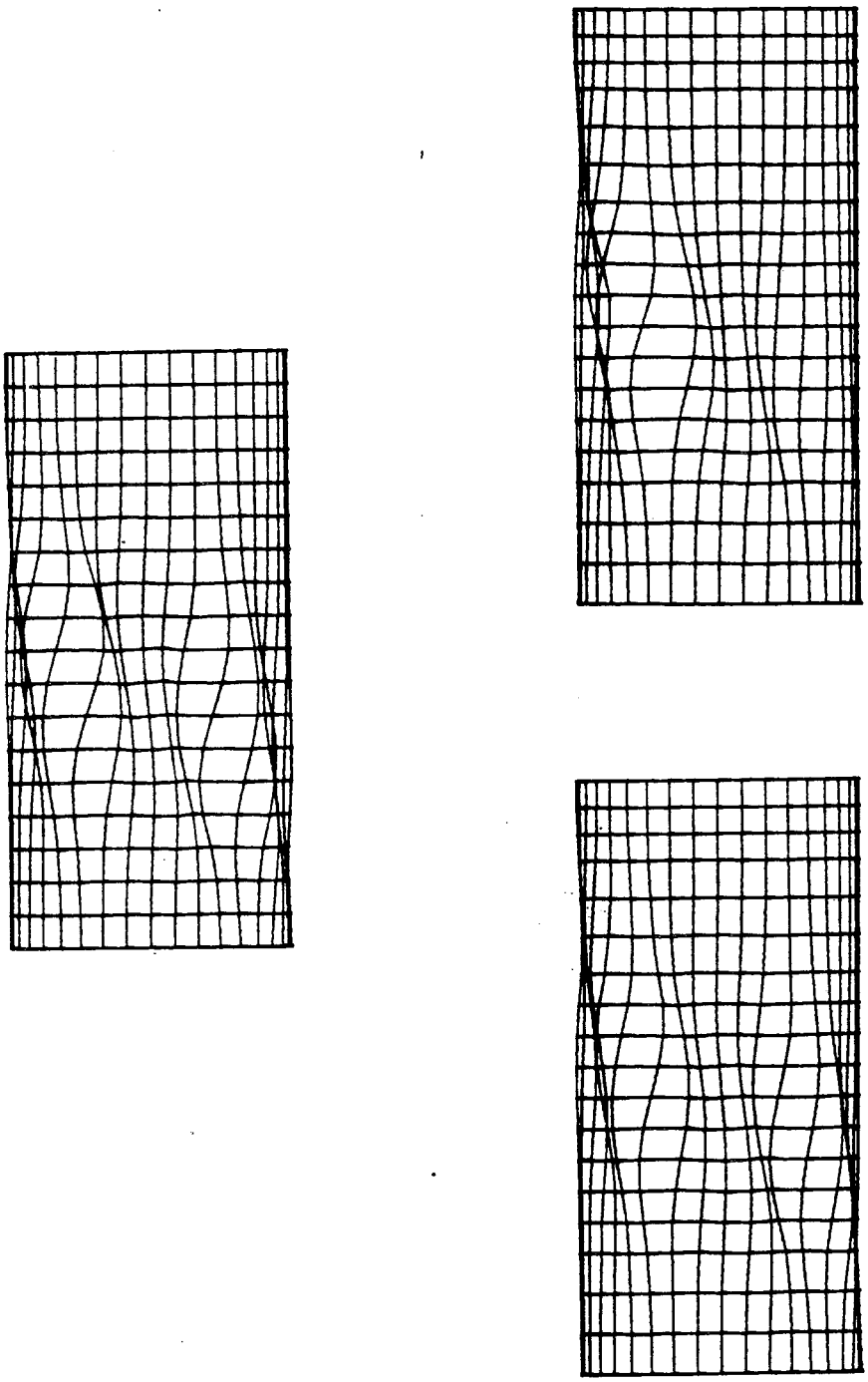

Figure 3.9 First Buckling Modes of Models B1, B3 and B4 in Series B

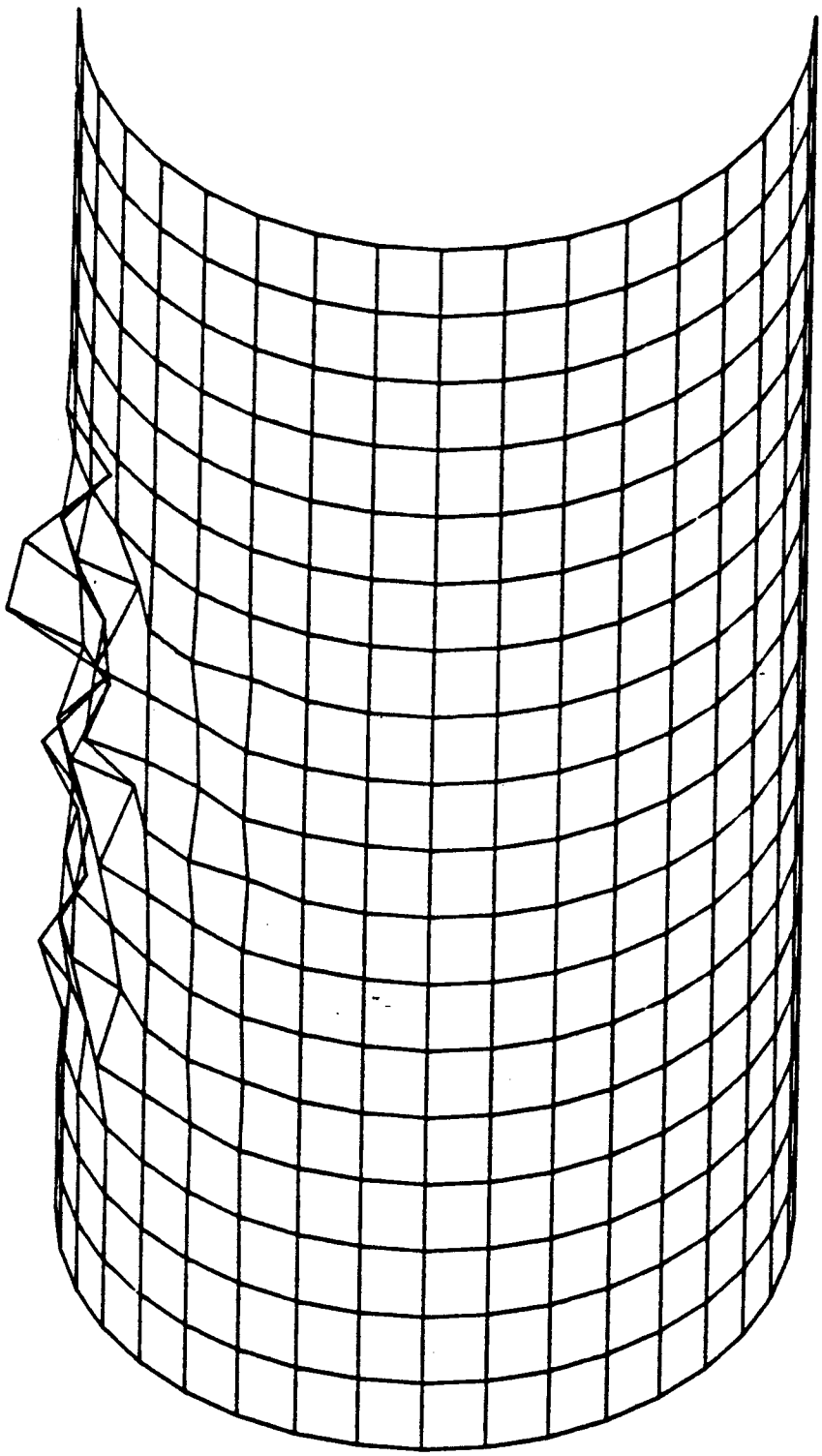

Figure 3.10 First Buckling Modes of Model B2 in Series B

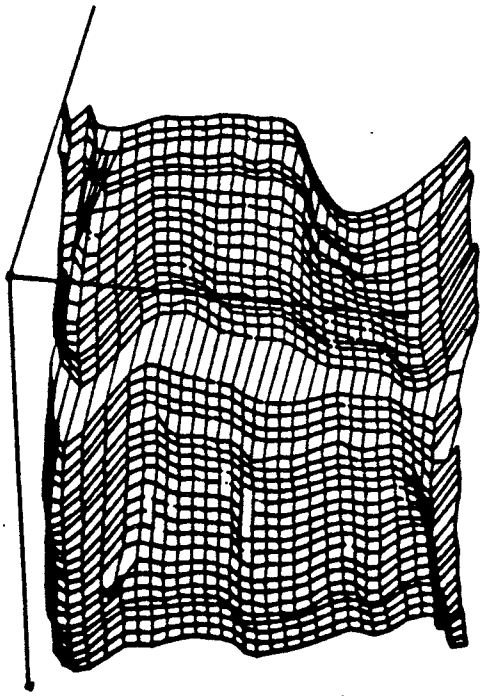

(a) Full Specimen

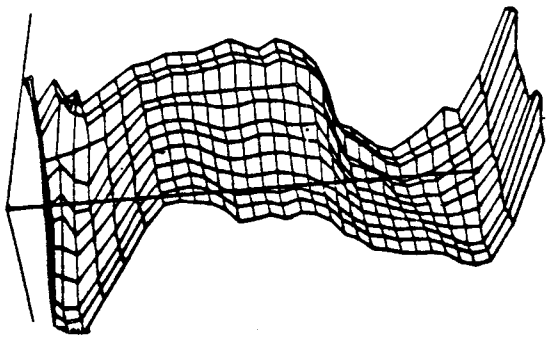

(b) Test Span 1

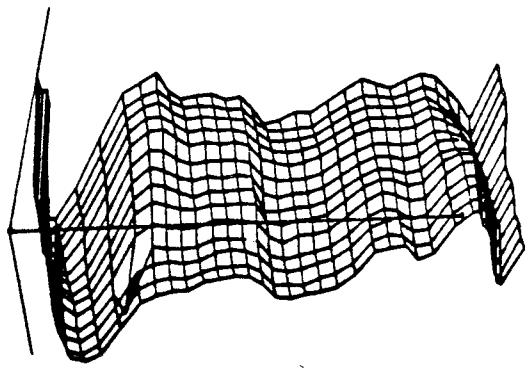

(c) Test Span 2

Figure 3.11 Actual Imperfection Profiles of Bailey and Kulak's First Shear Specimen

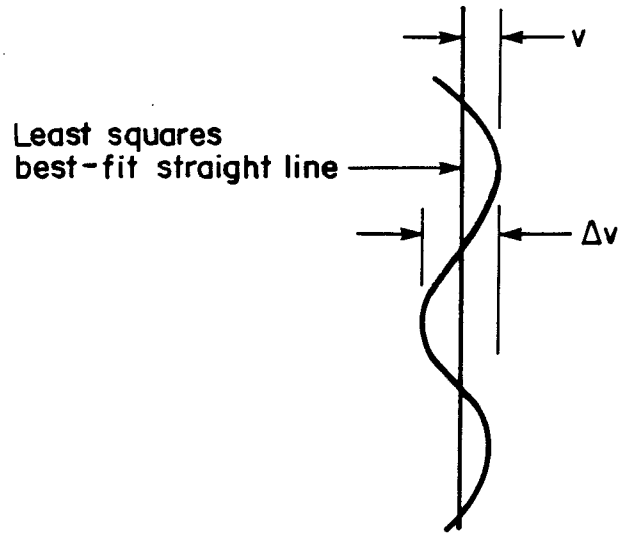

Figure 3.12 Initial Imperfection Measures

Table 3.1 Boundary Conditions of Models in Series A

	Boundary Conditions			Remarks
	Fixed Edge	Top and Bottom Longitudinal Edges	Loading Edge	
Model A1	All Fixed	XT,ZT,YR - Free YT,XR,ZR - Fixed	XT,ZT - Coupled YT,XR - Free YR,ZR - Fixed	Model A1 simulates a "Fixed-End" problem loaded in shear.
Model A2	All Fixed	XT,ZT,YR - Free YT,XR,ZR - Fixed	XT,ZT - Free YR - Coupled YT,XR,ZR - Fixed	Model A2 simulates a "Free-Cantilever" problem loaded in bending.
Model A3	All Fixed	XT,ZT,YR - Free YT,XR,ZR - Fixed	XT,ZT - Free YR - Coupled YT,XR,ZR - Fixed	Model A3 simulates a "Free-Cantilever" problem loaded in shear. Loading edge is stiffened with nine vertical truss elements.

[1] For the models under consideration, all degrees of freedom are defined with respect to the global system, except ZR,
and XT: X-translation, YT: Y-translation, ZT: Z-translation,
XR: X-rotation, YR: Y-rotation, ZR: Z-rotation.

Table 3.2 Material and Geometric Properties of Models in Series A

	Material Properties			Geometric Properties					Remarks
	^{1}E (MPa)	σ_{ys} (MPa)	ν 0.33	^{2}R (mm)	L (mm)	t (mm)	$\frac{R}{t}$	$\frac{L}{t}$	
All Models	204,400	301	0.33	190.0	808.5	0.76	250	1063.8	Constant thickness along the length of the shells.

[1] Strain hardening is assumed to be zero.
[2] Radius of mid-surface.

Table 3.3 Boundary Conditions of Models in Series B

	Boundary Conditions			Remarks
	Fixed Edge	Top and Bottom Longitudinal Edges	[1]Loading Edge	
Model B1	All Fixed	XT,ZT,YR - Free YT,XR,ZR - Fixed	ZT - Coupled XT,YT,XR,YR,ZR - Fixed	"Fixed-end" problem.
Model B2	All Fixed	XT,ZT,YR - Free YT,XR,ZR - Fixed	ZT,ZT - Free YR - Coupled YT,XR,ZR - Fixed	"Free-cantilever" problem. Loading edge is stiffened with truss elements.
[2]Model B3	All Fixed	XT,ZT,YR - Free YT,XR,ZR - Fixed	YT,ZT,XR - Free XT,YR,ZR - Fixed	"Fixed-end" problem.
[2]Model B4	All Fixed	XT,ZT,YR - Free YT,XR,ZR - Fixed	YT,ZT,XR - Free XT - Coupled YR,ZR - Fixed	"Fixed-end" problem.

[1] Refers to the free edge for models B3 and B4.
[2] For models B3 and B4, the loading edge is 72.5 mm from free edge.

Table 3.4 Material and Geometric Properties of Models in Series B

	Material Properties				Geometric Properties				Remarks
	[1]E (MPa)	σ_{ys} (MPa)	ν	[2]R (mm)	L (mm)	t (mm)	$\frac{R}{t}$	$\frac{L}{t}$	
Model B1	204,400	301	0.33	190.0	[3]404.3 [4](134.8,269.5)	[3]0.76 [5](1.52)	[3]250	[3]532	Variable thickness. Each model consists of two end spans and a test span.
Model B2	204,400	301	0.33	190.0	404.3 (134.8,269.5)	0.76 (1.52)	250	532	
Model B3	204,400	301	0.33	190.0	381.0 (165.0,262.5)	0.76 (1.52)	250	501	
Model B4	204,400	301	0.33	190.0	381.0 (165.0,262.5)	0.76 (1.52)	250	501	

1 E-Hardening is assumed to be zero.
2 Radius of mid-surface.
3 Refers to test span.
4 First number in parentheses refers to the end span closer to the fixed edge, second number refers to the end span closer to the loading edge.
5 Refers to both end spans.

Table 3.5 Shear Buckling Loads Predicted by NISA80 and Batdorf's Equation

Series B	Buckling Load (kN)		
	NISA80	Batdorf's Equation	
		Simple Supports	Clamped Edges
Model B1	33.4	30.4	32.4
Model B2	NA	NA	NA
Model B3	34.4	32.0	33.1
Model B4	34.3	32.0	33.1

NA - Not Applicable

Table 3.6 Initial Imperfection Characteristic of Test Span 1 of Bailey and Kulak's First Shear Specimen

Generator	$\|v\|_{max}$ (mm)	$\|\Delta v\|_{max}$ (mm)	$\|v\|_{mean}$ (mm)	v_{RMS} (mm)
1	0.484	0.730	0.156	0.200
2	0.049	0.083	0.017	0.022
3	0.127	0.175	0.027	0.042
4	0.231	0.319	0.056	0.080
5	0.147	0.257	0.058	0.076
6	0.098	0.184	0.041	0.051
7	0.206	0.314	0.055	0.080
8	0.136	0.232	0.055	0.066
9	0.117	0.215	0.065	0.073
10	0.116	0.217	0.047	0.059
11	0.092	0.165	0.033	0.044
12	0.099	0.149	0.036	0.042
13	0.087	0.155	0.031	0.040
14	0.086	0.157	0.040	0.046
15	0.088	0.146	0.033	0.040
16	0.102	0.170	0.043	0.049
17	0.092	0.183	0.045	0.053
18	0.062	0.111	0.033	0.039
19	0.101	0.178	0.040	0.052
20	0.079	0.124	0.025	0.033
21	0.099	0.189	0.058	0.066
22	0.259	0.461	0.074	0.107
23	0.228	0.394	0.063	0.092
24	0.231	0.390	0.090	0.109
25	0.129	0.195	0.042	0.053
26	0.139	0.246	0.041	0.058
27	0.199	0.368	0.062	0.088
28	0.188	0.371	0.101	0.118
29	0.222	0.345	0.060	0.084
30	0.144	0.244	0.062	0.074
31	0.165	0.327	0.097	0.110
32	0.662	1.079	0.355	0.401

Table 3.7 Initial Imperfection Characteristics of Test Span 2 of Bailey and Kulak's First Shear Specimen

Generator	$\|v\|_{max}$ (mm)	$\|\Delta v\|_{max}$ (mm)	$\|v\|_{mean}$ (mm)	v_{RMS} (mm)
1	0.331	0.572	0.174	0.195
2	0.347	0.615	0.131	0.159
3	0.294	0.587	0.190	0.205
4	0.125	0.233	0.059	0.072
5	0.197	0.357	0.068	0.090
6	0.061	0.107	0.026	0.030
7	0.568	0.736	0.107	0.173
8	0.130	0.250	0.075	0.084
9	0.069	0.129	0.032	0.038
10	0.086	0.156	0.046	0.051
11	0.088	0.157	0.040	0.045
12	0.089	0.174	0.042	0.051
13	0.088	0.168	0.032	0.040
14	0.124	0.204	0.059	0.005
15	0.126	0.245	0.060	0.073
16	0.111	0.182	0.040	0.049
17	0.178	0.299	0.061	0.075
18	0.168	0.314	0.075	0.087
19	0.093	0.182	0.040	0.053
20	0.127	0.225	0.067	0.076
21	0.133	0.255	0.069	0.079
22	0.093	0.175	0.042	0.052
23	0.136	0.258	0.053	0.071
24	0.105	0.194	0.049	0.056
25	0.137	0.255	0.078	0.088
26	0.119	0.225	0.058	0.066
27	0.148	0.257	0.059	0.074
28	0.173	0.294	0.072	0.095
29	0.094	0.179	0.046	0.055
30	0.207	0.384	0.082	0.098
31	0.291	0.509	0.128	0.162
32	0.240	0.386	0.084	0.108

Table 3.8 Experimental vs. Scaled Mode-1 Imperfection Measures (Test Span 1)

	Model B1 Generator 9		Model B2 Generator 11		Model B3 Generator 15		Model B4 Generator 8	
	Test	Mode-1	Test	Mode-1	Test	Mode-1	Test	Mode-1
$\|v\|_{max}$ (mm)	0.117	1.400	0.092	1.890	0.088	1.390	0.136	1.910
$\|\Delta v\|_{max}$ (mm)	0.215	0.959	0.165	1.273	0.146	0.955	0.232	1.345
$\|v\|_{mean}$ (mm)	0.065	0.954	0.033	1.162	0.033	1.048	0.055	1.235
v_{RMS} (mm)	0.073	1.008	0.044	1.246	0.040	1.150	0.066	1.309

Table 3.9 Experimental vs. Scaled Mode-1 Imperfection Measures (Test Span 2)

	Model B1 Generator 12		Model B2 Generator 3		Model B3 Generator 2		Model B4 Generator 3	
	Test	Mode-1	Test	Mode-1	Test	Mode-1	Test	Mode-1
$\|v\|_{max}$ (mm)	0.089	0.314	0.294	0.271	0.347	0.193	0.294	0.335
$\|\Delta v\|_{max}$ (mm)	0.174	0.251	0.587	0.268	0.615	0.171	0.587	0.261
$\|v\|_{mean}$ (mm)	0.042	0.198	0.190	0.125	0.131	0.108	0.198	0.207
v_{RMS} (mm)	0.051	0.216	0.205	0.154	0.159	0.123	0.216	0.227

4. ANALYTICAL PREDICTION OF SHELL BEHAVIOR

4.1 Introduction

As indicated in Chapter 1, the purpose of the analytical program is to investigate the shear behaviour of large diameter steel cylinders loaded in transverse shear. The cylinders treated herein have a radius to thickness ratio (R/t) of 250. Four cylinders are analysed with various boundary conditions and different levels of initial geometric imperfections. All cylinders considered have the same or approximately the same configuration as the first shear specimen (R/t = 251) experimentally tested by Bailey and Kulak (1984). The loading set up in this analytical program is similar to that in Bailey and Kulak's experiment (1984).

In this chapter the numerical results from the finite element technique are compared to the existing experimental data. In addition the effects of initial geometric imperfections (the magnitude of, and the method of introducing the geometric imperfections) on the buckling load and the load-response path of a cylindrical shell are examined.

4.2 Preliminary Considerations

It is shown in Chapter 3 that the variation in cylinder thickness which formed a part of the experimental set up has little influence on the buckling pattern of transversely

loaded thin cylindrical shells, and that the diagonal buckling pattern is a characteristic mode of buckling for thin cylindrical shells loaded in double curvature.

However, the theoretical and experimental work discussed in Chapter 2 indicates that initial geometric imperfections have an effect on the load at which first buckling occurs in thin-walled cylinders. Hence, it is important to include initial geometric imperfections in the analysis. Because of the small thickness of the shells under consideration, the effect of geometric imperfections can be pronounced and the problem can become imperfection sensitive.

In Chapter 2, it is mentioned that the buckling load may depend on the boundary conditions of the shells. In order to determine the variation of the buckling load due to the types of edge supports, notwithstanding the Bailey and Kulak test conditions, several sets of boundary conditions are imposed on the models in this analysis.

4.3 Description of Models

A series of four geometrically imperfect cylinders (Series S) are analysed using the finite element program NISA80. The analyses are based on a bilinear elastic-perfectly-plastic (von Mises) material response in the context of a total Lagrangian formulation. The geometry of the four models are the same as those in Series B of the preliminary study except that initial imperfections based on

buckling modes are superimposed onto the shell geometry. Each model consists of three spans representing one half of the Bailey and Kulak test set-up. The middle span is the test span having a smaller thickness than the two end spans. The test span has a thickness of 0.76 mm and is intended to fail first. The two end spans have a thickness of 1.52 mm. Configurations of the models are shown in Fig. 4.1.

Since the problem is symmetric about the longitudinal axis, only one longitudinal half of a cylinder is modelled. A uniform 6 x 6 finite element mesh is used for models S1 and S2. The lengths of the three spans are thus 134.75 mm for the end span closer to the fixed edge, 404.28 mm for the test span and 269.50 mm for the other end span. For models S3 and S4, a nonuniform 6 x 6 mesh is used in order to exactly fit the geometry of the shells. Hence, the lengths of the three spans are 165 mm, 381 mm and 262.5 mm respectively. In both cases, 36 bicubic 16-node Lagrangian 3-D degenerated plate-shell elements (Ramm 1977) are employed.

Integration of the finite elements is based on a 3 x 3 Gaussian scheme in the plane of each element, and on a Simpson's rule with 7 layers in the thickness direction. Eigenvalue analyses are carried out at different load levels using the subspace iteration technique (Bathe 1982). Equilibrium iterations are carried out employing the modified or standard Newton-Raphson iterative method up to a

certain load level and the Riks-Wempner iterative algorithm thereafter (Wempner 1971; Riks 1979; Crisfield 1980; Ramm 1980).

Models S1, S2 and S3 are designed to simulate "fixed-end" conditions with unrestrained vertical translations but restrained horizontal movements at the loading edge (Figs. 4.2a and 4.2b). Model S4 is also designed to provide a "fixed-end" condition but with unrestrained vertical and horizontal translations (Fig. 4.2c). In all cases, the vertical translations of all the nodes on the loading edge are coupled in order to prevent local failure. Note that the loading edge in models S3 and S4 is 72.5 mm from the far edge. Table 4.1 shows the details of the boundary conditions for the four models. The material and geometric properties are listed in Table 4.2.

In order to study the effect of initial geometric imperfections on the buckling loads of the models, different scaled mode-1 imperfection values and different combinations of buckling modes are used in the models. Model S1 contains a set of initial imperfections which is comprised of only the shear buckling mode obtained from model B1 in the preliminary analysis. The scaled mode-1 imperfection value used for model S1 is 1/100 times the shell thickness, or 0.0076 mm. In model S2, a combination of the shear buckling mode from model B1 and the compression buckling mode from model B2 is used. The contributions from each buckling mode are proportioned according to the maximum bending moment in

the top compression region of the test span in each case. The scaled mode-1 imperfection value used in model S2 is half the shell thickness and one and a half times the thickness for the shear mode and the bending mode respectively. The shear buckling mode from model B3 is used in model S3 while the shear buckling mode from model B4 is used in model S4. In both models, the scaled mode-1 imperfection value is one times the shell thickness, or 0.76 mm. The scaled mode-1 imperfection values for the four models are listed in Table 4.3.

4.4 Loading Procedure

Loads are applied transversely to the models through all the nodes at the loading edge as shown in Figure 4.3. A linear eigenvalue analysis is done at an early stage of loading for each model in order to obtain an estimate of the ultimate loads. Subsequent loading is then applied stepwise and the size of the loading is adjusted as the load-response behaviour becomes nonlinear. Different equilibrium iteration methods are used, accordingly, to achieve convergence. Subsequent eigenvalue analyses are then carried out at different load levels as the effects of prebuckling deformation become pronounced.

4.5 Results

4.5.1 General

In the following, the loading behaviour for each model

is described. The deformed shapes and the buckling modes for each model at different stages of loading are presented. The presentation of the results consists of two groups since there are two basic sets of shell geometry and loading conditions. The first group includes models S1 and S2 while the second group is related to models S3 and S4.

4.5.2 Behaviour During Loading

The behaviour during loading for models S1 and S2 and models S3 and S4 is shown in Figs. 4.4 and 4.5 respectively, where plots of load versus the vertical deflection at the top node of the loading edge of the models are presented. In all cases the finite element models were about four times as stiff as Bailey and Kulak's first shear specimen.

In model S1, which incorporated an infinitesimal initial imperfection and suppressed rotations and longitudinal translations at the loading edge, the behaviour is practically linear up to a maximum load of 32.42 kN (Fig. 4.4a). The buckling loads obtained from eigenvalue analyses at different load levels showed little variation, mostly falling between 33.4 kN and 33.7 kN. At about 30 kN, no nonlinearity can be seen from that load-response curve. However, the size of the incremental load had to be adjusted in order to achieve convergence. At 32.92 kN, the model showed very little stiffness and the solution diverged even though very small load size and different iteration schemes such as the standard Newton-Raphson method and the Riks-

Wempner algorithm were tried. At this stage, it is believed that a limit point is reached or within proximity. The deformed mesh of model S1 at this load level is plotted (Fig. 4.6a). It is noted that inclined buckles are formed in the test span of the model in a manner similar to that obtained in Baily and Kulak's first shear specimen.

The load-response behaviour for model S2, which incorporated large initial imperfections based on a combination of shear and bending buckling modes, is practically linear up to a maximum load of 24.16 kN (Fig. 4.4b). Thereafter, no further load could be applied to the model. This occurred rather abruptly since no sign of nonlinearity was found in the load-deflection curve and little indication of failure was detected in the previous load steps. At this point, the size of the incremental load was adjusted and other iteration schemes were used; however, no further results could be obtained. The buckling loads obtained from eigenvalue analyses at two different load stages show little variation, both of them are approximately equal to 33.9 kN. The deformed shape of the model at the maximum load level is plotted (Fig. 4.6b). A combination of deformation modes is found to exist in the model. Inclined buckles are obtained in the test span. Compression buckles are also found along the top region of the test span. This mode of failure, a combination of shear buckling and compression buckling, is similar to the failure mode of Bailey and Kulak's first shear specimen. However, this

conclusion is not firm because no nonlinearity is apparent in the load-deflection curves. These buckles may be magnifications of the superimposed prebuckling deformations. In addition, it should be noted that the analysis of model S2 has been carried out on a new version of the program NISA80. Tests of this version are not complete. Hence, no inferences can be made from this model's results.

Fig. 4.5a shows the load-response behaviour of model S3. This model incorporates initial imperfections based on a shear buckling mode of the order of the shell thickness, and boundary conditions consisting of suppressed rotations and longitudinal translations at the far edge. It can be seen that the behaviour is practically linear up to a load of about 15 kN. An eigenvalue analysis was done at an early stage of loading. The buckling load obtained from the eigenvalue analysis was 15.74 kN. Loading was then resumed. A second eigenvalue analysis with 6 subspace iteration vectors was attempted at a load level of 13.59 kN. No positive eigenevalues were obtained. Another trial was made with 10 subspace iteration vectors but again no positive eigenvalues were found. The eigenvalue analysis was then abandoned and loading was resumed. At this load level, it was necessary to change the iteration scheme from the modified Newton-Raphson technique to the standard Newton-Raphson technique in order to achieve equilibrium convergence although no nonlinearity was observed in the

load-response curve. However, the model was able to take load up to and beyond the ultimate load of 14.7 kN achieved by Bailey and Kulak in the experiment as well as the buckling load of 15.74 kN obtained in the early eigenvalue analysis. Thus, it was suspected that a critical point may have been missed due to large incremental load steps and an alternative primary path was followed. Hence, the loading was backed up to 13.59 kN and was restarted with a smaller incremental load size using the Riks-Wempner iteration scheme in hope of tracing the secondary path. The solution, however, continued along the previously established curve and no branching occurred. At a load of about 13.6 kN, the load-response behaviour started to become nonlinear, but the model was able to take load above the predicted buckling load of 15.74 kN. At 18.12 kN, it was necessary to adjust the size of the incremental load in order to achieve equilibrium convergence. An eigenvalue analysis was attempted at a load level of 18.88 kN with 10 subspace iteration vectors; however, no positive eigenvalues were found. Loading was then resumed. At a load of 19.63 kN, although the model may be able to take more loading, application of load was stopped.

The load-response behaviour of model S4 is shown in Fig. 4.5b. This model incorporated initial imperfections based on a shear buckling mode of the order of the shell thickness and the boundary conditions consisted of suppressed rotations and coupled longitudinal translations

at the far edge. The behaviour is similar to that obtained for model S3. It is practically linear up to a load of about 13.6 kN. An eigenvalue analysis was carried out with 6 subspace iteration vectors at an early stage of loading. The buckling load obtained from the eigenvaue analysis was 17.19 kN. All subsequent eigenevalue analyses were done using 12 subspace iteration vectors to generate the first and the second buckling modes. The next three eigenvalue analyses were carried out at load levels of 10.57 kN, 12.84 kN and 14.35 kN. The buckling loads corresponding to the first mode were 17.96 kN, 18.49 kN and 18.95 kN while those corresponding to the second mode were 21.84 kN, 21.88 kN and 22.07 kN respectively. It can be seen that at this stage there is a substantial increase in the predicted first buckling load. This suggests that the model stiffens as it is being loaded and that the effect of prebuckling deformations on the buckling load should not be neglected. At a load level of 12.08 kN, it is necessary to adjust the incremental load size and to change the iteration scheme from the modified Newton-Raphson technique to the standard Newton-Raphson technique in order to achieve equilibrium convergence although the load-response curve is still linear. As in the case of model S3, model S4 was able to absorb loads up to 15.86 kN. Loading was then backed up to a level of 12.84 kN and restarted using a smaller incremental load size along with the Riks-Wempner iteration scheme. The load-response behaviour, however, continued on

the previous curve. At about 15 kN, the load-response curve began to stiffen although the effect of nonlinearity is not severe. An eigenvalue analysis was carried out at load level of 15.86 kN. The first and the second buckling loads were found to be 19.50 kN and 22.30 kN respectively. Loading was then resumed. Two subsequent eigenvalue analyses were attempted at load levels of 17.36 kN and 18.88 kN but no positive eigenvalues were obtained. At a load of 19.63 kN, although the model may continue to take more loading, the application of load was stopped.

4.5.3 Specific Load-Deflection Curves

In the previous section, the load-response curves are plotted with respect to the vertical deflection at the far edge of the models. It is mentioned that "at some stages of the loading, the size of the incremental load and the iteration scheme had to be adjusted in order to achieve equilibrium convergence", which indicates that some nonlinear behaviour may have been encountered. The load-response curves, however, remain linear under most of these circumstances. This leads to the suggestion that the vertical deflection at the far edge is a necessary, but not sufficient, deflection parameter to describe the load-response behaviour of the models under consideration. In order to have a better understanding of the load-response behaviour of the problem, it is necessary to examine, in more detail, the deflections at other critical locations

such as the regions in which inclined buckles and compression buckles were found.

Four nodal points were selected as the representative locations to describe the formation and behaviour of the inclined buckles which exist in the test span. The four nodal points are nodes 194, 198, 215 and 238. Nodes 286 and 287 were chosen to represent the behaviour at the top compression region of the test span. In all models, however, deflections of nodes 286 and 287 are almost the same. Hence, only node 286 is used. The locations of these nodes on the finite element mesh are shown in Fig. 4.7.

To examine the effects of the prebuckling deformation on the behaviour of the models, plots of the applied load versus the lateral translations (y-translations) of nodes 194, 198, 215 and 238 are presented in Figs. 4.8 and 4.9 for models S1 and S2 and models S3 and S4, respectively.

For model S1 (Fig. 4.8a), the load-deflection curves begin to show nonlinearity at a load of about 30 kN. At this point, the lateral deflections of the buckles start to increase substantially in a nonlinear manner. It is concluded that buckling has occurred in a shear mode in model S1 at this load level. For model S2 (Fig. 4.8b), the load-deflection curves are linear up to the maximum load. No nonlinearity is observed. It is concluded that the effect of the prebuckling deformation is linear in model S2.

Very similar results are obtained for model S3 and model S4 (Fig. 4.9). In both models, the load-deflection

curves show nonlinearity at a rather early load stage, 10 kN. Thereafter, the nonlinear effects due to the prebuckling deformations become quite substantial.

Another area of interest is the top compression region in the test span at which compression buckling may occur. Again, plots of the applied load versus the vertical translations (z-translations) of node 286 are presented in Fig. 4.10 for models S1 and S2, and in Fig. 4.11 for models S3 and S4 respectively.

For model S1 (Fig. 4.10a), the curve is practically linear up to 30 kN. Beyond this point, the slope of the curve increases, which may indicate that a compression buckle is in the process of formation in the opposite direction to the overall deflection pattern. The curve corresponding to model S2 (Fig. 4.10b) does not show any nonlinear behaviour although compression buckles can be seen at the top compression region of the test span in the deformed shape shown in Fig. 4.6b. In Fig. 4.11, models S3 and S4 show similar load-response behaviour. In both cases, nonlinearity becomes obvious at about 13.6 kN. Beyond this point, the slope decreases. This indicates that the models, in so far as this deflection parameter is concerned, are softening under the application of load.

4.5.4 Deformed Shapes

The deformed shapes and the buckling shapes from the eigenvalue analyses are presented in this section. For each

model, a series of deformed shapes at different load levels is shown in order to describe the behaviour of the model during the loading process.

In Fig. 4.12, the deformed shapes of model S1 at five different load levels are shown, along with the buckling shapes at two load levels. The deformed mesh at failure (at 32.9 kN) shows inclined buckles in the test span similar to those predicted from the buckling analyses. No compression buckles are found. This suggests that model S1 is exhibiting a shear buckling failure mode.

The deformed shapes for model S2 are shown in Fig. 4.13 at four different load steps along with two buckling shapes. The buckling shapes show only inclined buckles in the test span. At the maximum load (24.16 kN), inclined buckles and compression buckles in the top compression region are both found in the test span. However, these buckles may be magnifications of the superimposed prebuckling deformations.

In Fig. 4.14, five deformed shapes of model S3 and one buckling shape are shown. Inclined buckles are found at about 15 kN but no compression buckles are evident. A similar situation is found in model S4. Five deformed shapes and three buckling shapes are shown in Fig. 4.15. At about 15 kN, inclined buckles are found in the test span. However, no compresion buckles are obtained in the top compression region.

4.6 Further Investigation

A model S5 is analysed in this section. This model has the same geometry, boundary and loading conditions as in model S3. The only difference is that in model S5, the scaled mode-1 imperfection value is twice the shell thickness while in model S3, it is only one times the shell thickness. This model incorporates large initial imperfections based on the shear buckling mode obtained from model B3 in the preliminary investigation. Model S5 simulates a "fixed-end" problem with restrained longitudinal movements and suppressed rotations at the far edge. The loading face is stiffened by coupling all vertical translations at this face.

During the analysis of this model, numerical difficulties were found. This model was able to take load up to about 6 kN. The load-response behaviour is linear up to this load. Thereafter, the solution diverges and no further results can be obtained. Smaller incremental load size was used along with the Riks-Wempner iteration technique, however, no convergence is reached.

4.7 Comparison of FEM Results with Classical Theories and Test Results

In Chapter 2, the classical solution developed by Batdorf et al. (May, 1947) based on the small-displacement theory was discussed. Solutions exist for both simply-supported and clamped-edge cylinders. For models S1 and S2,

the critical buckling stress according to Batdorf et al. is 140 MPa for simply supported edges and 167 MPa if the edges are clamped. These stress levels correspond to shear buckling loads of 31.76 kN and 37.81 kN, respectively for the two edge conditions.

The shear yield strength for cylinders can be conveniently calculated by multiplying the cross-sectional area by the shear yield stress and dividing by the shape factor. In this study, the shear yield stress, τ_y, is assumed to be $\sigma_y/\sqrt{3}$. For thin-walled cylinders, the shape factor can be taken as 2.0. Hence, the resulting shear yield strength for models S1 and S2 is 39.46 kN. Comparing the shear yield strength with those predicted by Batdorf et al. (1947), it is obvious that models S1 and S2 should reach the shear buckling loads before shear yielding occurs.

Stephens et al. (1982) developed a semi-empirical formula to predict the strength of axially loaded cylinders. They suggest that the flexural buckling capacity of fabricated steel cylinders can be approximated on the basis of the test results for uniformly compressed cylinders. Since the models considered in this study are susceptible to compression buckling, it is necessary to calculate the flexural capacity of the models. According to Stephens et al., the critical flexural buckling stress for models S1 and S2 is 168 MPa, which corresponds to an ultimate transverse load of 26.81 kN. This leads to the suggestion that compression buckling will occur prior to

shear buckling in models S1 and S2. It should be noted, however, the solutions by Stephens et al., are semi-empirical solutions based on testing of real structures. Hence, the effects of initial imperfections (material and geometric) have been accounted for. Batdorf's classical solutions, on the other hand, are for perfect shells based on the small-displacement theory and no initial imperfections are considered. Since shear buckling is detected prior to compression buckling in model S1, the implications are that either Stephen's et al. (1982) predictions are conservative or that Batdorf's classical solution should be modified in the presence of initial imperfections.

The actual maximum load from the finite element analysis is 32.92 kN for model S1, and 24.16 kN for model S2. Comparing these results to Batdorf's shear buckling values, models S1 and S2 reached 104% and 76% respectively of the predicted values, if simply supported edges are assumed, and 87% and 64% for clamped edge condition. If compared to the shear yield strength, model S1 reached 83% of yield, while model S2 reached 61%. The actual results can also be compared with the ultimate strengths predicted by Stephens et al. (1982) based on pure bending. The maximum load reached 123% of the predicted value for model S1, and 90% for model S2. Table 4.4 shows the comparisons clearly.

When the numerical analysis values are compared with

the experimental load of 14.7 kN obtained by Bailey and Kulak, little agreement exists. In both models, the actual values exceed the experimental result by a considerable factor. This lack of agreement can be attributed to the following factors. First, the models in this analysis and the test specimen have slight differences in the lengths of the three spans and in the position of the transverse load. The effects due to these differences may be small, nevertheless, they should not be neglected. The second factor may be attributed to the inadequate modelling of the boundary conditions. It is known that different sets of boundary conditions result in different failure loads. Initial imperfections, both geometric and material, are also important factors in determining the ultimate load of a structure. In model S1, the scaled mode-1 imperfection magnitude is 1/100 times the shell thickness. This level of imperfection is relatively small and hence model S1 remains approximately close to a perfect shell. It can, thus, reach a buckling load close to the critical buckling load predicted by Batdorf's classical theory. In model S2, the scaled mode-1 imperfection magnitude is relatively large. A combination of shear buckling mode and compression buckling mode was used in preparing the initial imperfections. Having this level of imperfection, model S2 no longer behaves like a perfect shell. In fact, it reaches a maximum load close to the predicted value according to the semi-empirical equations developed by Stephens et al. Finally,

residual stresses and, hence, their effects leading to premature failure have not been accounted for in this study. In the actual experiment, it is conceivable that residual stresses played an important role in determining the ultimate capacity of the specimen.

For models S3 and S4, the critical buckling stress according to Batdorf et al. is 105 MPa for simply supported edge and 120 MPa for clamped edges. These stress levels correspond to shear buckling loads of 23.82 kN and 27.22 kN for the respective two edge conditions. The shear yield strength for models S3 and S4 is 39.46 kN. Comparing the shear yield strength with those predicted by Batdorf et al., it is apparent that models S3 and S4 should reach the shear buckling loads before shear yielding occurs. According to Stephens et al., the critical buckling stress for models S3 and S4 is 168 MPa which corresponds to an ultimate transverse load of 30.22 kN. It is apparent that shear buckling should occur before compression buckling.

In Bailey and Kulak's experiment, the failure load obtained for the first shear test is 14.7 kN, which is below all the predicted values above. In the analysis, however, this is not the case. Models S3 and S4 are able to absorb loads up to and above 14.7 kN although nonlinearity became obvious. Simultaneous eigenvalue analyses indicate the buckling loads of model S4 are increasing, which implies that the model is stiffening under the application of load (see Fig. 4.5). The same behaviour is assumed to exist in

model S3 although no verification can be drawn from the eigenvalue analyses. This stiffening phenomenon may be attributed to the existence of a tension field. However, for a tension field to develop, shear buckling in the test span has to occur first. This leads to the suggestion that models S3 and S4 buckled in a shear mode at a load between 10 kN and 16 kN since most of the eigenvalue analyses are carried out between these two load levels.

It is apparent that models S3 and S4 can absorb load above the test load by a considerable amount. The lack of agreement between the results and the test value can be attributed to several factors. First, residual stresses have not been accounted for in this analysis. In the test specimen, residual stresses exist as a consequence of fabrication and subsequent welding. This may lead to a substantial decrease in the ultimate load of the test specimen. As before, the second factor is due to the inaccuracy of the modelled boundary conditions. More accurate representation of the test support conditions should give a better agreement between the results from the test and from the computer models.

4.8 Observations on Results of Numerical Investigation

From the analyses presented in this chapter, it is apparent that the numerical results do not agree with the test results obtained by Bailey and Kulak (1984). The program NISA80 appears to be insufficiently developed at

this time to predict reliably the behaviour of the test specimen. The most obvious discrepancies between the numerical results and the experimental results are: a) the measured stiffness for the first experimental shear specimen are approximately 1/4 times the predicted stiffness, as shown in Figs. 4.4 and 4.5; and, b) the predicted 'failure' loads range from 133% to 224% of the experimental failure loads (Table 4.4).

It is reasonable to argue that the initial response of the shells would be expected to be similar to that of a fixed-end beam. Hence it is of interest to compare the measured and predicted deflections with those from simple beam theory. Table 4.5 shows the results for flexibilities (Δ/P) where they are compared with NISA80 and experimental values. The beam theory computations indicate that approximately 70% of the deflection is due to shear deformation. The total beam theory agrees very well with the NISA80 deflections. This indicates that the predicted flexibility is approximately equal to that predicted by the beam theory. However, the experimental results are approximately 4 times as flexible as the NISA80 predictions. An upper bound on beam theory deflections can be obtained by using simple support conditions. The results are also shown in Table 4.5. The flexural deflections predicted by beam theory increase by a factor of approximately 4.5 and the total deflection is increased by a factor of approximately 2. However, the effect of such a

relaxation of boundary conditions on the NISA80 solution is difficult to predict. If these deflections were also increased by a factor of 2, the flexibility of the NISA80 solution would still be only 1/2 of the experimental results.

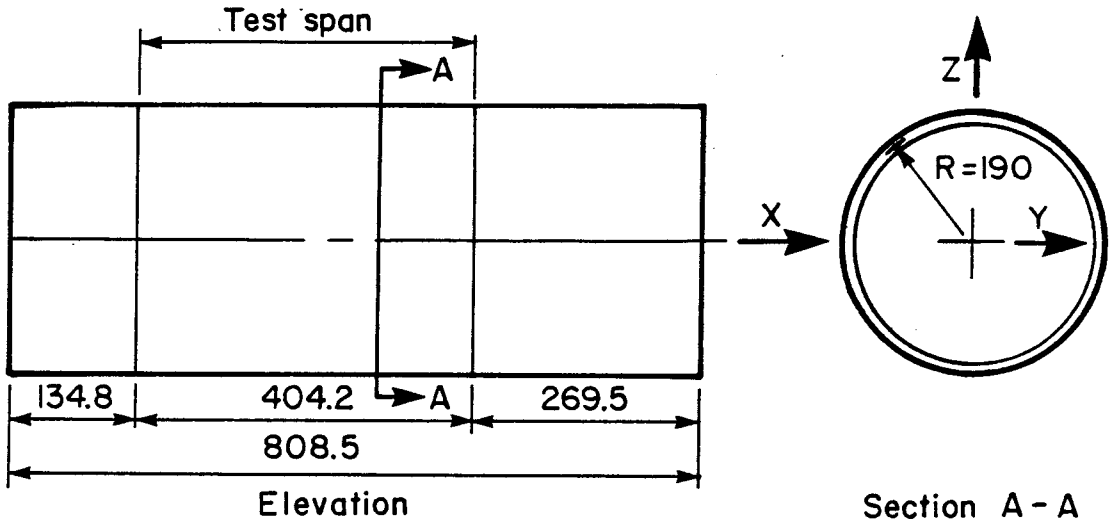

(a) MODELS S1 and S2

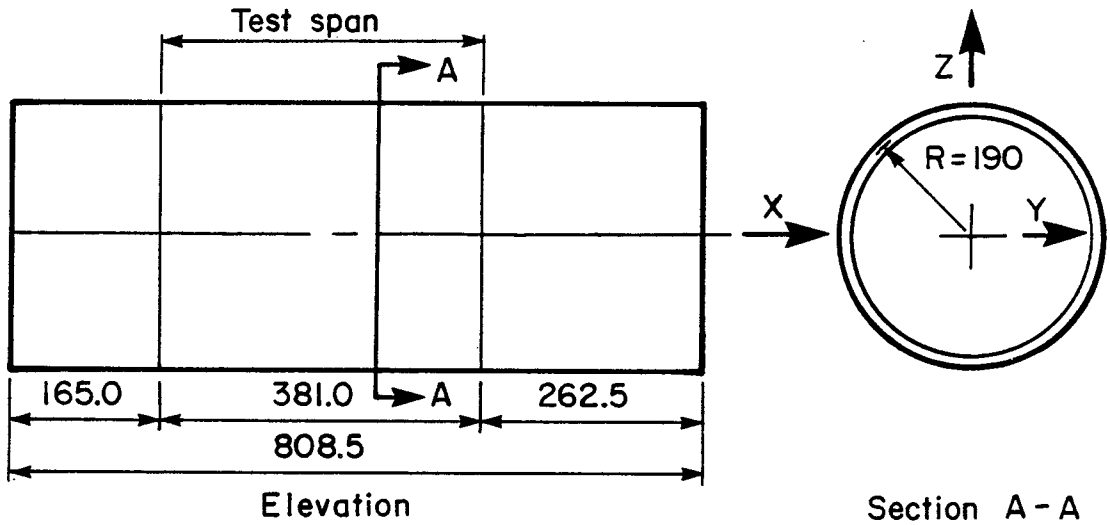

(b) MODELS S3 and S4

Test span : t = 0.76 mm
Other span : t = 1.52 mm
R = Radius of mid-surface (all spans)

Figure 4.1 Configurations of Models in Series S

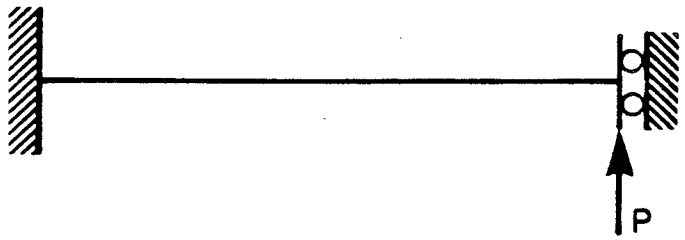

(a) MODELS S1 and S2

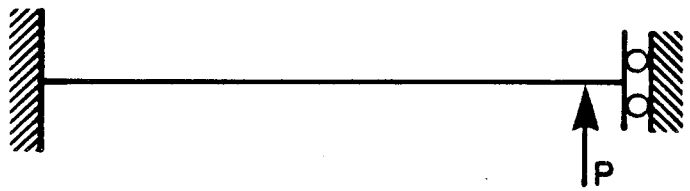

(b) MODEL S3

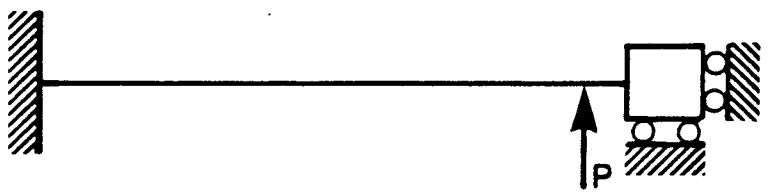

(c) MODEL S4

Figure 4.2 End Conditions of Models in Series S

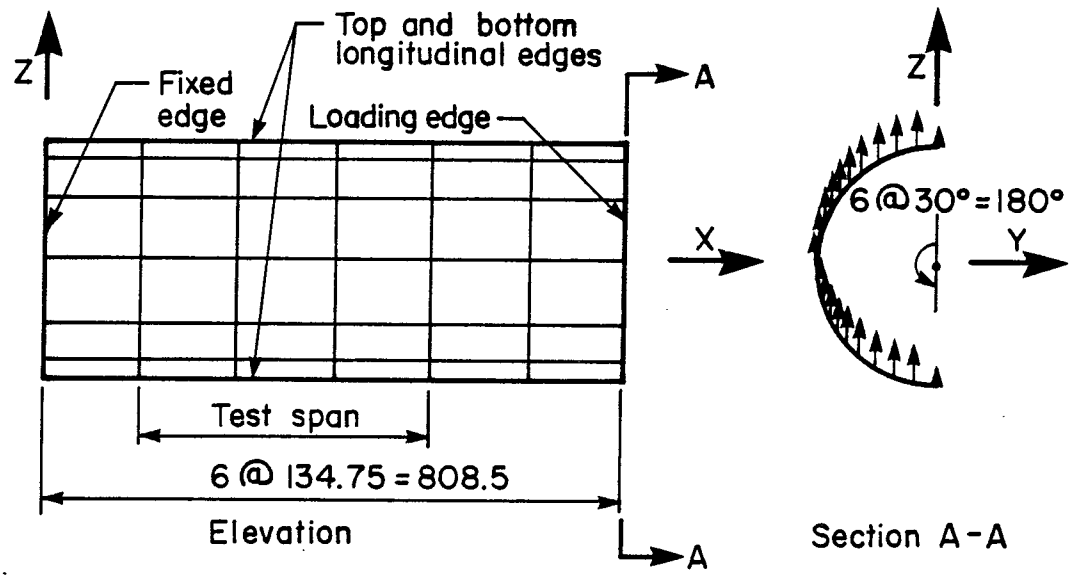

(a) MODELS S1 and S2: uniform 6x6 mesh

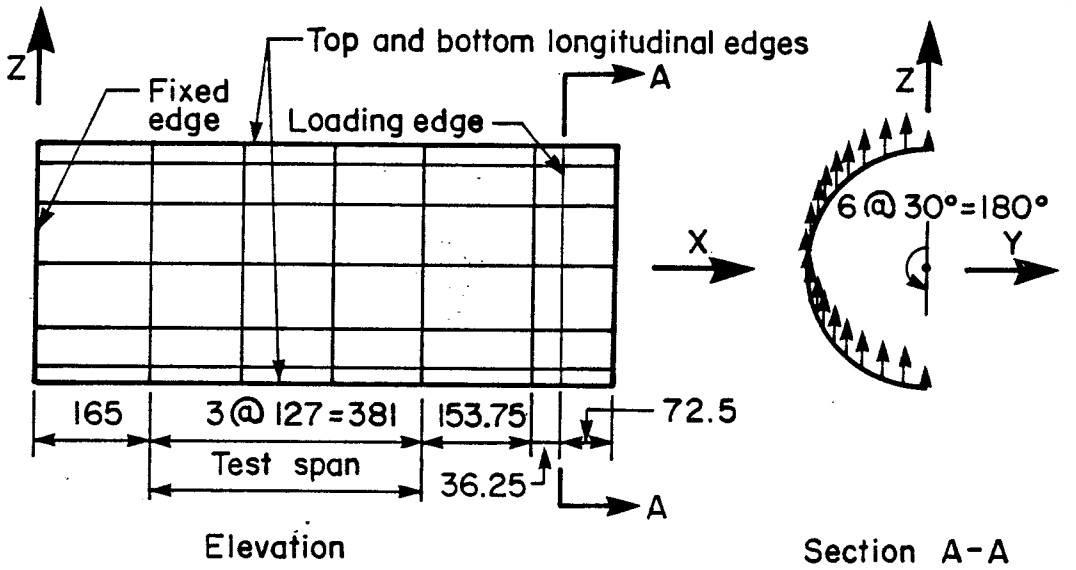

(b) MODELS S3 and S4: nonuniform 6x6 mesh

Figure 4.3 Finite Element Meshes and Loading Conditions of Models in Series S

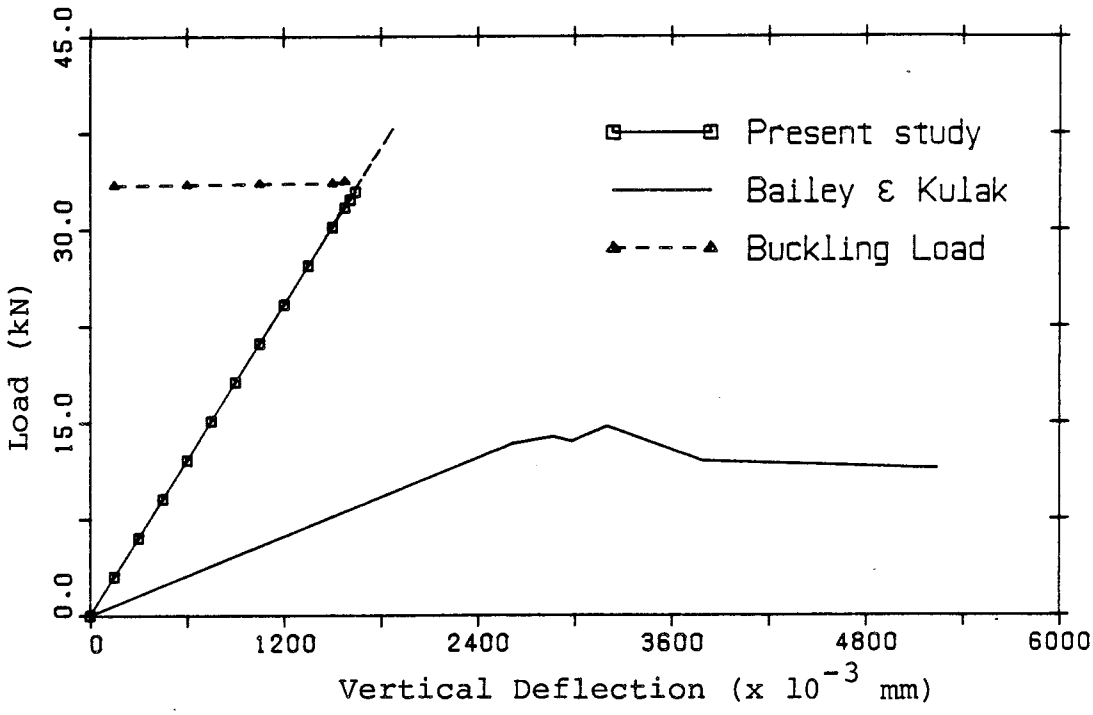

(a) Model S1

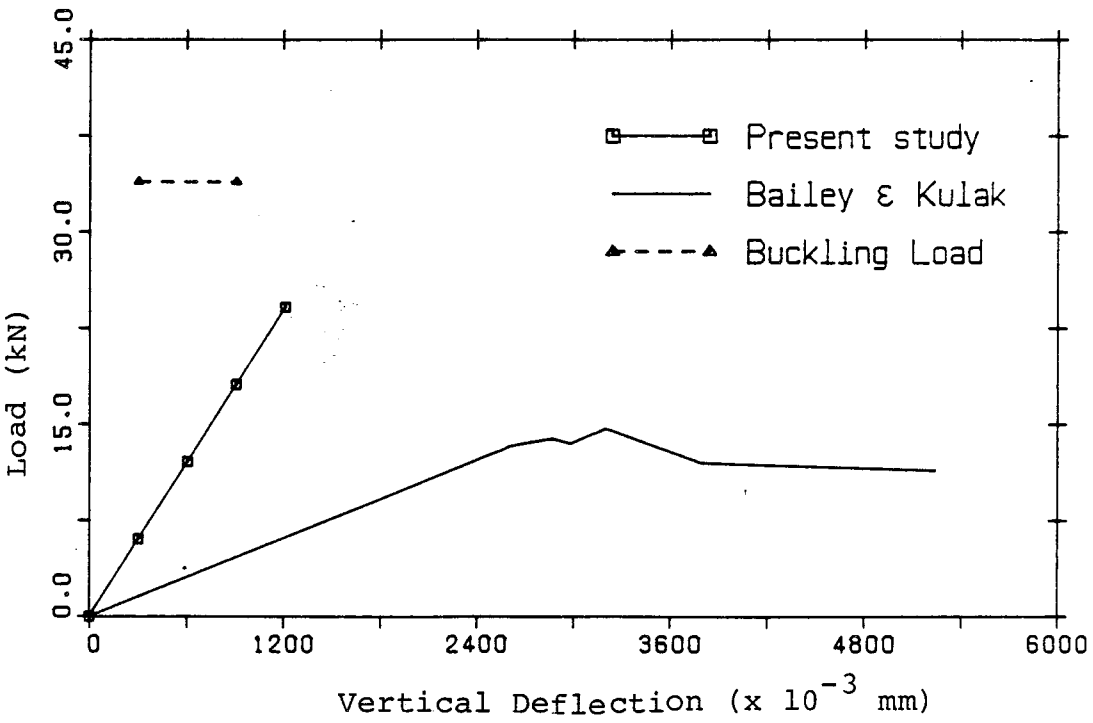

(b) Model S2

Figure 4.4 Load-Response Curves of Models S1 and S2

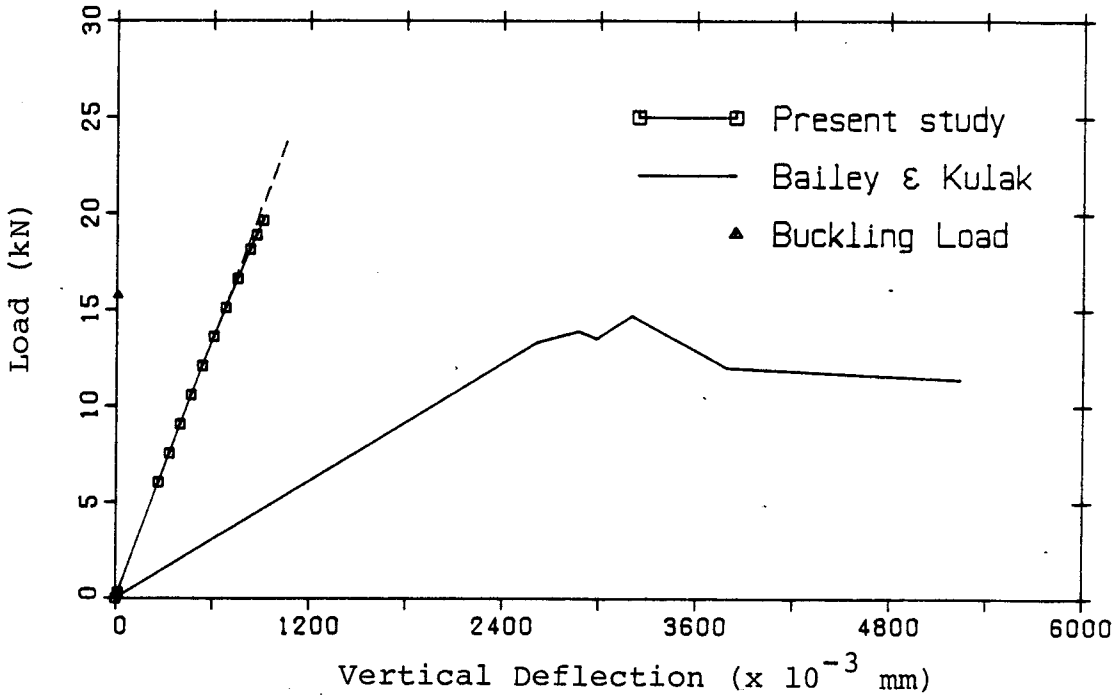

(a) Model S3

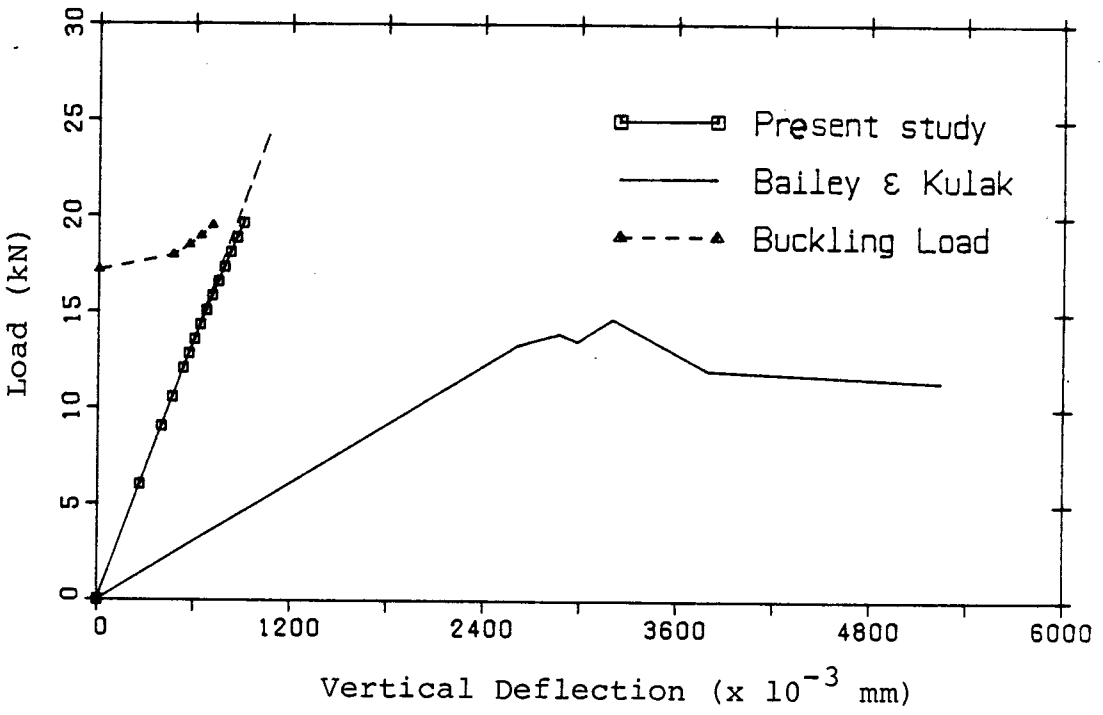

(b) Model S4

Figure 4.5 Load-Response Curves of Models S3 and S4

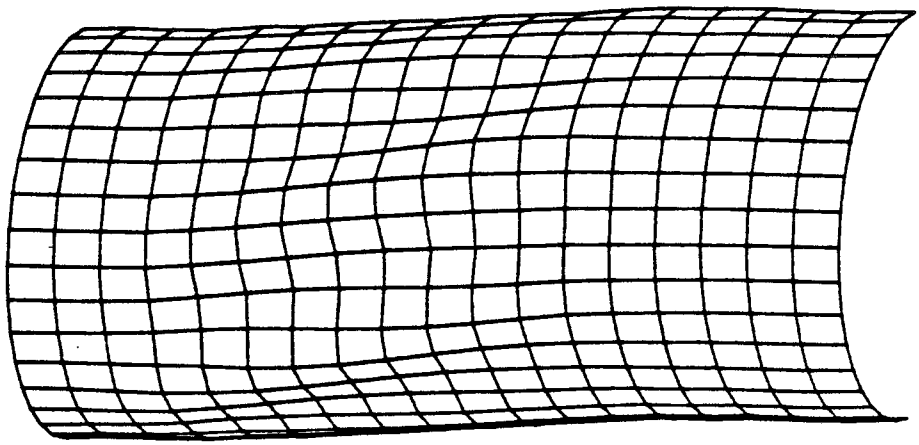

(a) Model S1

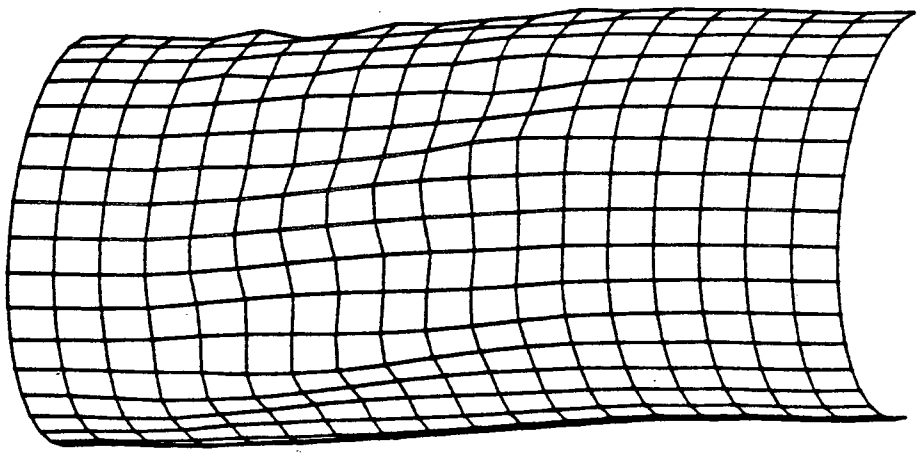

(b) Model S2

Figure 4.6 Deformed Meshes at Maximum Loads for Models S1 and S2

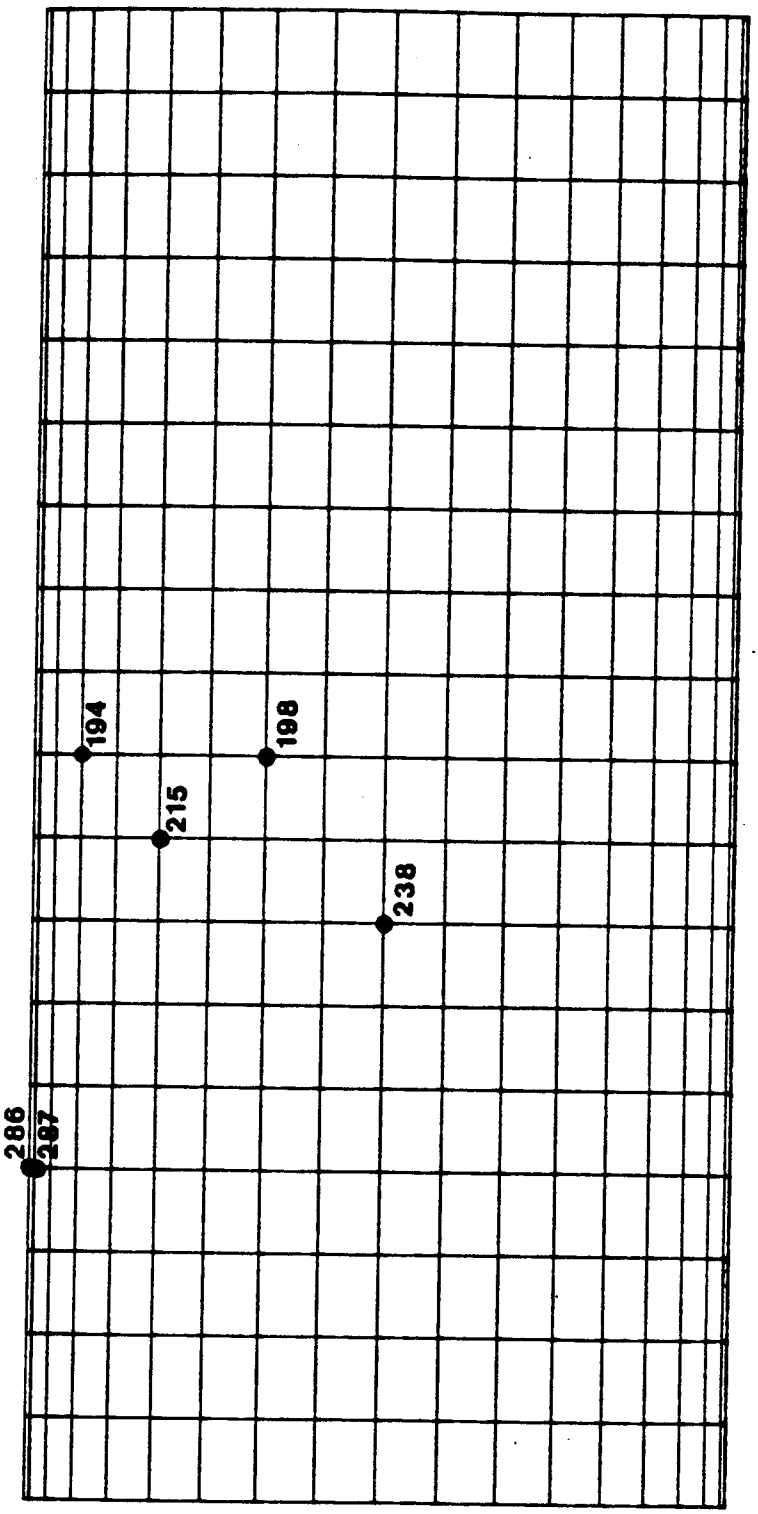

Figure 4.7 Locations of Representative Nodes

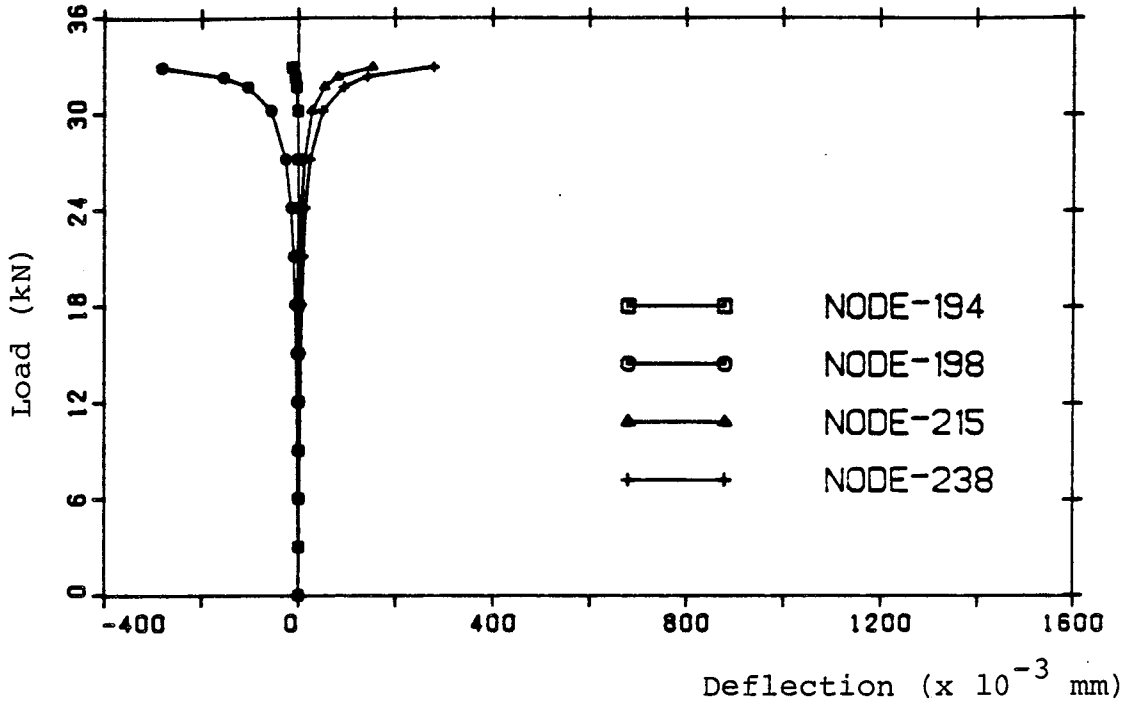

(a) Model S1

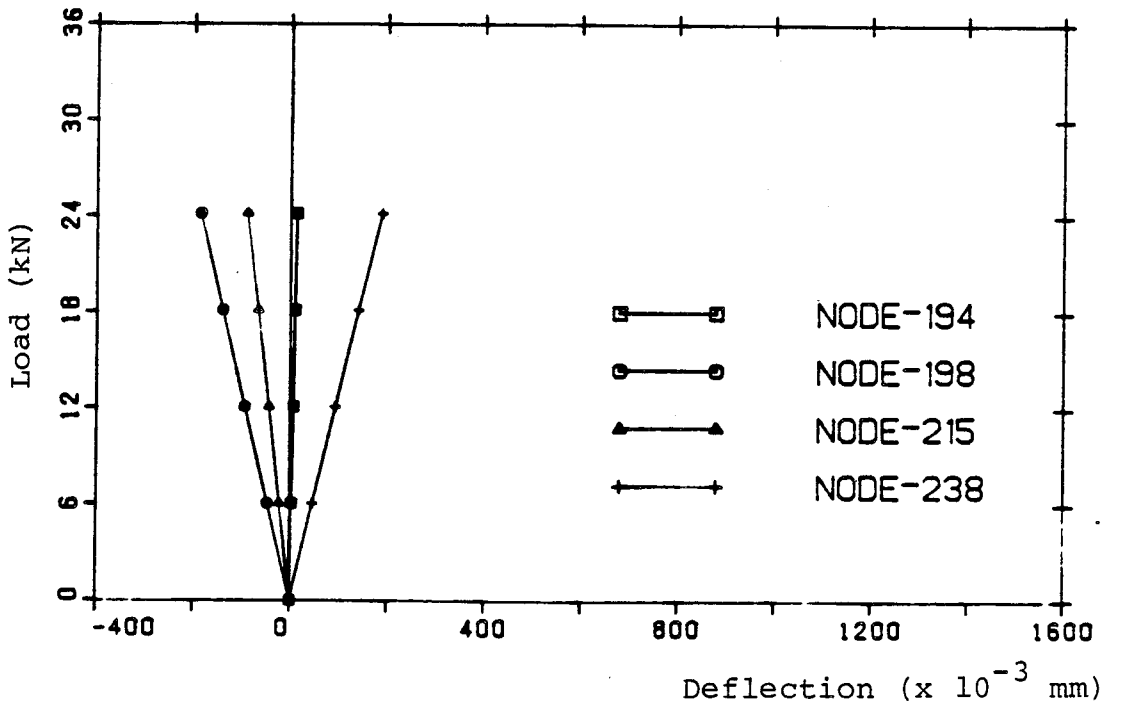

(b) Model S2

Figure 4.8 Load versus Lateral Deflection of Test Span in Models S1 and S2

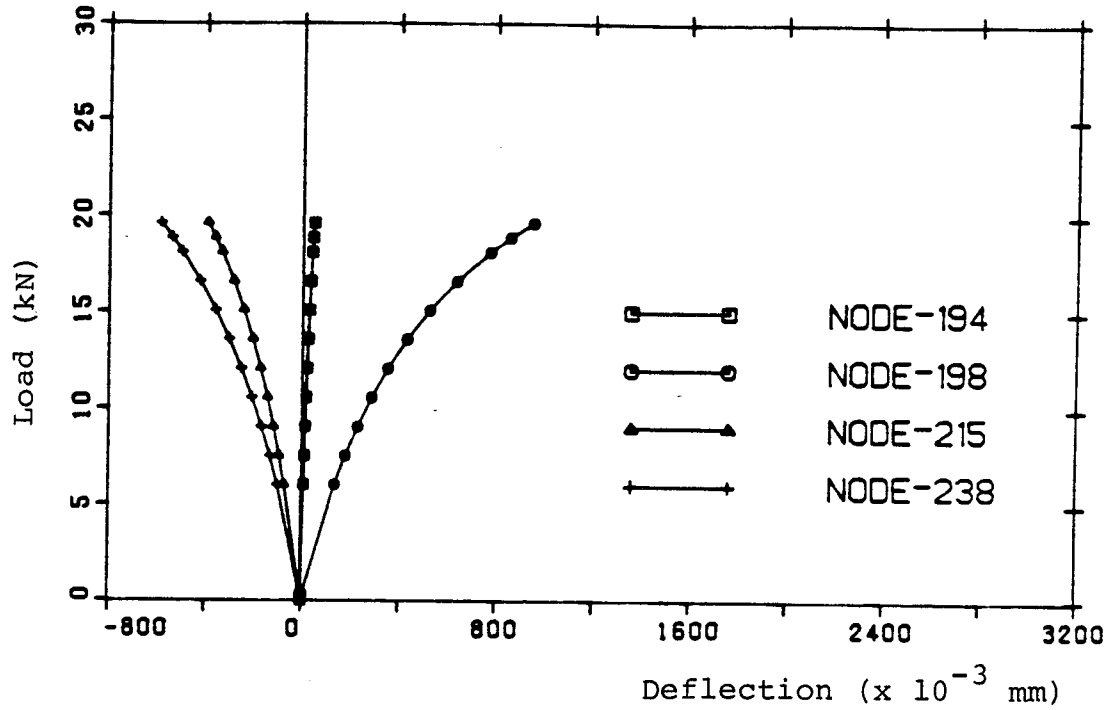

(a) Model S3

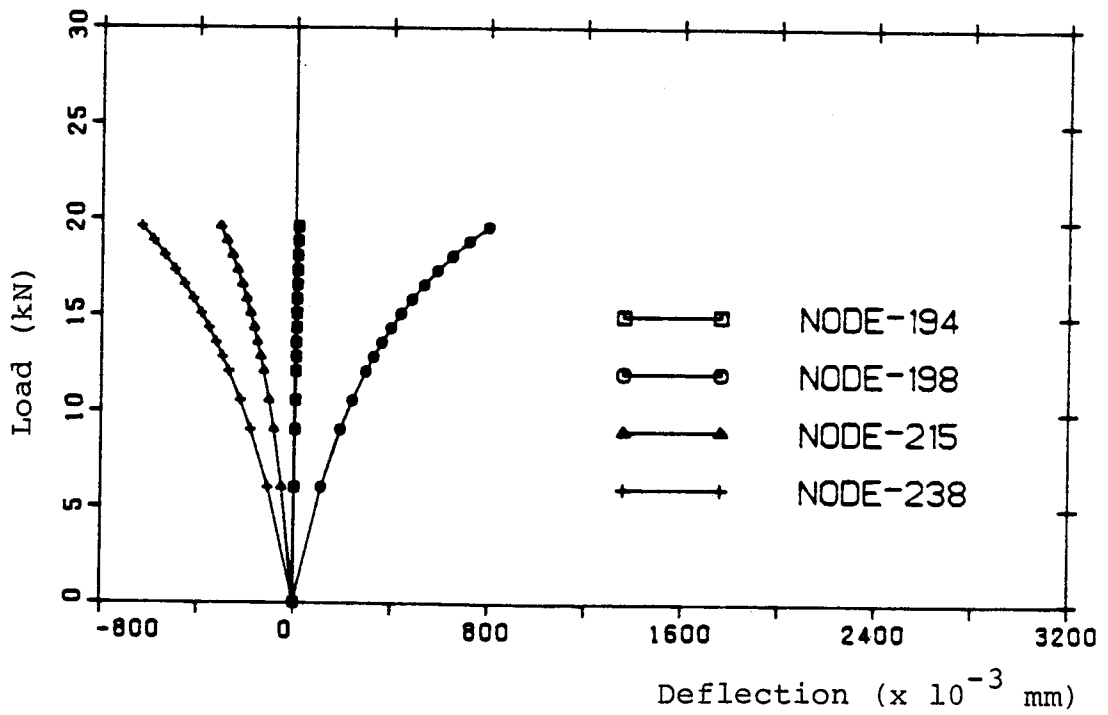

(b) Model S4

Figure 4.9 Load versus Lateral Deflection of Test Span in Models S3 and S4

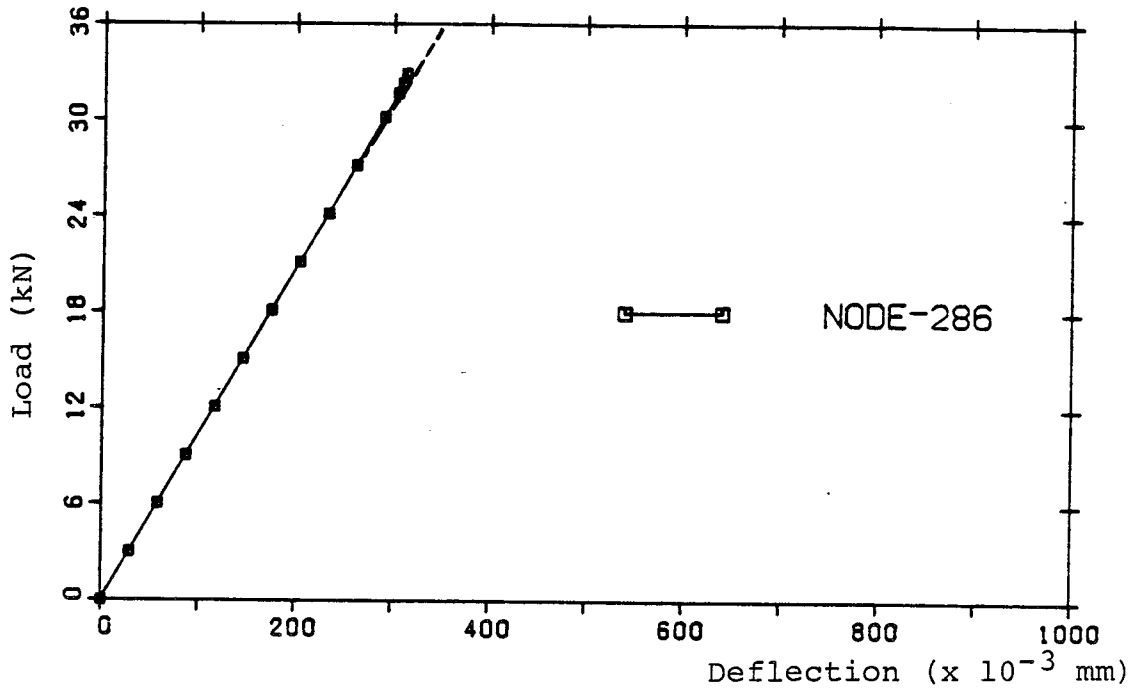

(a) Model S1

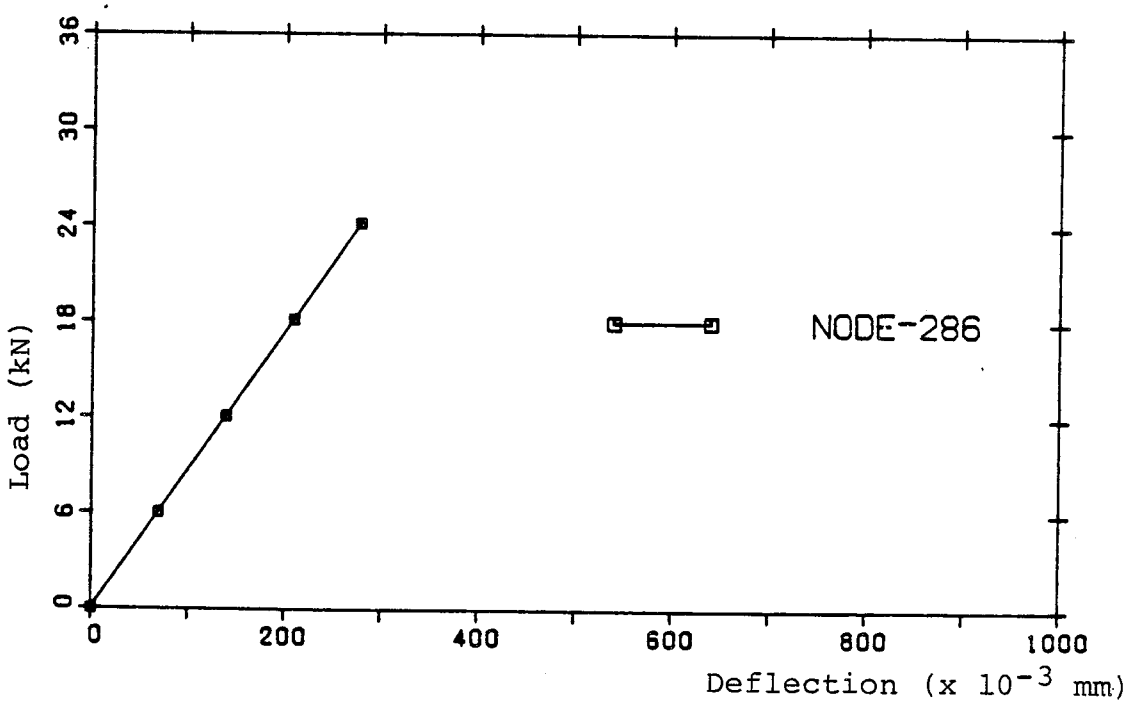

(b) Model S2

Figure 4.10 Load versus Vertical Deflection of Compression Region in Models S1 and S2

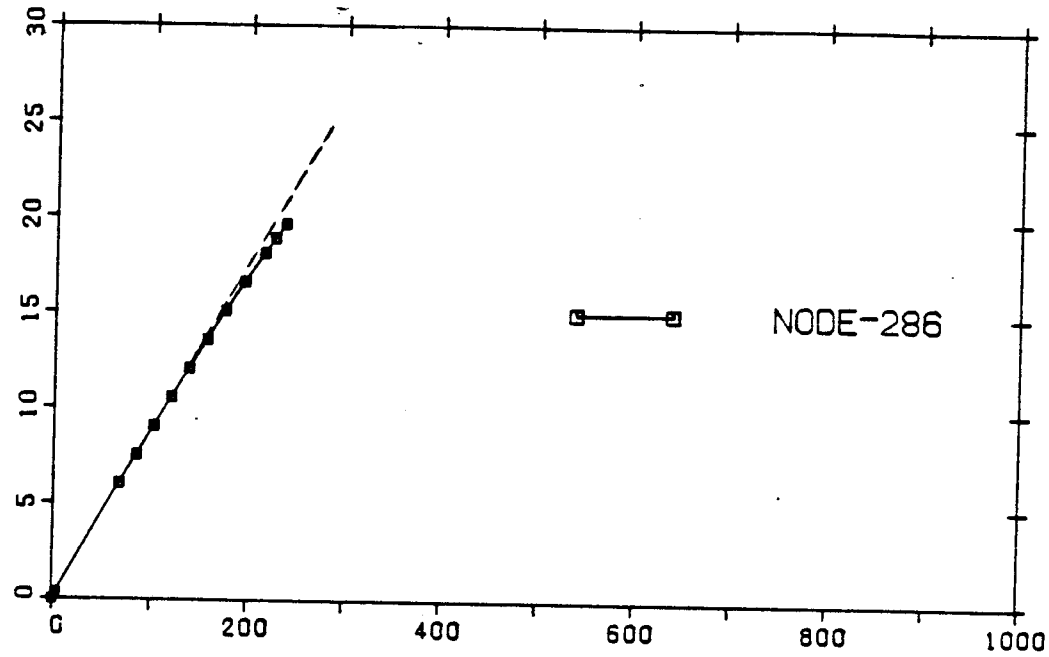

(a) Model S3

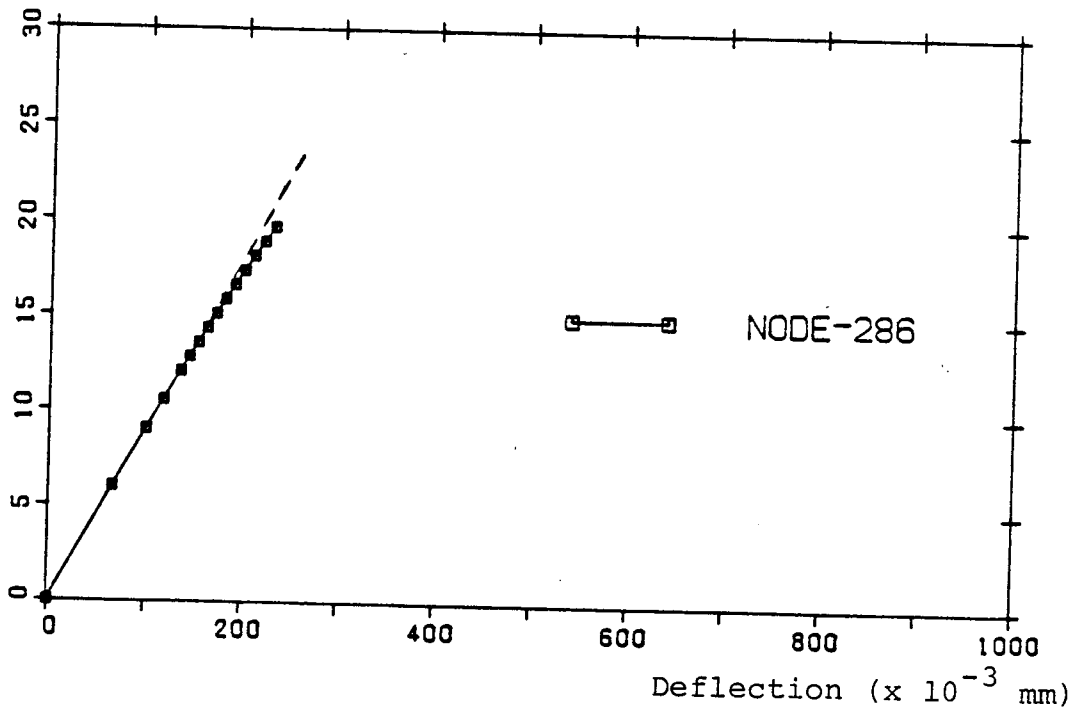

(b) Model S4

Figure 4.11 Load versus Vertical Deflection of Compression Region in Models S3 and S4

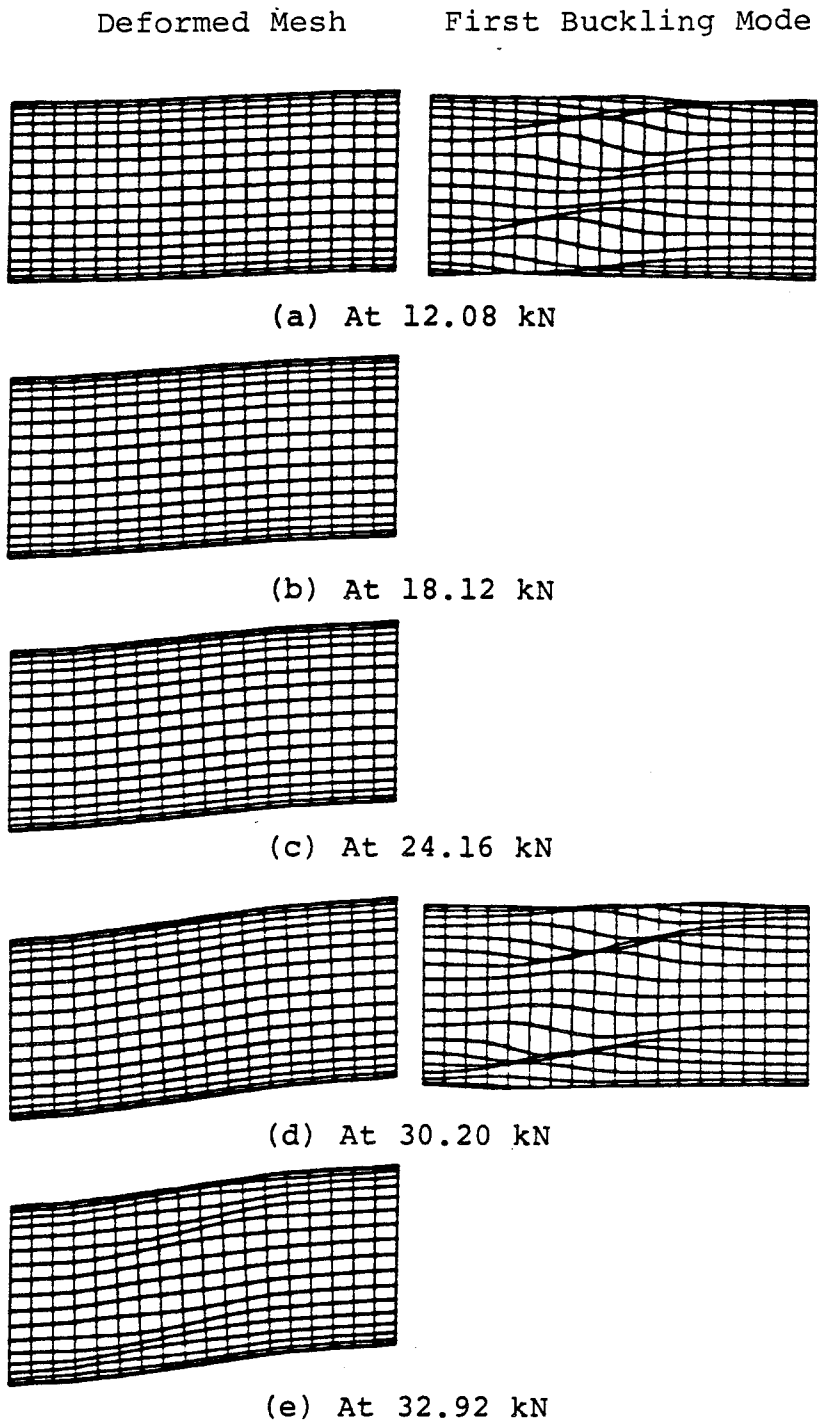

Figure 4.12 Deformed Shapes and Buckling Shapes of Model S1

Deformed Mesh First Buckling Mode

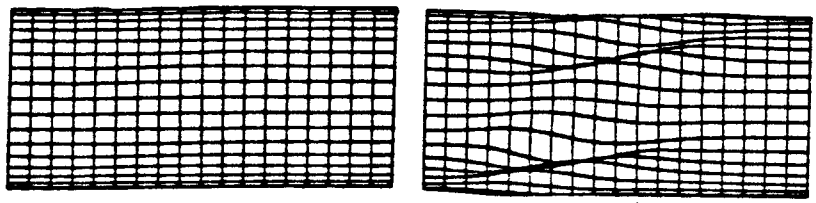

(a) At 6.04 kN

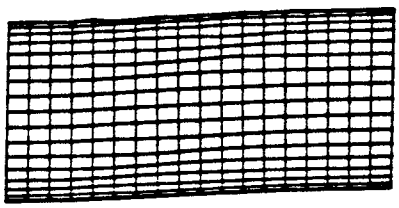

(b) At 12.08 kN

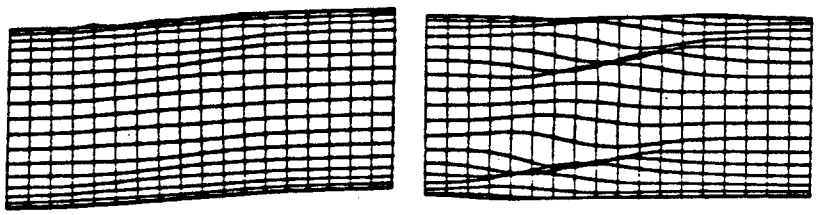

(c) At 18.12 kN

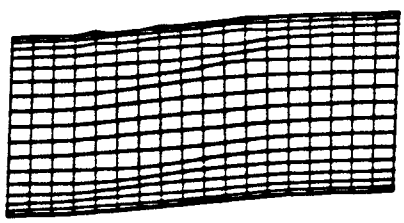

(d) At 24.16 kN

Figure 4.13 Deformed Shapes and Buckling Shapes of Model S2

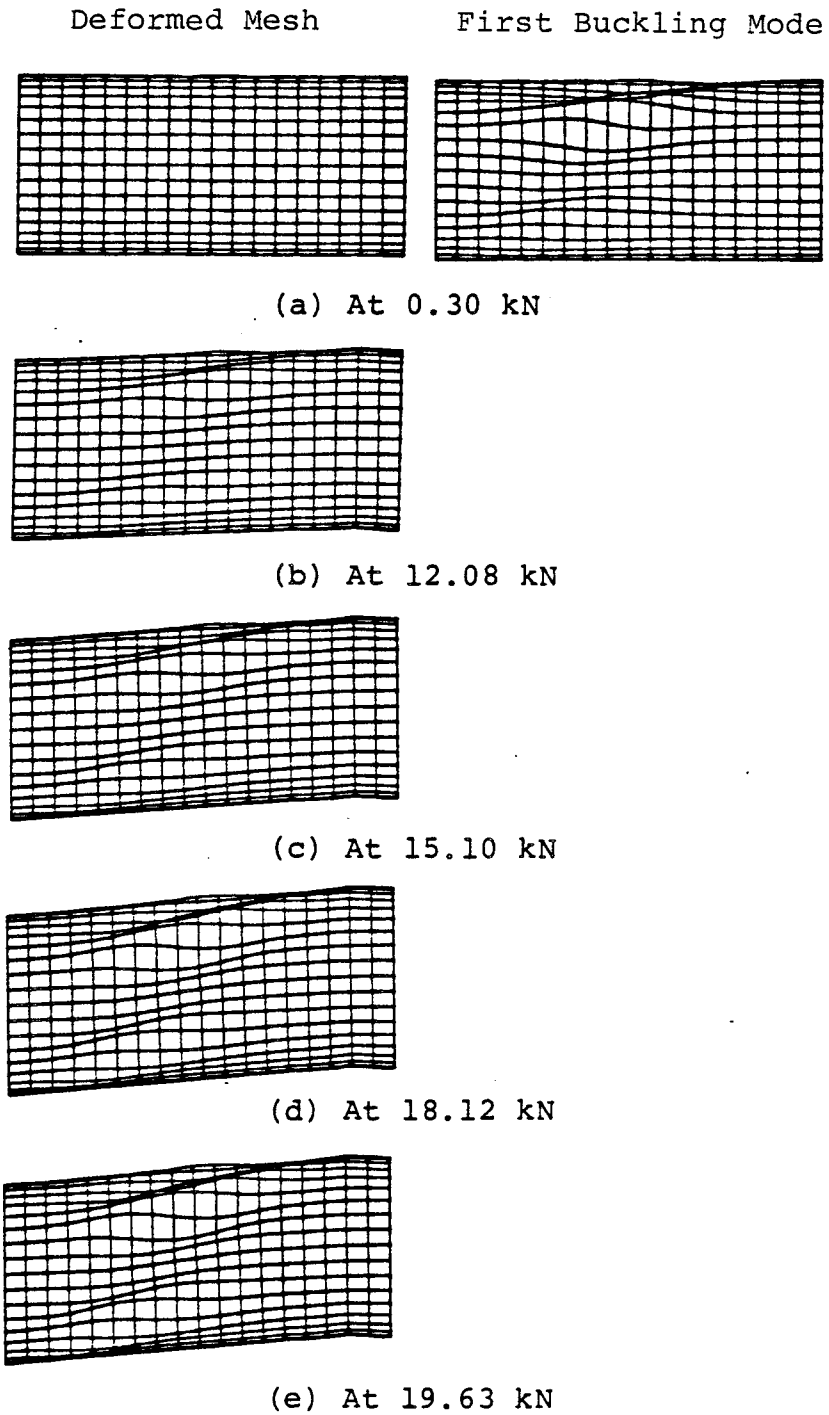

Figure 4.14 Deformed Shapes and Buckling Shape of Model S3

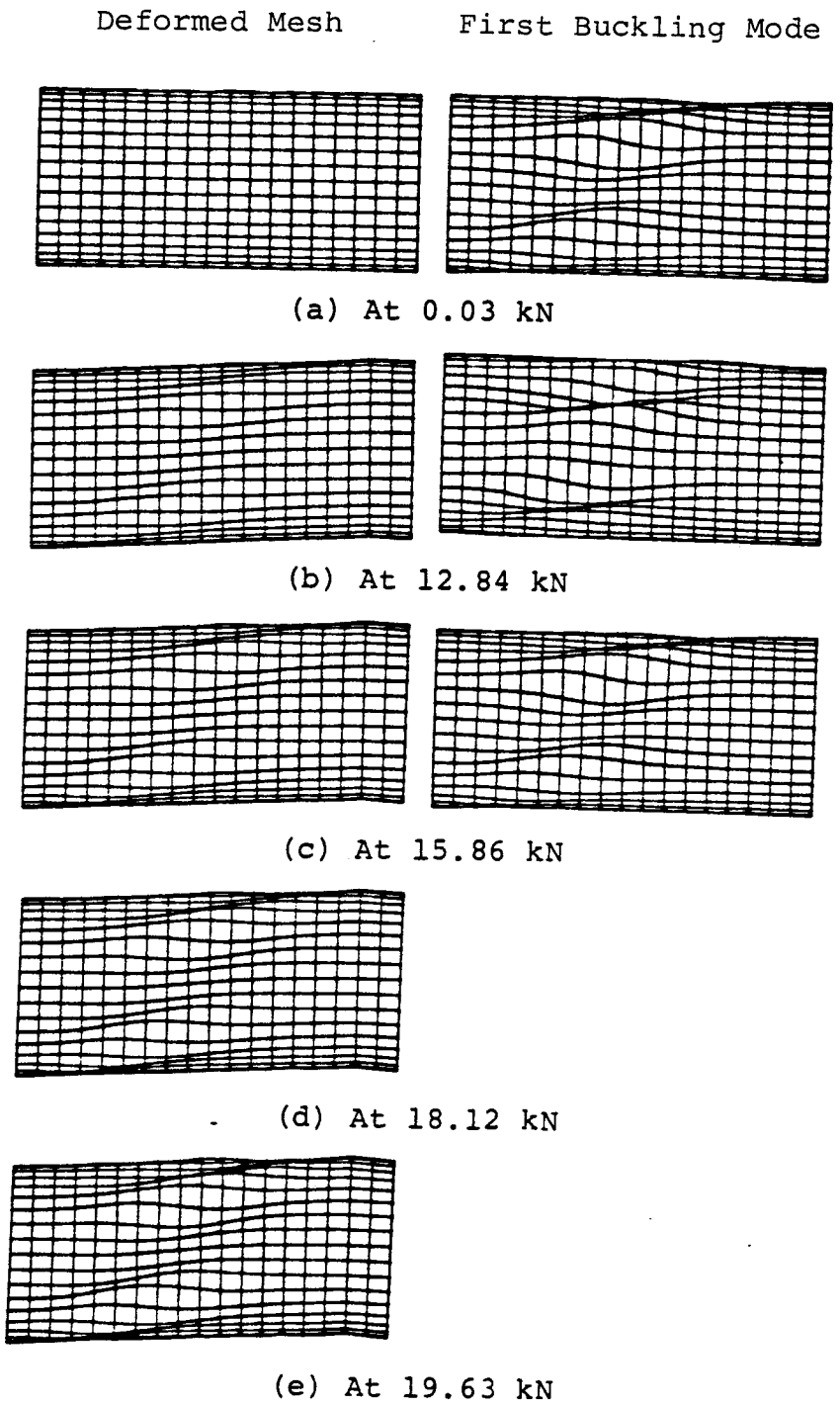

Figure 4.15 Deformed Shapes and Buckling Shapes of Model S4

Table 4.1 Boundary Conditions of Models in Series S

	Boundary Conditions			Remarks
	Fixed Edge	Top and Bottom Longitudinal Edges	[1]Loading Edge	
Model S1	All Fixed	XT,ZT,YR - Free YT,XR,ZR - Fixed	ZT - Coupled XT,YT,XR,YR,ZR - Fixed	All models provide "Fixed-End" conditions. All ZT are coupled at loading edge.
Model S2	All Fixed	XT,ZT,YR - Free YT,XR,ZR - Fixed	ZT, - Coupled XT,YT,XR,YR,ZR - Fixed	
[2]Model S3	All Fixed	XT,ZT,YR - Free XT,XR,ZR - Fixed	YT,ZT,XR - Free XT,YR,ZR - Fixed	
[2]Model S4	All Fixed	XT,ZT,YR - Free YT,XR,ZR - Fixed	XT - Coupled YT,ZT,XR - Free YR,ZR - Fixed	

[1] Refers to the free edge for models S3 and S4.
[2] For models S3 and S4, the loading edge is 72.5 mm from free edge.

Table 4.2 Material and Geometric Properties of Models in Series S

	Material Properties				Geometric Properties				Remarks
	[1]E (MPa)	σ_{ys} (MPa)	ν	[2]R (mm)	L (mm)	t (mm)	$\frac{R}{t}$	$\frac{L}{t}$	
Model S1	204,400	301	0.33	190.0	[3]404.3 [4](134.8,269.5)	[3]0.76 [5](1.52)	[3]250	[3]532	Variable thickness. Each model consists of two end spans and a test span. Initial geometric imperfections are incorporated.
Model S2	204,400	301	0.33	190.0	404.3 (134.8,269.5)	0.76 (1.52)	250	532	
Model S3	204,400	301	0.33	190.0	381.0 (165.0,262.5)	0.76 (1.52)	250	501	
Model S4	204,400	301	0.33	190.0	381.0 (165.0,262.5)	0.76 (1.52)	250	501	

1 E-Hardening is assumed to be zero.
2 Radius of mid-surface.
3 Refers to test span.
4 First number in parentheses refers to the end span closer to the fixed edge, second number refers to the end span closer to the loading edge.
5 Refers to both end spans.

Table 4.3 Scaled Mode-1 Imperfection Values used in the Models of Series S

	[1]Scaled Mode-1 Imperfection Values
Model S1	$\frac{1}{100}$ t
[2]Model S2	$\frac{1}{2}$t (shear), $\frac{3}{2}$t (bending)
Model S3	t
Model S4	t

[1] t = thickness of test span i.e. 0.76 mm

[2] For model S2, effective initial imperfection consists of a linear combination of the shear buckling mode and the compression buckling mode in the ratio according to their respective maximum bending moments in the top compression region of the test span.

Table 4.4 Comparison Between Predicted and Experimental Results

	Batdorf's Prediction (kN)		Stephen's Prediction (kN)	NISA80 Prediction (kN)	$\frac{\text{NISA80}}{\text{Experiment}} \times 100\%$
	Simply-supported	Clamp-edge			
Model S1	31.76	37.81	26.81	32.92	224%
Model S2	31.76	37.81	26.81	24.16	164%
Model S3	32.82	27.22	30.22	19.63	133%
Model S4	23.82	27.22	30.22	19.63	133%

Table 4.5 Comparison of Flexibilities

		Flexibilities $(\frac{\Delta}{P})$, x 10^{-6}mm/N
Simple Beam Theory	Fixed End	$^{1}\Delta_f/P = 15.18$ $^{2}\Delta_v/P = 34.80$ $^{3}\Delta_T/P = 49.98$
	Simple Support	$\Delta_f/P = 67.98$ $\Delta_v/P = 34.80$ $\Delta_T/P = 102.78$
NISA80 Fixed End		$\Delta/P = 48.0$
Experiment		$\Delta/P \simeq 190$

1. Deflections due to flexural deformation.
2. Deflections due to shear deformation.
3. Total deflections.

5. EXAMINATION OF THE TENSION FIELD THEORY

5.1 Introduction

It is suggested by Bailey and Kulak that a tension field develops after buckling of the shell has occurred, it is necessary, as a part of the analysis, to verify the existence of the tension field and to find out the effect on the shear strength of the shell due to such action. Finally, the lack of information and guidelines on this subject in many of the existing design specifications warrants the development of an ultimate strength equation for thin cylindrical shells loaded in shear. In this chapter a stress analysis which indicates the existence of a tension field is presented. Then a tension field analysis based on Basler's tension field theory is carried out, and the contribution to the shear strength is examined. Finally the determination of the total shear capacity of a thin cylindrical shell is presented.

5.2 Stress Analysis

5.2.1 Tension to Compression Ratio Variation

For structures loaded primarily in shear, the effect of a tension field which sets in after the shear portion of the structure loses its rigidity due to buckling should be considered since the influence due to such action could be important. In plate girders, the ability to perform in a manner similar to a truss was recognized as early as 1898

(Salmon, 1971). The tensile forces are carried by membrane action of the web while the compressive forces are carried by stiffeners. To determine the ultimate shear strength of a plate girder, it is necessary to consider the classical buckling theory until buckling has occurred, then the tension field membrane stresses along with the compression forces in stiffeners are used in the post-buckling condition. It is required then, to determine the stress at which first buckling takes place and tension field initiates.

In Bailey and Kulak's experiment, it is suggested that a tension field may have existed after shear buckling of the test span occurred. Any additional loads carried are assumed to be a consequence of the tension field action. In order to find out the contribution of the tension field to the ultimate shear strength of a transversely loaded cylindrical shell, the stress or the load at which the shell buckles has to be determined. From the finite element analyses, complete stress fields are obtained. The stresses are calculated at the Gaussian points in the global coordinate system. Hence, it is required to transform these global stresses to stresses in the local coordinate system. The transformation is done according to the following

$$[\sigma'] = [T]^T[\sigma][T] \qquad (5.1)$$

where [σ'] and [σ] represent the stresses in the local and global coordinate systems respectively, and [T] is the transformation matrix which contains the directional cosines between the two sets of coordinate axes. After [σ'] has been obtained, the principal stresses and their orientations are calculated in the local system. These procedures are repeated at each load step for each model.

To determine the load level at which shear buckling occurs in these models, the following assumptions are made:

1. An element subjected to pure shear in addition to an inclined tension force is considered.
2. After the shell buckles, the compressive principal stress, τ_{cr} remains constant at the buckling stress level.
3. Any subsequent load carried is due to the tension field stress σ_t in addition to the compressive principal stress τ_{cr}.

The above assumptions imply that the maximum principal stresses (tensile) increase while the minimum principal stresses (compressive) remain at a constant value. Hence, by examining the ratio of the tensile stress to compressive stress, the buckling stress is the level of stress at which this ratio begins to increase. Figs. 5.1 and 5.2 show the variations of the tension to compression ratio at several representative Gaussian points (local system) in the test spans.

In Fig. 5.1a, the tension to compression ratio starts

to increase at about 30 kN, which agrees with the previous observations made in Chapter 4 when the load-response curves were discussed. This implies that model S1 buckles in a shear mode at this load level and tension field action develops thereafter. Any subsequent load carrying capacity is contributed from the tension field action. In Fig. 5.1b, however, the curve does not show any increase in the ratio and this suggests that no tension field is developed in model S2. This further indicates that the shear buckling stress had not been reached and no shear buckling occurs in the test span of model S2.

The curves for model S3 and model S4 are shown in Fig. 5.2. The tension to compression ratio gradually increases after a load of about 10 kN in both models. This level is determined by a visual examination of the departure from an initial straight line. Although there are some slight increases in the ratio before this load level, it is assumed that the models buckle at this load and any subsequent load carried is the result of the tension field action.

5.2.2 Principal Stresses

In order to have a better understanding of the pattern of the tension field, the principal stresses at the maximum load level of the mid-surface in the local coordinate system are plotted in Fig. 5.3 for models S1 and S2 and in Fig. 5.4 for models S3 and S4. The principal stresses are shown on flat meshes instead of curved ones and are plotted at the

four Gaussian points for each of the 36 elements in each model. The scale for the stresses is 312 MPa/cm. Any tensile stress above 90 MPa is shown with a large arrowhead.

In Fig. 5.3a, the principal stresses for model S1 are shown. It is clear that a tension field is well developed in this model. The tension field in the test span is anchored along the two edges which are attached to the two thicker end spans which in turn find anchorage from the boundary supports at the two ends. In Fig. 5.3b, it is obvious that a tension field does not exist in the test span of model S2. This agrees with the observation made earlier in the previous section that in model S2, the shear buckling stress has not been reached.

Fig. 5.4 shows that the principal stress patterns obtained for model S3 and model S4 are very similar. It can be seen that in both models some tension field action, although not fully developed, exists in the test span. Anchorage for the tension field is provided by the two edges attached to the two thicker spans as in model S1.

Another point of interest is the orientation of these principal stresses. According to Salmon (1971) the angle between the tension field stress and the horizontal, ζ, is always less than 45°. Hence, the angle of inclination of the maximum principal stress, ζ', resulting from the combined stress conditions is also less than 45°. For the models in the present analysis, the central region of the test span, at which flexural stresses are minimum, is

closest to the pure shear condition. In models S1 and S2, ζ' is found to fall in the neighborhood of 45° while in models S3 and S4, ζ' is between 30° and 45°.

5.3 Tension Field Analysis

5.3.1 General

As indicated in the previous section, tension field action exists in all models except model S2. The contribution of the tension field action to the ultimate shear strength, however, is still unknown. In the literature, little theoretical work has been done in determining the tension field strength of a transversely loaded cylindrical shell. The tension field theory in plate girders developed by Basler (1961) and modified for cylinders by Bailey and Kulak (1984) is adopted with some changes in this analysis and is used as the guideline to develop the ultimate shear strength equation.

5.3.2 Angle of Inclination of Tension Field

The tension field develops only through a strip of the test span, as shown in Fig. 5.5. The following assumptions have been made:

1. The top and bottom longitudinal edges do not provide any anchorage for the tension field action, because of the small local bending stiffness of the shell top and bottom edges.
2. The tension field stress σ_t is constant and uniform.

Using the notation shown in Fig. 5.5, the arc covered by the tension field is

$$\alpha = \cos^{-1}\left(1 - \frac{y_1}{R}\right) \tag{5.2}$$

where $y_1 = 2R - y_2$ (5.3a)

$y_2 = L \tan \zeta$ (5.3b)

Substituting Eqs. 5.3a and 5.3b into Eq. 5.2, the following is obtained

$$\cos \alpha = \left(\frac{L}{R} \tan \zeta - 1\right) \tag{5.4}$$

Since σ_t is inclined at an angle of ζ to the horizontal, the set of stresses obtained through a rotation of $-\zeta$ (clockwise direction) is given as

$$\sigma_x = \frac{\sigma_t}{2} + \frac{\sigma_t}{2} \cos (2\zeta) \tag{5.5a}$$

$$\sigma_y = \frac{\sigma_t}{2} - \frac{\sigma_t}{2} \cos (2\zeta) \tag{5.5b}$$

$$\tau_{xy} = \frac{\sigma_t}{2} \sin (2\zeta) \tag{5.5c}$$

Calculation of the vertical force component of the tension field can be carried out by dividing the tension field into narrow strips of width dW, where

$$dW = Rd\phi \tag{5.6}$$

The vertical force component dF in each strip, can be described as

$$dF = \tau_{xy} \cdot \sin \phi \cdot t \cdot dW \tag{5.7}$$

Substituting Eqs. 5.5c and 5.6 into Eq. 5.7, the following is obtained

$$dF = \frac{\sigma_t}{2} \sin (2\zeta) \sin \phi \cdot t \cdot R \cdot d\phi \tag{5.8}$$

Integrating the vertical force component dF over the arc α, the total vertical force V_t for a full shell is given as

$$V_t = 2 \int_o^{\alpha} d\ F \tag{5.9}$$

Substituting Eq. 5.8 into Eq. 5.9, V_t can be expressed as

$$V_t = \sigma_t \cdot t \cdot R \sin (2\zeta) (1 - \cos \alpha) \tag{5.10}$$

Substituting Eq. 5.4 into Eq. 5.10, V_t can be rewritten as

$$V_t = \sigma_t \cdot t \cdot R \cdot \sin (2\zeta) \left(2 - \frac{L}{R} \tan \zeta\right) \tag{5.11}$$

It is reasonable to expect that the direction of the tension field assumes the most efficient orientation

(Basler, 1961). Differentiating Eq. 5.11 with respect to ζ and setting the derivative equal to zero gives the angle of inclination of the tension field, ζ. as

$$\zeta = \frac{1}{2} \tan^{-1} \left(2 \frac{R}{L}\right) \qquad (5.12)$$

In this study, the radius to the mid-surface of the shells is 190 mm and the length of the test span is 404.2 mm for models S1 and S2, and 381 mm for models S3 and S4. Substituting these values into Eq. 5.12, the angle of inclination, ζ, of the tension field is obtained for each model. ζ is found to be 21.6° for models S1 and S2, and 22.5° for models S3 and S4.

These values are compared with the angle of inclination measured from the deformed meshes of the models. By measurement, ζ is 20° for model S1, 22° for model S3 and 23° for model S4. In addition, the angle of inclination of the buckles in the Bailey and Kulak test was 24°. Good agreement exists between the measured values and the predicted values based on Eq. 5.12. No comparison is made for model S2 since it does not buckle in the shear mode. It is concluded that Eq. 5.12 describes the angle of inclination, ζ, of the tension field for a thin cylindrical shell loaded in transverse shear.

5.3.3 Contribution of Tension Field Action

In order to determine the shear contribution due to the

tension field action, it is required to determine the additional tensile stress, σ_t, existing after the shell buckles. A method to obtain σ_t is presented here. Besides the assumptions made earlier, the following assumptions are necessary.

1. The shell behaves elastically and linearly before the onset of buckling.
2. After the shell buckles, additional shear is carried by tension field action only. Thus, the tension field stress, σ_t, acts in addition to the critical principal stresses, τ_{cr}, as shown in Fig. 5.6b.

In section 5.2.1, the load levels at which the shells buckle in a shear manner are determined based on the deviation of the tension compression ratio of the principal stresses in the zero bending region of the shell, from an initial straight line portion. It is found that model S1 buckles at 30 kN, model S2 does not show any evidence of shear buckling, and models S3 and S4 both buckle in a shear mode at 10 kN. The difference between these buckling loads and the maximum loads achieved in the analyses are the tension field contributions. The additional tensile stress, σ_t is obtained as follows:

1. At an early stage of loading, the stresses [σ] at several Gaussian points in the regions of small bending moments (central portion of the test span) are obtained.
2. These stresses are then scaled linearly by a factor,

Q, equal to the ratio between the buckling load and the early load in step 1 to obtain Q[σ].

3. The difference between the set of stresses $[\sigma_{MAX}]$ at the maximum load and the set of scaled stresses Q[σ] is the additional set of stresses, [Δσ], arising after the shell buckles.
4. The result from step 3 is then transformed from the global coordinate system to the local coordinate system, thus local stresses $[\Delta\sigma]_{LOCAL}$ are obtained.
5. The principal stresses corresponding to these local stresses are then calculated. Theoretically, only the tensile (maximum) principal stress should exist since the shell cannot take any compression in the minor principal direction after buckling occurs. The tensile principal stress obtained is the additional tensile stress, σ_t, existing in the tension field.

Employing the above procedures, an average value of σ_t for the tension field region is obtained for each model. σ_t is found to be 35 MPa for model S1, 55 MPa for model S3, and 60 MPa for model S4. Using these σ_t values and the angle of inclination, ζ, according to Eq. 5.12, the shear contribution, V_t, due to the tension field action for each model can be calculated from Eq. 5.11. V_t is found to be 2.15 kN for model S1, 3.55 kN for model S3, and 3.88 kN for model S4. These values are then compared with the actual shear contributions which are obtained as the differences

between the maximum loads and the buckling loads established previously. The actual shear contribution is 2.92 kN for model S1, and 9.63 kN for models S3 and S4. The percentage difference between the actual values and the predicted values from Eq. 5.11 is found to be 26% for model S1, 63% for model S3, and 60% for model S4.

It is apparent that better agreement exists in model S1. This may be explained by the fact that, in models S3 and S4, there is some nonlinearity existing before the assumed buckling load is reached, while in model S1, the behaviour is linear before the buckling load is reached, which in fact is one of the assumptions required.

5.3.4 Determination of Total Shear Capacity

In this section, the shear strength of a full cylindrical shell is examined. As mentioned previously, it has been suggested by Bailey and Kulak that provided reaction points exist for the development of tension field action, the shear capacity of a thin shell, consists of two components; namely, the "beam shear" component and the "tension field" component. The relationship can be described as follows:

$$V_u = V_b + V_t \tag{5.13}$$

where V_u is the ultimate strength of the cylindrical shell, V_b is the beam shear strength, and V_t is the tension field

strength.

The beam shear strength, V_b, is simply that capacity attained at the point of theoretical shear buckling, if no shear yielding nor compression buckling occurs prior to this. For thin cylindrical shells, shear buckling usually occurs before the shear yield stress is reached. In pure shear conditions or in situations where the bending stresses are small, compression buckling is unlikely to occur. In that case, V_b can be expressed as

$$V_b = \frac{\tau_{cr} A}{2} \tag{5.14}$$

where A is the cross-sectional area of the shell, 2 is the shape factor for thin shells, and τ_{cr} is the theoretical buckling stress for shells under transverse shear. In the literature, a source for τ_{cr} is contained in the work by Batdorf et al. (1947). Batdorf's solution, however, is obtained based on the small-displacement theory of perfect shells. The effect of initial imperfection, hence, is precluded. In order to account for this, a critical-shear-stress reduction factor, F, is applied to τ_{cr}. The determination of F, which requires more testing of thin cylindrical shells with different magnitudes of initial geometric imperfections, is not available at this time. However, a sketch of the variation of the "reduction" factor is shown in Fig. 5.7 in which F is expressed as P_b/P_{cr}, and is plotted against the scaled mode-1 imperfection values

used in the models of series S in this study. P_b is the actual buckling load and P_{cr} is the predicted buckling value according to Batdorf et al.

Applying the "reduction" factor to the critical buckling stress and realizing that the cross-sectional area A of a shell can be expressed as $2\ V_{ys}/\tau_y$ at shear yielding, Eq. 5.14 can be rewritten as

$$V_b = F\ \tau_{cr}\ \frac{V_{ys}}{\tau_y} \tag{5.15}$$

where τ_y is the shear yield stress, and V_{ys} is the shear yield strength. In general, τ_y is taken as $\sigma_y/\sqrt{3}$. Hence, V_b can be expressed as

$$V_b = \sqrt{3}\ F\ \tau_{cr}\ \frac{V_{ys}}{\sigma_y} \tag{5.16}$$

or

$$V_b = K_{ys}\ V_{ys} \tag{5.17}$$

where K_{ys} is a dimensionless parameter defined as

$$K_{ys} = \sqrt{3}\ F\ \frac{\tau_{cr}}{\sigma_y} \tag{5.18}$$

The second component of the ultimate shear capacity is the tension field contribution, V_t defined by Eq. 5.11. In order to compute the tension field stress σ_t explicitly, the

following assumptions are required:

1. No compression buckling occurs at the compression regions after shear buckling has occurred. This assumption implies that failure takes place by yielding of the diagonal element.
2. The superposition of the stresses resulting from the tension field stress and the beam shear stress is limited by the state of stress which fulfills the yield conditions, as shown in Fig. 5.6b.

According to the second assumption, the tension field stress σ_t is defined as the stress which can be added to the state of shear stress at the point of shear buckling (where $\tau_{xy} = F\tau_{cr}$) such that unrestricted yielding occurs in the tension field. Note that the buckling stress is $F\tau_{cr}$ since this is the stress at which a real shell buckles. The following derivation follows Basler's work on the tension field analysis of plate girders (1961). Attention is given to the subscripts used (Fig. 5.6b). The fixed coordinates are x and y. The Cartesian coordinates u and v are generated by rotating x and y in the counterclockwise direction by the magnitude of ζ. When ζ equals 45°, these are called axis 1 and 2. By means of Mohr's circle, the state of shear stresses ($\tau_{xy} = F\tau_{cr}$) superimposed on the diagonal tension stress σ_t under the inclination ζ is:

$$\sigma_u = F\,\tau_{cr} \sin(2\zeta) + \sigma_t \qquad (5.19a)$$

$$\sigma_v = - F \tau_{cr} \sin (2\zeta) \tag{5.19b}$$

and

$$\tau_{uv} = F \tau_{cr} \cos (2\zeta) \tag{5.19c}$$

Substituting this set of stresses into von Mises' yield criterion,

$$\sigma_u^2 + \sigma_v^2 - \sigma_u\sigma_v + 3\tau_{uv}^2 - \sigma_y^2 = 0 \tag{5.20}$$

the following result for the tension field stress σ_t is obtained:

$$\sigma_t = K_t \sigma_y \tag{5.21}$$

where,

$$K_t = \sqrt{1 + \left(\frac{F\tau_{cr}}{\sigma_y}\right)^2 \left\{\left[\frac{3}{2} \sin (2\zeta)\right]^2 - 3\right\}} - \frac{3}{2} \frac{F\tau_{cr}}{\sigma_y} \sin (2\zeta) \tag{5.22}$$

With this expression for σ_t, the tension field strength V_t defined by Eq. 5.11 can be rewritten as

$$V_t = R\ t \sin 2\zeta \left(2 - \frac{L}{R} \tan \zeta\right) K_t \sigma_y \tag{5.23}$$

For thin cylindrical shells, the cross-sectional area A can

be approximated as $2\pi Rt$, hence Eq. 5.23 becomes

$$V_t = \sin 2\zeta \left(2 - \frac{L}{R} \tan \zeta\right) K_t \frac{A}{2\pi} \sigma_y \tag{5.24}$$

Noting that the tensile yield strength Vy_t of a shell loaded in tension is $A\sigma_y$, Eq. 5.24 can be rewritten as

$$V_t = Ky_t \, Vy_t \tag{5.25}$$

where Ky_t is a dimensionless parameter and is given as

$$Ky_t = \frac{K_t}{2\pi} \sin 2\zeta \left(2 - \frac{L}{R} \tan \zeta\right) \tag{5.26}$$

With this expression the ultimate shear strength computation for a thin cylindrical shell is completed. According to Eqs. 5.13, 5.17 and 5.25 the ultimate shear strength is given as

$$V_u = Ky_s \, Vy_s + Ky_t \, Vy_t \tag{5.27}$$

where Vy_s and Vy_t are the shear yield strength and the tensile yield strength respectively, Ky_s and Ky_t are dimensionless parameters which depend on E, σ_y, ν, R, L, t and F.

In summary, the main parameters that appear to govern the shear strength of thin cylindrical shells are the R/t ratio, L/t ratio, the yield stress, the level of initial

geometric imperfections and the level of residual stress which, however, is not considered in this study. The ultimate shear strength V_u as described in Eq. 5.28, obviously, needs further modifications and comparison with experimental results before it can be used for design purposes. In addition, a parallel development should be carried out in which the limit of tension field action is the buckling of the compression element. Further analysis should include residual stresses and wider ranges of initial geometric imperfection levels. Better assessment should also be made in the preparation of geometric imperfections and in the modelling of boundary conditions.

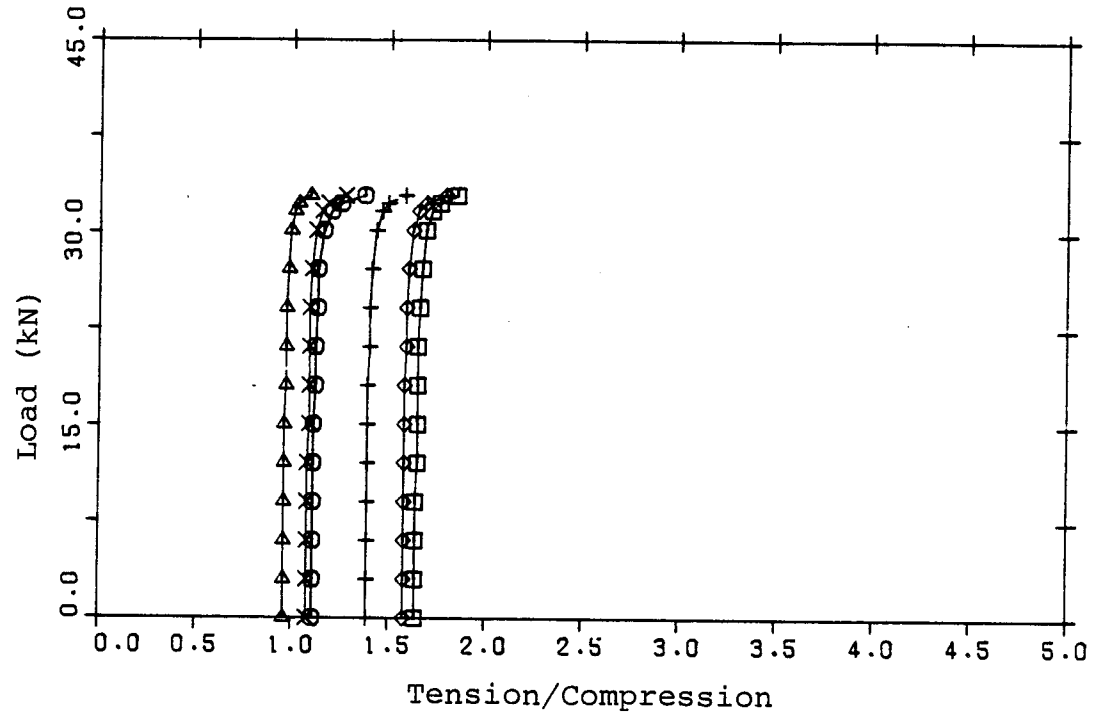

(a) Model S1

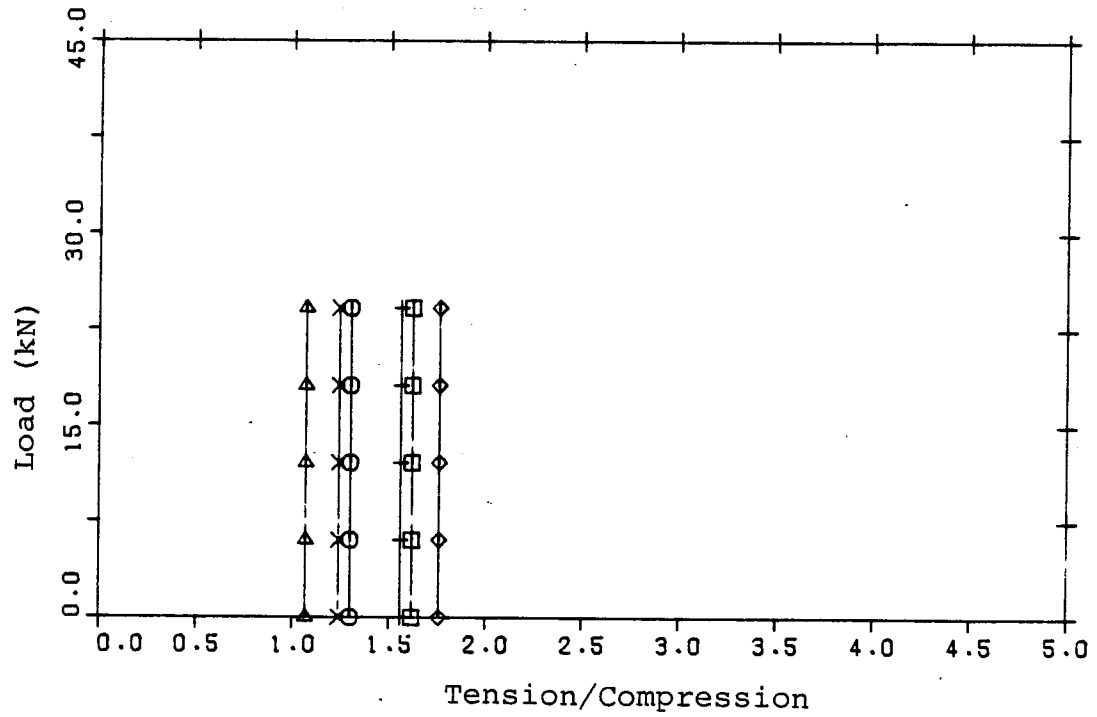

(b) Model S2

Figure 5.1 Variation of Tension to Compression Ratio for Models S1 and S2

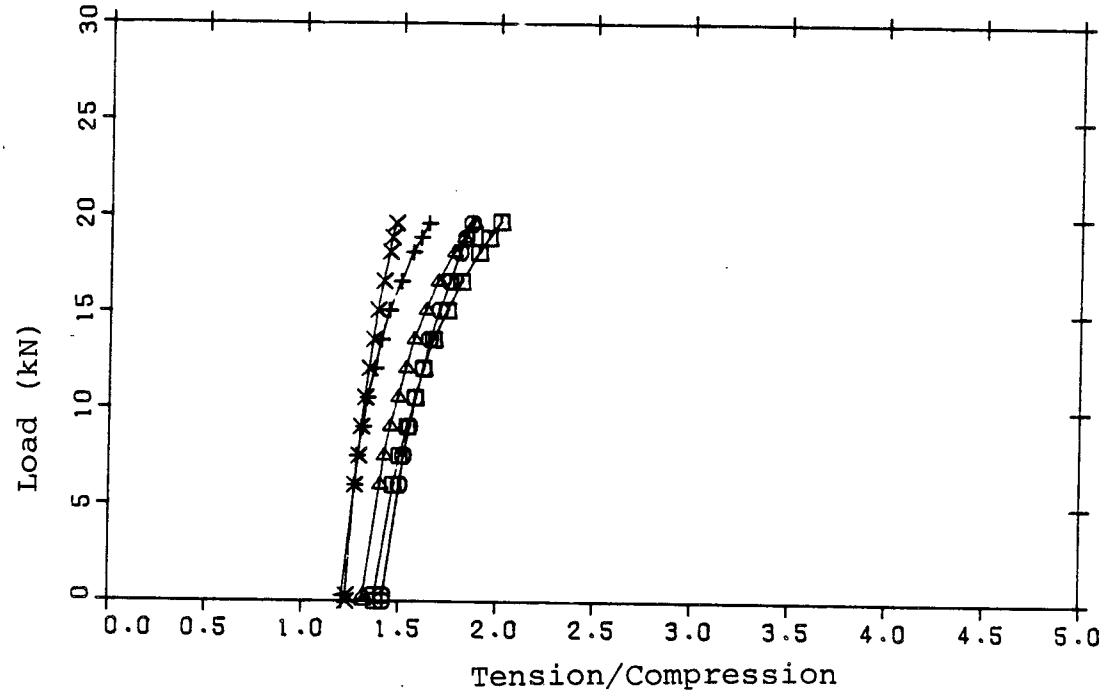

(a) Model S3

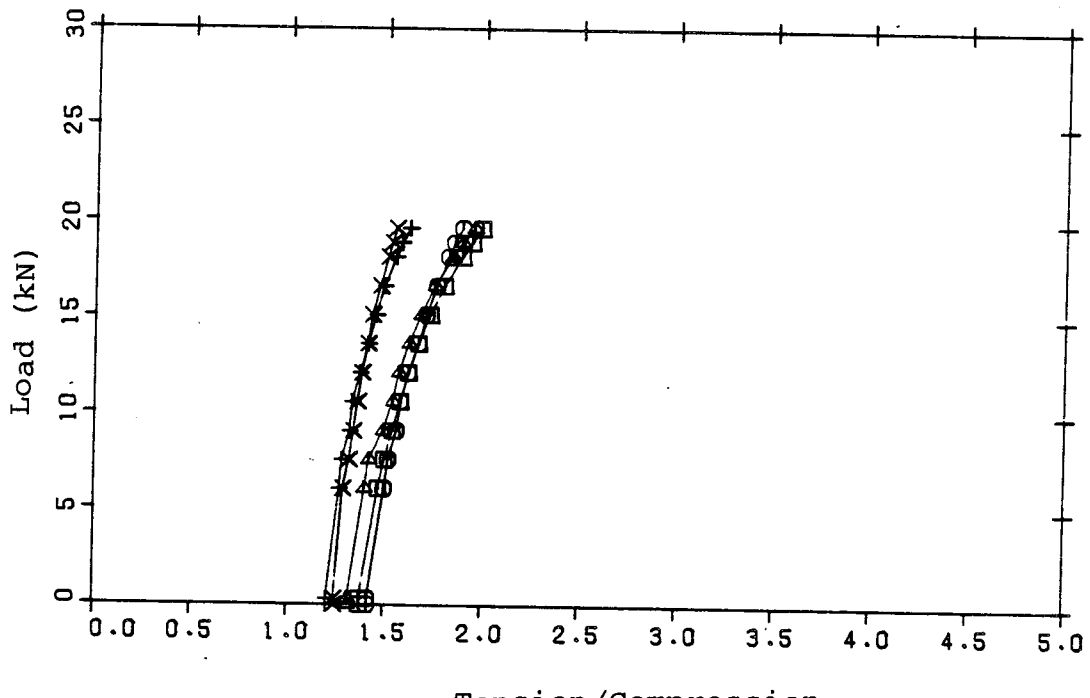

(b) Model S4

Figure 5.2 Variation of Tension to Compression Ratio for Models S3 and S4

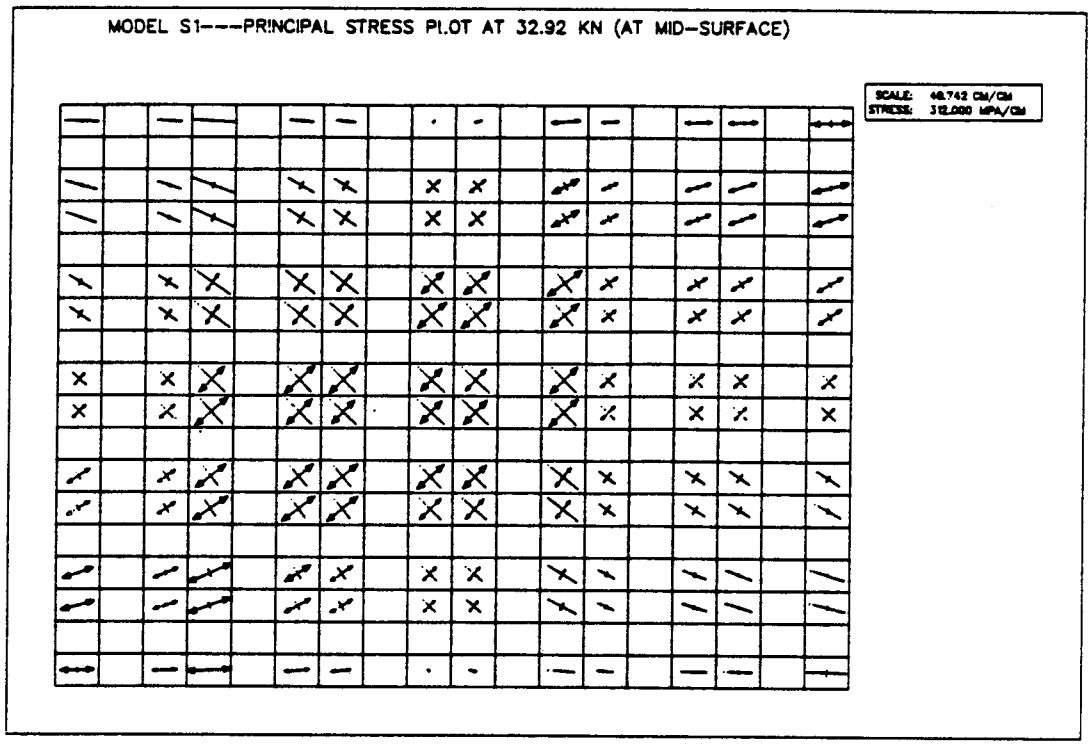

(a) Model S1

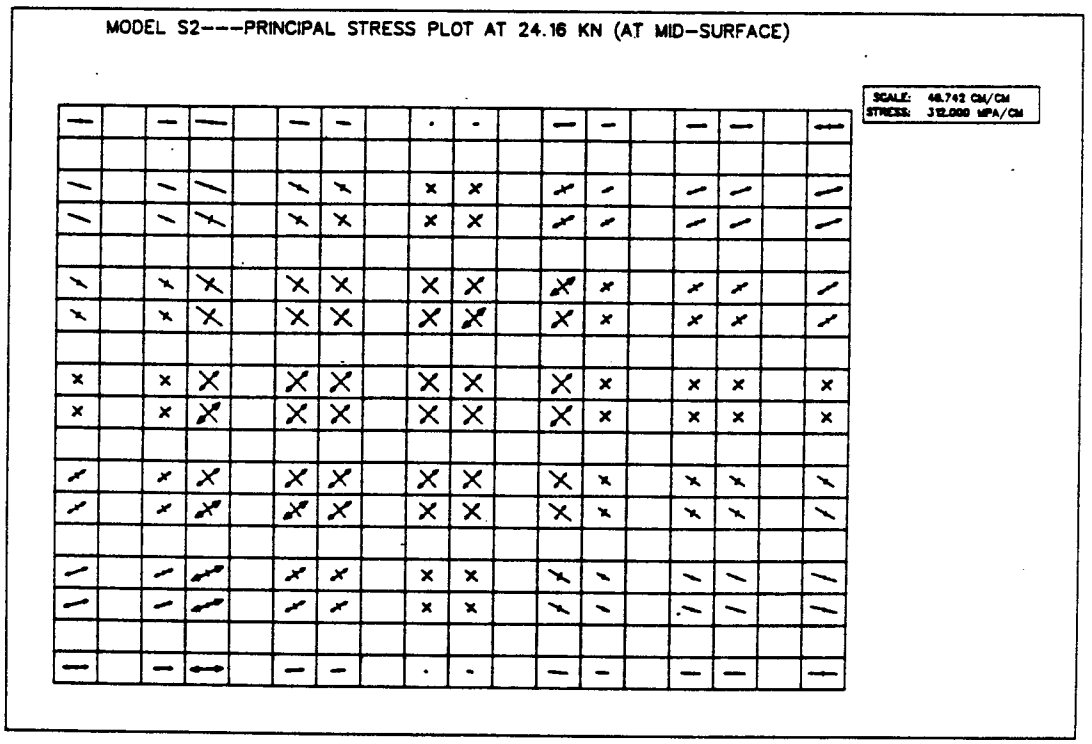

(b) Model S2

Figure 5.3 Principal Stress Plots for Models S1 and S2

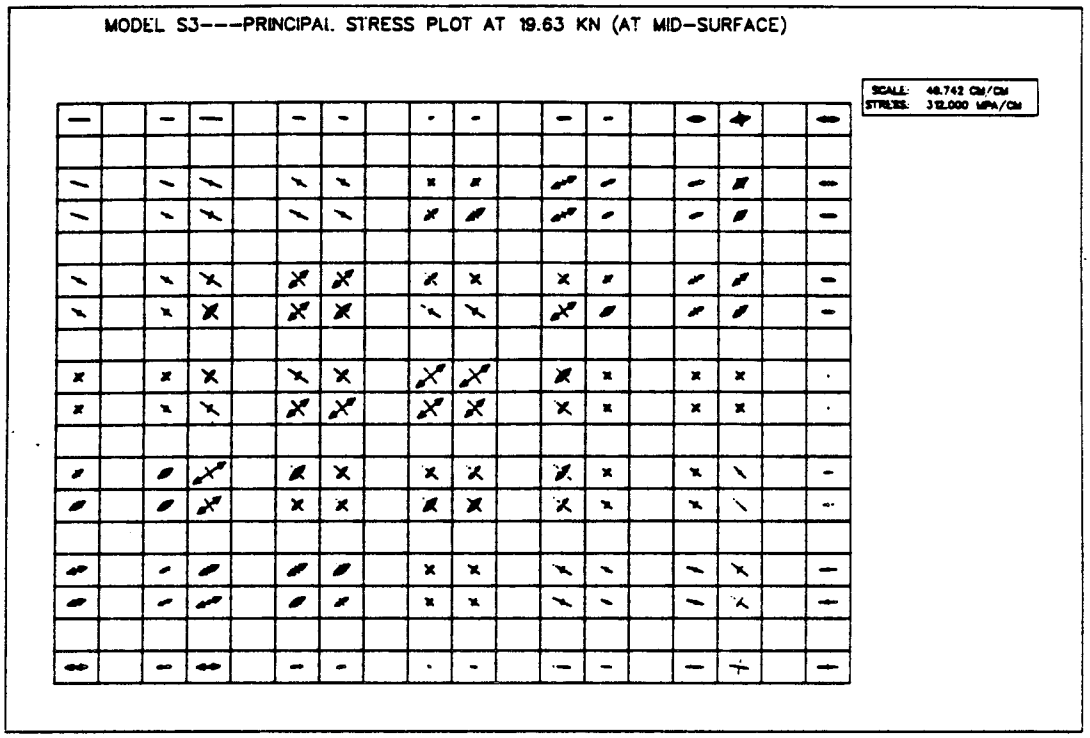

(a) Model S3

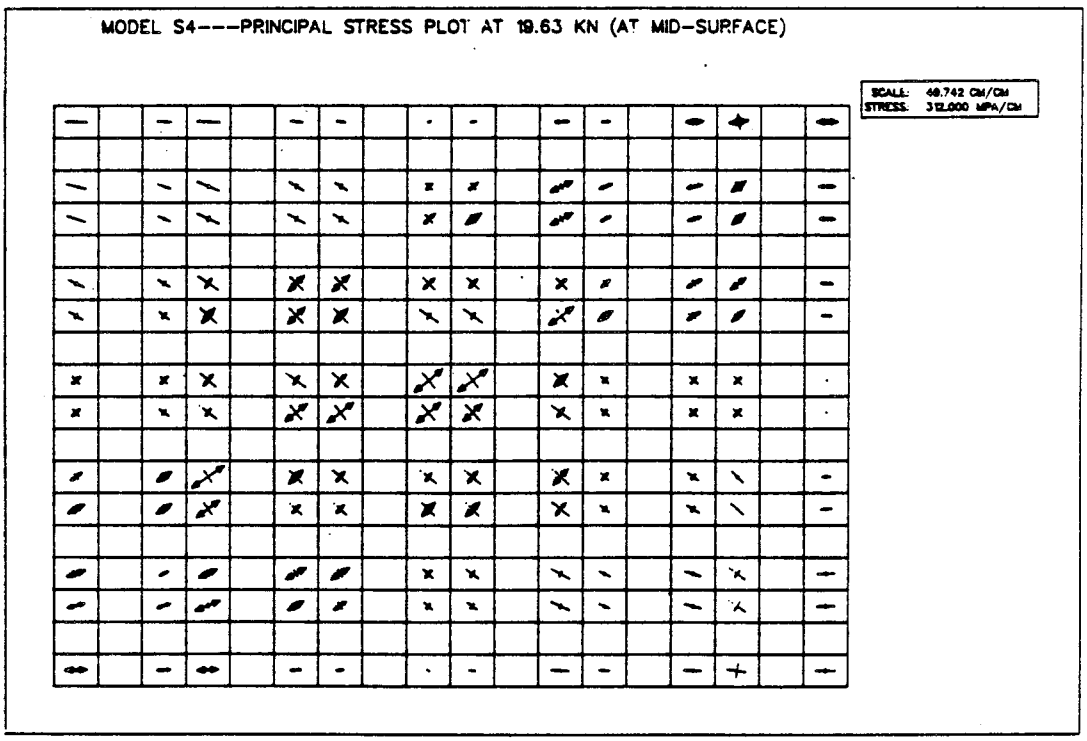

(b) Model S4

Figure 5.4 Principal Stress Plots for Models S3 and S4

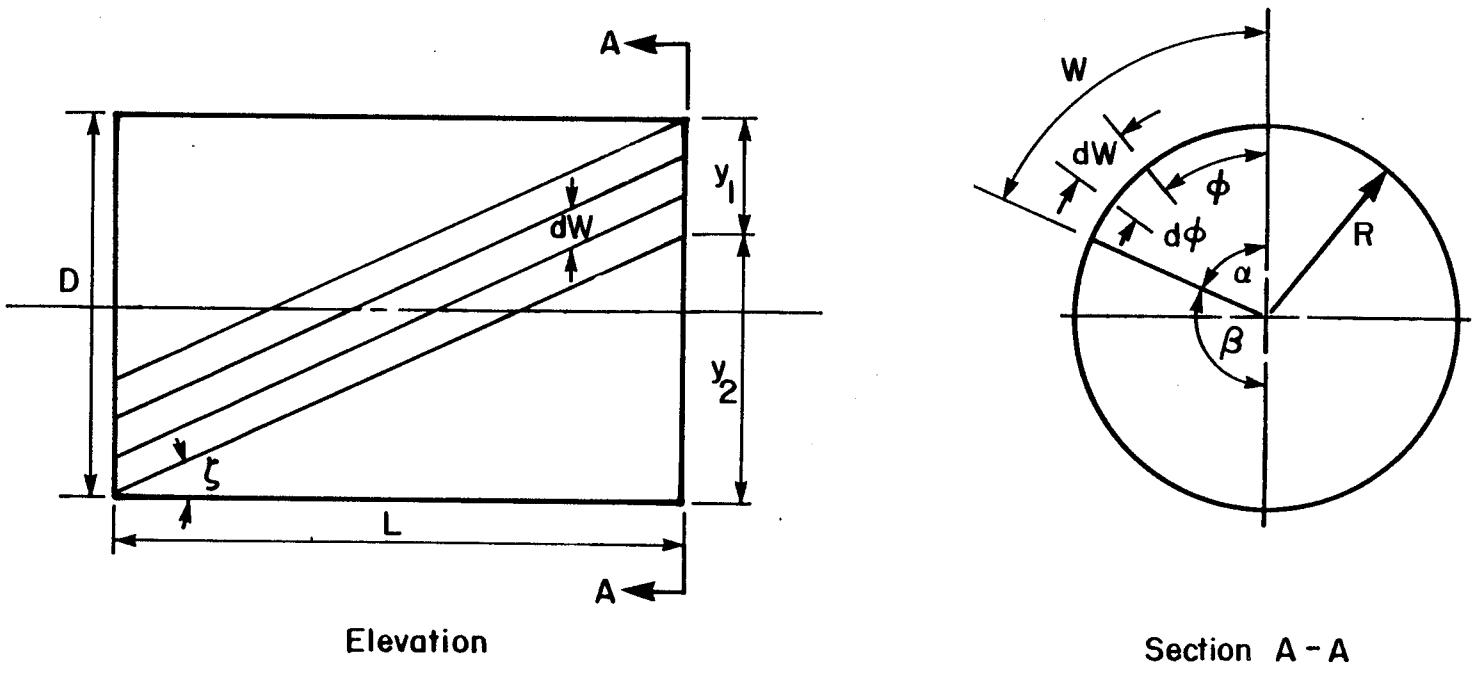

Figure 5.5 Proposed Geometry of the Tension Field

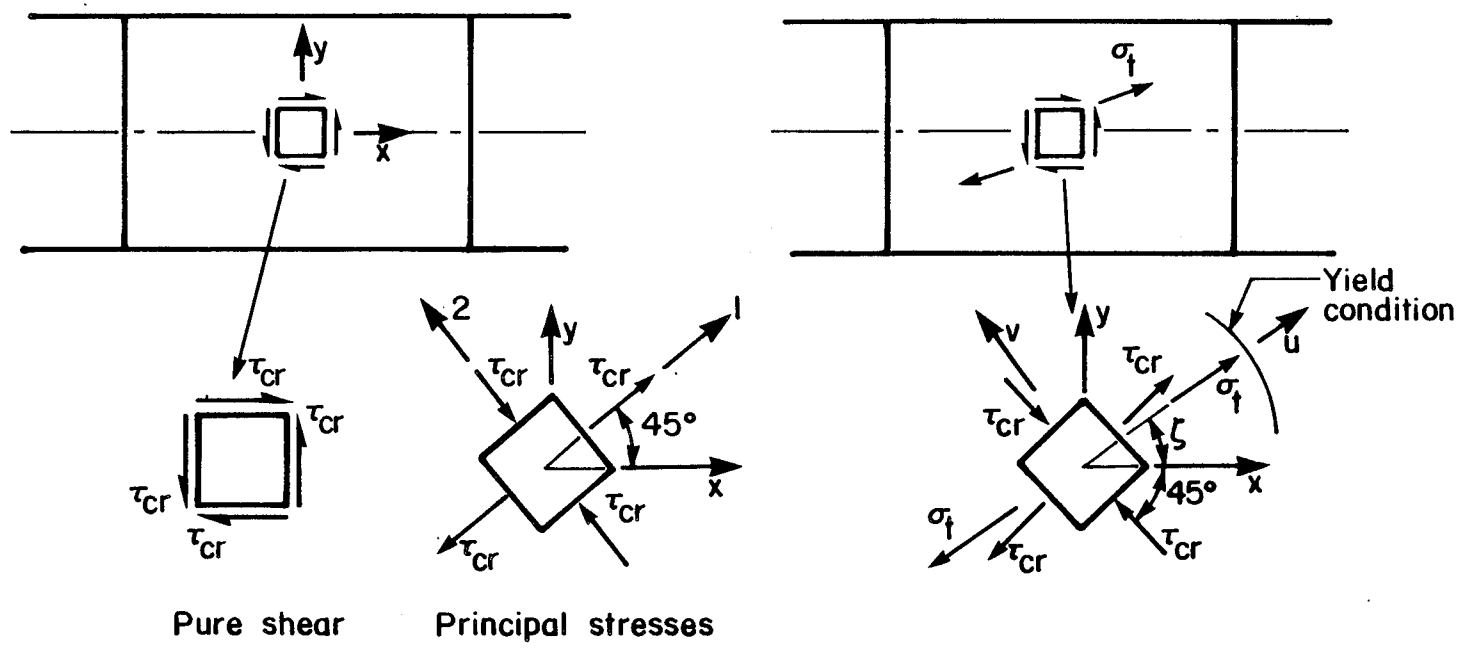

Figure 5.6 State of Stress at Buckling Load and at Ultimate Load

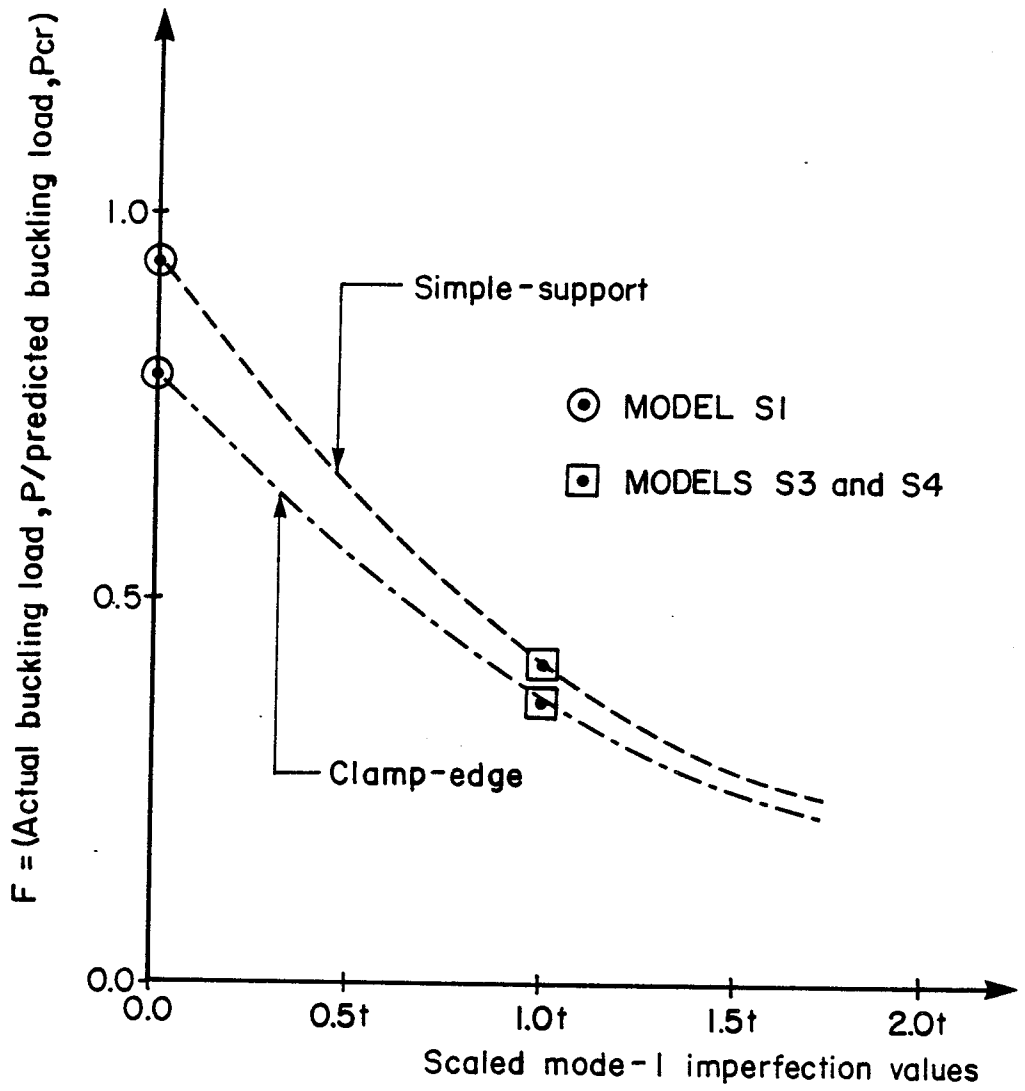

Figure 5.7 Variation of Critical-Shear-Stress Reduction Factor

P: Initial Buckling Load from Numerical Analysis
P_{cr}: Predicted Buckling Load According to Batdorf

6. SUMMARY, CONCLUSIONS AND RECOMMENDATIONS

6.1 Summary and Conclusions

This study was undertaken to investigate the shear behaviour of large diameter fabricated steel cylinders. Specifically, stability failure caused by the transverse shear loading at stress levels below the yield point was considered. The analytical phase of the study used the finite element code NISA80 as a tool to numerically analyse thin imperfect cylindrical shells. In particular, the geometry and the initial imperfection level of previously tested cylinders were used. Cylinders of this type are usually found in conveyor support systems where transverse shear is of primary concern.

The analysis of the results obtained in this study and the comparison with the results obtained by others on large diameter fabricated steel cylinders have led to the following conclusions:

1. The inclined buckling pattern of large diameter fabricated steel cylinders is a characteristic mode of initial buckling in shells loaded in double curvature. Thus, the patterns obtained in the Bailey and Kulak (1984) tests are not a special feature of that test.
2. Program NISA80 predicts reasonably well the shear buckling load of cylinders with small or no initial geometric imperfection, compared to the classical

theory for curved rectangular panels in pure shear according to Batdorf et al.

3. This inital buckling load is sensitive to geometric imperfections.
4. The stiffness of the shells is not sensitive to the level of geometric imperfections.
5. Program NISA80 load deflection response, although in agreement with beam theory results, exhibits far more stiffness than that obtained in the Bailey and Kulak test results.
6. In addition program NISA80, for levels of initial imperfections half those of the test specimen, failed to predict ultimate strength values anywhere near to the test results.
7. A definite tension field develops in the buckled regions subsequent to shear buckling, provided sufficient reaction (anchorage) elements exist.
8. The total shear capacity of large diameter fabricated steel cylinders consists of two parts, the "beam shear" component and the "tension field" component.
9. The R/t ratio is an important factor in determining the proportion of each shear component. As R/t increases the "tension field" component is expected to increase while the "beam shear" component decreases.

6.2 Recommendations

Future investigations should take into account the following aspects.

1. Some means of decreasing the overall stiffness of the models is needed, since in most cases of this study, the models exhibit much higher stiffness than the first shear specimen of Bailey and Kulak. It is possible that residual stresses may play a greater role than anticipated. Therefore, simulation of residual stresses is recommended.
2. Continuous eigenvalue analysis requires increasing the number of subspace iterations as the load level increases.
3. Shifting the solution strategy from Newton-Raphson to Riks-Wempner proved to be difficult. Therefore, it is recommended that Riks-Wempner strategy be used throughout an analysis.
4. Better assessment of how to correlate the measured imperfection values to the modal shapes is required in order to predict realistic scaling factors.
5. A parallel development of the tension field equations should be carried out in which the buckling of the compression element is the limit of the tension field action.

LIST OF REFERENCES

1. Almroth, B.O., "Influence of Edge Conditions on the Stability of Axially Compressed Cylindrical Shells", NASA CR-161, February, 1965.
2. Arbocz, J., "The Effect of Initial Imperfections on Shell Stability", Thin-Shell Structures, edited by Y.C. Fung and E.E. Sechler, Prentice-Hall, Englewood Cliffs, N.J., 1974.
3. Arbocz, J., and Babcock, C.D., "Prediction of Buckling Loads Based on Experimentally Measured Initial Imperfections", Buckling of Structures, edited by B. Budiansky, Springer-Verlag, New York, N.Y., 1976, pp. 295-296.
4. Arbocz, J., "The Imperfection Data Bank, A Mean to obtain Realistic Buckling Loads", Buckling of Shells, edited by E. Ramm, Proceedings of a State-of-the-Art Colloquium, Universität Stuttgart, Germany, May 6-7, 1982.
5. American Society of Mechanical Engineers, Metal Containment Shell Buckling Design Methods, Case N-284 of the ASME Boiler and Pressure Vessel Code, 1980.
6. Babcock, C.D., "Experiments in Shell Buckling", Thin-Shell Structures, edited by Y.C. Fung and E.E. Sechler, Prentice-Hall, Englewood Cliffs, N.J., 1974.

7. Bailey, R.W., and Kulak, G.L., "Flexural and Shear Behaviour of Large Diameter Steel Tubes", Structural Engineering Report No. 119, Dept. of Civil Engineering, University of Alberta, November, 1984.

8. Basler, K., "Strength of Plate Girders in Shear", Journal of the Structural Division, ASCE, Vol. 87, No. ST7, October, 1961.

9. Batdorf, S.B., Schildcrout, M., and Stein, M., "Critical Stress of Long Plates with Transverse Curvature", NACA TN-1346, June, 1947.

10. Batdorf, S.B., Stein, M., and Schildcrout, M., "Critical Stress of Curved Rectangular Panels", NACA TN-348, May, 1947.

11. Bathe, K.J., Finite Element Procedures in Engineering Analysis, Prentice-Hall, Englewood Cliffs, N.J., 1982.

12. Brazier, L.G., "On the Flexure of Thin Cylindrical Shells and Other Thin Sections", Proc. Roy. Soc. Lond., Series A., Vol. 116, 1927.

13. Brendel, B., Ramm, E., Fisher, D.F., and Rammerstorfer, F.G., "Stability Analysis of Thin Cylindrical Shells under Wind Loads", Journal of Structural Mechanics, Vol. 9, 1981, pp. 91-113.

14. Clough, R.W., and Penzien, J., Dynamics of Structures, edited by B.J. Clark and M. Gardner, McGraw-Hill, 1975, pp. 191-199.

15. Cook, R.D., Concepts and Applications of Finite Element Analysis, Second Edition, John Wiley and Sons, Inc., New York, 1981.

16. Crisfield, M.A., "Incremental/Iterative Solution Procedures for Non-linear Structural Analysis", Int. Conf. Num. Meth. for Nonlinear Problems, Swansea, Sept., 1980.

17. Donnell, L.H., "Stability of Thin-Walled Tubes under Torsion", NACA Rep. 479, 1933.

18. Donnell, L.H., "A New Theory for the Buckling of Thin Cylinders under Axial Compression and Bending", ASME Transactions, Vol. 56, 1934.

19. Donnell, L.H. and Wan, C.C., "Effect of Imperfections on Buckling of Thin Cylinders and Columns under Axial Compression", Journal of Applied Mechanics, Vol. 17, No. 1, 1950.

20. Everstine, G.C., "A Comparison of Three Resequencing Algorithms for the Reduction of Matrix Profile and Wavefront", IJNME, Vol. 14, No. 6, 1979, pp. 837-853.

21. Flügge, W., "Die Stabilität der Kreiszylinderschale", Ing.-Arch., Vol. 3, pp. 463-506, 1932.

22. Fung, Y.C., and Sechler, E.E. (editors), Thin Shell Structures/Theory, Experiment and Design, Prentice-Hall, Englewood Cliffs, 1974.

23. Harding, J.E., Dowling, P.J., and Agelidis, N. (editors), Buckling of Shells in Offshore

Structures, Granada, 1982.

24. Hoff, N.J., and Soong, T.E., "Buckling of Circular Cylindrical Shells in Axial Compression", SUDAER No. 204, Stanford, California, August, 1964.

25. Koiter, W.T., "On the Stability of Elastic Equilibrium", Thesis, Technical University Delft, Amsterdam, 1945; English Translation: Air Force Flight Dynamics Laboratory, Air Force Systems Command, Wright-Patterson Air Force Base, Ohio, Technical Report AFFDL-TR-70-25, 1970.

26. Koiter, W.T., "The Effect of Axisymmetric Imperfections on the Buckling of Cylindrical Shells under Axial Compression", Lockhead Missiles and Space Comp., Sunnyvale, Calif., U.S.A., Techn. Rep. 6-90-93-86, August, 1963, III.

27. Krätzig, W.B., Basar, Y., and Wittek, U., "Nonlinear Behaviour and Elastic Stability of Shells - Theoretical Concepts - Numerical Computations - Results", Buckling of Shells, edited by E. Ramm, Proceedings of a State-of-the-Art Colloquium, Universität Stuttgart, Germany, May 6-7, 1982.

28. Krätzig, W.B., Wittek, U., and Basar, Y., "Buckling of General Shells - Theory and Numerical Analysis", Collapse: the buckling of structures in theory and practice, edited by J.M.T. Thompson and G.W. Hunt, Cambridge University Press, Cambridge, 1983.

29. Lorenz, R., "Die nichtachsensymmetrische Knickung

dünnwanger Hohlzylinder", Phys. Z., Vol. 13, 1911, pp. 241-260.

30. Lundquist, E.E., "Strength Tests of Thin-Walled Duralumin Cylinders in Torsion", Technical Note 427, National Advisory Committee for Aeronautics, Washington, D.C., 1932.

31. Lundquist, E.E., "Strength Tests of Thin-Walled Duralumin Cylinders in Pure Bending", Technical Note 479, National Advisory Committee for Aeronautics, Washington, D.C. 1933.

32. Lundquist, E.E., "Strength Tests of Thin-Walled Duralumin Cylinders in Combined Transverse Shear and Bending", Technical Note 523, National Advisory Committee for Aeronautics, Washington, D.C., 1935.

33. Miller, C.D., "Buckling of Axially Compressed Cylinders", Journal of Structural Division, ASCE, Vol. 103, No. ST3, Proc. Paper 12823, 1977.

34. National Aeronautics and Space Administration, "Buckling of Thin-Walled Circular Cylinders", NASA Space Vehicle Design Criteria (Structures), NASA SP-8007, 1968.

35. Pinkney, R.B., Stephens, M.J., Murray, D.W. and Kulak, G.L., "Inelastic Buckling of Axially Loaded Cylindrical Shells", Proceedings, Annual Conference, CSCE, May 27-28, 1982, Edmonton, Alberta.

36. Pinkney, R.B., Stephens, M.J., Murray, D.W., and Kulak,

G.L., "Use of Measured Imperfections to Predict Buckling of Axially Loaded Cylindrical Shells", Canadian Journal of Civil Engineering, Vol. 10, No. 4, September, 1983.

37. Plantema, F.J., "Collapsing Stresses of Circular Cylinders and Round Tubes", Nat. Luchtvaartlaboratorium Rep. S.280, Amsterdam, 1946.

38. Ramm, E., "A Plate/Shell Element for Large Deflections and Rotation", Formulations and Computational Algorithms in Finite Element Analysis, edited by Bathe, K.J., Oden, J.T., and Wunderlich, W., MIT Press, 1977.

39. Ramm, E., "Strategies for Tracing the Nonlinear Response near Limit Points", Nonlinear Finite Element Analysis in Structural Mechanics, edited by W. Wunderlich, E. Stein, and K.J. Bathe, Proceedings of the Europe-U.S. Workshop, Ruhr-Universität Bochum, Germany, July 28-31, 1980.

40. Ramm, E., "Nichtlineare Struktur Analyse (NISA) Computer Code", Institute für Baustatik, University of Stuttgart, Stuttgart, W. Germany, 1980.

41. Ramm, E., and Stegmüller, H., "The Displacement Finite Element Method in Nonlinear Buckling Analysis of Shells", Buckling of Shells, edited by E. Ramm, Proceedings of a State-of-the-Art Colloquium, Universität Stuttgart, Germany, May 6-7, 1982.

42. Riks, E., "An Incremental Approach to the Solution of

Snapping and Buckling Problems", Int. J. Solids and Structures, Vol. 15, 1979, pp. 529-551.

43. Salmon, C.G., Steel Structures: Design and Behaviour, edited by Brinker, R.C., Intext Educational, San Francisco, 1971.

44. Schilling, G.G., "Buckling Strength of Circular Tubes", ASCE, Journal of Structural Division, Vol. 91, No. ST5, Proc. Paper 4520, Oct., 1965.

45. Schwerin, E., "Die Torsions - Stabilität des dünnwandigen Rohres", Z. Angew. Math. Mech., Vol. 5, 1925, pp. 235-243.

46. Seide, P., and Weingarten, V.I., "On the Buckling of Circular Cylindrical Shells and Other Thin Sections", J. Appl. Mech., Vol. 28, No. 1, 1961.

47. Singer, J., and Rosen, A., "The Influence of Boundary Conditions on the Buckling of Stiffened Cylindrical Shells", Buckling of Structures, edited by B. Budiansky, Springer-Verlag, New York, N.Y., 1976, pp. 227-250.

48. Southwell, R.V., "On the Collapse of Tubes by External Pressures", Phil. Mag., Vol. 25, 1913, pp. 687-698.

49. Southwell, R.V., "On the General Theory of Elastic Stability", Phil. Trans. Roy. Soc. Lond., Series A, No. 213, 1914.

50. Stephens, M.J., Kulak, G.L. and Montgomery, C.J., "Local Buckling of Thin-Walled Tubular Steel Members", Structural Engineering Report No. 113, Dept. of

Civil Engineering, University of Alberta, February, 1982.

51. Thorburn, L.J., Kulak, G.L. and Montgomery, C.J., "Analysis of Steel Plate Shear Walls", Structural Engineering Report No. 107, Dept. of Civil Engineering, University of Alberta, May, 1983.

52. Timler, P.A., and Kulak, G.L., "Experimental Study of Steel Plate Shear Walls", Structural Engineering Report No. 114, Dept. of Civil Engineering, University of Alberta, Nov., 1983.

53. Timoshenko, S., and Gere, J., Theory of Elastic Stability, McGraw-Hill, New York, N.Y., 1961.

54. von Karmań, T., and Tsien, H.S., "The Buckling of Thin Cylindrical Shells under Axial Compression", J. Aeron. Sci., Vol. 8, No. 8, 1941.

55. von Mises, R., "Der Krtische Ausendruck zylindrischer Rohre", Z. Ver. Deutsch. Ing., Vol. 58, 1914, pp. 750-755.

56. Webster, R.L., "On the Static Analysis of Structures with Strong Geometric Nonlinearity", Comp. St., Vol. 11, Nos. 1/2, 1980, pp. 137-145.

57. Weller, T., Singer, J., and Batterman, S.C., "Influence of Eccentricity of Loading on Buckling of Stringer-Stiffened Cylindrical Shells", Proceedings of the Thin Shell Structures Symposium, Prentice-Hall, 1974, pp. 305-324.

58. Wempner, G.A., "Discrete Approximations Related to

Nonlinear Theories of Solids", Int. J. Solids and Structures, 7(1971), pp. 1581-1599.

59. Wilson, W.M. and Olson, E.D., "Tests of Cylindrical Shells", U. of Illinois Engineering Experimental Station Bulletin Series, No. 331, 1941.

60. Zienkiewicz, O.C., and Irons, B.M., "Matrix Iteration and Acceleration Processes in Finite Element Problems of Structural Mechanics", Methods for Nonlienar Algebraic Equations, edited by P. Rabinowitz, Gordon and Breach, London, 1970, pp. 183-194.

61. Zienkiewicz, O.C., The Finite Element Method, 3rd edition, McGraw-Hill, London, 1977.